IDENTIFICATION AND QUANTIFICATION OF INORGANIC NANOPARTICLES IN WASTEWATER

by

Yinduo Chen

A Dissertation

Submitted to the Faculty

of the

WORCESTER POLYTECHNIC INSTITUTE

in Partial Fulfillment of the Requirements for the

Degree of Doctor of Philosophy

in

Civil Engineering

April 2022

APPROVED:

Dr. John A. Bergendahl, Assoc. Professor, Civil, Environmental and Architectural Engineering, Worcester Polytechnic Institute, Thesis Advisor

Dr. Harold W. Walker, Schwaber Professor, Civil, Environmental and Architectural Engineering, Worcester Polytechnic Institute, Committee Member

Dr. Nancy A. Burnham, Professor, Physics, Worcester Polytechnic Institute,
Committee Member

IDENTIFICATION AND QUANTIFICATION OF INORGANIC NANOPARTICLES IN WASTEWATER

By
Yinduo Chen
A Dissertation
Submitted to the Faculty
of the
WORCESTER POLYTECHNIC INSTITUTE
in Partial Fulfillment of the Requirements for the
Degree of Doctor of Philosophy
in
Civil Engineering

April 2022

APPROVED:

Dr. John A. Bergendahl, Associate Professor
Civil, Environmental and Architectural Engineering
Worcester Polytechnic Institute
Thesis Advisor

Dr. Harold W. Walker, Schwaber Professor
Civil, Environmental and Architectural Engineering
Worcester Polytechnic Institute
Committee Member

Dr. Nancy A. Burnham, Professor
Physics
Worcester Polytechnic Institute
Committee Member

ABSTRACT

Increasing use of inorganic nanoparticles (INPs) in consumer products and industrial processes has resulted in a more significant presence of these nanoparticles in wastewater. It is essential to understand the occurrence and characteristics of various nanoparticles in community wastewater. The primary objectives of this research were (1) to further develop and improve techniques to identify, quantify, and characterize these inorganic nanoparticles; (2) to investigate the presence of nanoparticles from 14 elements in wastewater from a large community with diverse wastewater sources; and (3) to explore the impacts of the size and wastewater sources of wastewater treatment plants (WWTPs) on the occurrence of inorganic nanoparticles. These objectives were motivated by the lack of information on the fate and transport of inorganic nanoparticles in wastewater streams and in the environment after consumer and industrial use. The presence of these nanoparticles in various water sources could pose a potential risk to public health and the environment. Extraction and concentration protocols were developed to prepare samples for instrumental analysis. Single Particle Inductively Coupled Plasma Mass Spectrometry (spICP-MS) was utilized, along with other nanoparticle characterization techniques.

Specific accomplishments of this research were: (1) the detection of inorganic nanoparticles from the 14 different targeted elements (Mg, Al, Mn, Fe, Cu, Sr, Mo, Ag, Sn, Ba, Pb, Zr, Ti, Zn) in municipal wastewater at different concentrations in influent and effluent streams; (2) the sizes and concentrations of these inorganic nanoparticles were variable over time due to the complexity of wastewater sources and the sampling period; and (3) the preparatory method developed in this work achieved good removal efficiencies of dissolved materials to minimize matrix-effects in single-particle ICP-MS analysis; (4) the nanoparticle size ranges obtained from different analytical techniques showed significant differences due to size distribution limits and agglomeration; (5) spICP-MS analysis coupled with statistical analysis indicated various levels of differences in nanoparticle concentrations between the WWTPs with different sizes and wastewater sources; (6) the effects of WWTP size (i.e., flowrate) and wastewater sources on detection of inorganic nanoparticles; and (7) the INPs removal efficiencies (10% -100%) between the influent and effluent vary with WWTPs sizes, sources and treatment. This work provides (1) a protocol to collect wastewater samples & analyze various INPs in complex wastewater systems; (2) a framework to assess some major factors affecting the nature of nanoparticles which are of importance to those determining environmental impacts; and (3) valuable information on the concentrations and size of different INPs in wastewater for realistic risk assessment.

This thesis is dedicated to my parents, my grandmother, and my fiancée

For their endless love, support and encouragement.

ACKNOWLEDGEMENTS

First and foremost, I would like to express my sincere gratitude to my advisor Prof. John Bergendahl for the continuous support of my Ph.D. study and related research, for his patience, motivation, and immense knowledge. His guidance helped me in all the time of research and writing of this dissertation. I could not have imagined having a better advisor and mentor for my Ph.D. study.

Besides my advisor, I would like to thank the rest of my dissertation committee: Prof. Harold Walker and Prof. Nancy Burnham, for their insightful comments, encouragement, and the complex and constructive questions that incented me to widen my research from various perspectives.

I would also like to thank the Department of Civil, Environmental, and Architectural Engineering at Worcester Polytechnic Institute for the assistantship awarded to me that enabled this research. I want to give special thanks to Dr. Wenwen Yao and Russell Lang for their support with laboratory procedures. I would also like to thank Prof. Dudle and Prof. Abu-Lail, whom I have had the great opportunity to work with.

Lastly, a special thanks to my family. Words cannot express how grateful I am to my grandmother and my parents for all the sacrifices you have made on my behalf. Your devotion, unconditional love and support, patience, optimism, and advice were more valuable than you could ever imagine. I would also like to thank my fiancée, Jihan. Thank you for supporting me in everything, and especially I cannot thank you enough for encouraging me throughout this experience.

TABLE OF CONTENTS

LIST OF TABLES

LIST OF FIGURES

LIST OF SYMBOLS AND ABBREVIATIONS

ENPs	Engineered nanoparticles
nAg (AgNPs)	Nanosized silver
nAu (AuNPs)	Nanosized gold
$nTiO_2$	Nanosized titanium dioxide
Fe	Iron
Ag	Silver
Ce	Cerium
W	Tungsten
Pd	Palladium
Pt	Platinum
Rh	Rhodium
Zn	Zinc
Ti	Titanium
Si	Silicon
Cu	Copper
Mo	Molybdenum
B	Boron
nZnO	Nanosized zinc oxide
W_2S	Tungsten disulfide
Mo_2S	Molybdenum disulfide
BN	Boron nitride

CeO_2	Ceric oxide
C_{60}	Buckminsterfullerene
TiO_2	Titanium dioxide
Fe_3O_4	Iron oxide black
Al_2O_3	Aluminum oxide
CrO_3	Chromium trioxide
spICP-MS	Single particle inductively coupled plasma mass spectrometry
WWTP	Wastewater treatment plant
UV	Ultraviolet
CFC	Chlorofluorocarbon
MNP	Magnetic nanoparticle
γ-Fe_2O_3	Maghemite
FePt	Iron-platinum
SiO_2	Silica
H_2	Hydrogen
CH_3OH	Methanol
CH_3CH_2OH	Ethanol
Li	Lithium
Mg	Magnesium
Na	Sodium
NPs	Nanoparticles
MgO	Magnesium oxide
CuO	Copper (II) oxide

FDA	Food and Drug Administration
ZVI	Zero-valent iron
INPs	Iron nanoparticles
TCE	Trichloroethylene
NINPs	Natural inorganic nanoparticles
Mn	Manganese
Cr	Chromium
Ba	Barium
Pb	Lead
H_2S	Hydrogen sulfide
HS	Hydrosulfide
O_2	Oxygen
CNTs	Carbon nanotubes
NOM	Natural organic matter
ROS	Reactive oxygen species
NINPs	Natural inorganic nanoparticles
Fe^{3+}	Iron (3+) ion
Mg^{2+}	Magnesium (2+) ion
Ca^{2+}	Calcium ion
RT	Room temperature
MIC	Minimum inhibitory concentrations
GP	Gram-positive
GN	Gram-negative

MGD	Million gallons per day
CBOD	Carbonaceous biochemical oxygen demand
TSS	Total suspended solids
H_2O_2	Hydrogen peroxide
HNO_3	Nitric acid
Sr	Strontium
Zr	Zirconium
Mo	Molybdenum
Sn	Tin
Ba	Barium

EXECUTIVE SUMMARY

Increasing use of inorganic nanoparticles in consumer products and industrial processes has resulted in a more significant presence of these nanoparticles in wastewater. It is essential to understand the occurrence and characteristics of various nanoparticles in wastewater systems.

The primary objectives of this research were to (1) further develop and improve techniques to identify, quantify, and characterize these inorganic nanoparticles; (2) investigate the presence of nanoparticles from 14 elements in wastewater treatment plants (WWTPs) influent & effluent streams from a large community with diverse wastewater sources; and (3) explore the impacts of the size and wastewater sources of wastewater treatment plants (WWTPs) on the occurrence of inorganic nanoparticles. These objectives were motivated by the lack of information on the fate and transport of inorganic nanoparticles in waste streams and in the environment after consumer and industrial use; the presence of these nanoparticles in various water sources could pose a potential risk to public health and the environment.

In this work, sampling and analyses were performed in two phases on various wastewaters from four WWTPs in Massachusetts. Wastewater samples were collected over monthly time intervals from UB WWTP (Phase I) and four WWTPs: AC, SB, UB, and DI (Phase II). Extraction and concentration protocols were developed to prepare samples for further analysis. Single Particle Inductively Coupled Plasma Mass Spectrometry (spICP-MS) was utilized, along with other analytical nanoparticle characterization techniques, including Scanning Electron Microscopy (SEM), Dynamic Light Scattering (DLS), and Atomic Force Microscopy (AFM).

Specific accomplishments of Phase I research were: (1) the detection of inorganic nanoparticles from the 14 different targeted elements (Mg, Al, Mn, Fe, Cu, Sr, Mo, Ag, Sn, Ba, Pb, Zr, Ti, Zn) in wastewater samples via spICP-MS, with significant variability in concentrations over time; (2) the size distributions of detected inorganic nanoparticles in the wastewater samples were revealed, highlighting the most frequent sizes in these samples which varied from 16 nm (Pb) to 139 nm (Ti); and (3) the effectiveness of the sample preparatory method developed in this study in removing dissolved, background, concentrations that interfere with the single-particle analysis was examined.

Specific accomplishments of Phase II research were: (1) spICP-MS analysis coupled with statistical analysis indicated various levels of differences in nanoparticle concentrations between the WWTPs with different sizes and wastewater sources; (2) the effects of WWTP size (i.e., flowrate) and wastewater sources on detection of inorganic nanoparticles; and (3) the INPs removal efficiencies (10% -100%) between the influent and effluent vary with WWTPs sizes, sources and treatment.

This research on nanoparticles in wastewater contributes to our knowledge of community impact on public health and the environment. In particular, the findings of this research: (1) provided a framework/protocol to collect wastewater samples & analyze various inorganic nanoparticles in complex wastewater systems; (2) explored factors affecting the nature of nanoparticles which are of importance to those determining environmental impacts; and (3) provided valuable information on the concentrations and size of these different INPs in wastewater for realistic risk assessment. For future perspectives, we recommend that (1) research on wastewater composed of different sources and sampling periods can be conducted to gain a better understanding of the origin, fate, and transport of INPs in wastewater; (2) an improvement in the

spICP-MS sensitivity is needed to detect the smaller INPs than the current cut off point; (3) a development of new analytical techniques and novel approaches to detect, quantify and differentiate natural from engineered INPs; and (4) studies in organisms exposed to treated effluents could consider these measurements, in order to obtain a realistic scenario for organisms exposed to INPs.

I. INTRODUCTION

Inorganic nanoparticles, defined as solid particulate material with dimensions of 1-100 nm, are widely used for various purposes in agricultural, domestic, and industrial sectors. The production and application of engineered nanoparticles (ENPs) have grown dramatically over the past decades and become a significant constituent of global material flow (Keller *et al.* 2013). Because their surface area to volume ratio is high, nanoparticles have unique properties and are used beneficially in many practical applications. Nanosized silver (nAg) is employed in some healthcare products (Foss Hansen et al. 2016). Nanosized gold (nAu) is applied in components of various electronic equipment and is also utilized as a catalyst in different industrial processes (Toro *et al.* 2007). Nanosized titanium dioxide ($nTiO_2$) is a common constituent in domestic products such as sunscreens, cosmetics, toothpaste, paintings, and certain food products (e.g., chewing gum) (Helsper *et al.* 2016; Peters *et al.* 2014). In the automobile industry, nanomaterials composed of metals such as Fe, Ag, Ce, W, Pd, Pt, Rh, Zn, Ti, Si, Cu, as well as Mo and B, are used in many components such as brake linings and engine parts. Nanosized zinc oxide (nZnO) is used as a vulcanization activator in car tires (Semaan, Quarles, and Nikiel 2002). In addition, nanosized W_2S, Mo_2S, BN, CeO_2, and C_{60} are used as additives in engine oils and fuels to improve engine performance (Jung, Kittelson, and Zachariah 2005; Lahouij *et al.* 2012). Clearly, many types of inorganic nanoparticles have been used in a multitude of applications for beneficial purposes, and there is little doubt that the amount of nanoparticles used and produced by society will increase.

Many nanoparticles have been found to produce deleterious impacts on various lifeforms, presumably due to their high surface activity as a result of their high surface-area-to-volume ratio. It has been demonstrated that nanoparticles may damage DNA in microorganisms (Auffan et al.

2009). In the presence of ultraviolet (UV) light, some nanoparticles can produce reactive species resulting in cell damage (Alkahtane 2015). In addition to nanoparticle-induced toxicological problems, nanoparticles can disrupt vital functions of microbial cells through physical means, such as blocking pores (Elsaesser and Howard 2012).

Research has also been conducted to determine the effect of nanoparticles on animals. Lam *et al.* (2004) showed that carbon nanotubes induced dose-dependent granulomas in mice, and in some cases, the nanoparticles produced interstitial inflammation in the animals after seven days of exposure. Oberdörster *et al.* (2005) demonstrated that nanoparticles (C_{60} fullerenes) induced oxidative stress in a fish model. The toxicity of nanoparticles should be considered when producing, using, and releasing nanoparticles into wastewater. Thus, the need to determine the occurrence, concentrations, and types of nanoparticles in wastewater, as well as the consequences of their presence.

The release of nanoparticles is not only a concern due to possible deleterious impacts on aquatic life and the environment; there are also potential human health concerns. Hematopoietic human progenitor cells have been shown to be affected by a 5 μg/mL dose of antimony trioxide nanoparticles in a laboratory environment (Bregoli *et al*. 2009). A research study examined the relationship among working groups with vague symptoms of exposure to airborne polyacrylate nanoparticles (Song, Li, and Du 2009). Polyacrylate has been shown to be airborne in the workplace in a nano-particulate form. For specific working groups, diseases (i.e., non-specific pulmonary inflammatory disease, pulmonary fibrosis, and foreign-body granulomas of pleura) were reported in the pathological exam of seven young women aged 18-47. This study confirmed the chronic toxicity of nanosized polyacrylate in the lung (Song *et al.* 2009). Iron oxide nanoparticles were also found to cause cell death associated with membrane damage (Berry *et al*.

2004). And Jeng and Swanson (2006) found significant inorganic oxide nanoparticles (TiO_2, ZnO, Fe_3O_4, Al_2O_3, and CrO_3) toxicity in mammalian cells.

Even though the use of nanoparticles in many societal sectors is increasing, there is little data on the fate and transport of nanoparticles in our waste streams and in the environment after consumer and industrial use. And information on the ultimate disposal and release/emissions of nanoparticles is sparse. However, it is expected that the increasing use of nanoparticles in consumer products and in specific industrial processes will result in a growing number of nanoparticles in municipal wastewater streams.

Much research has focused on the advancement of analytical methods to identify certain nanoparticles in water (Choi *et al*. 2017). Yet, an accurate examination of the presence of a wide range of nanoparticles in actual wastewater utilizing these techniques has not been published. In addition, they are studies that only focused on nanoparticles identification in the different treatment steps in a single WWTP facility, but no study has compared WWTPs with various sizes and sources. Few studies collected actual samples so as to indicate the presence of different nanoparticles, regardless of whether inorganic or organic (Bäuerlein *et al*. 2017). Past notable research has included the characterization of Ti and Zn nanoparticles in actual wastewater samples (Choi *et al.* 2017). Research focusing on the broader population of nanoparticles in wastewater has not been performed. Most previous studies were focused only on nanoparticulate elemental Ti, Ag, and Zn. The results of earlier studies on the identification and quantification of nanoparticles under actual conditions at wastewater treatment plants are summarized in Table 1. Therefore, further research is needed to assess the occurrence of multiple types of nanoparticles under field conditions in wastewater is needed. In addition, an accurate and systematic identification and quantification

of INPs in wastewater is needed to determine their relations to the sources and sizes of WWTPs and their possible risks

Table 1 Identification and quantification of engineered nanoparticles under field conditions at wastewater treatment facilities.

Nanoparticles	Analytical techniques	Reference
$nTiO_2$	ICP-OES, SEM, EDX	Kiser *et al*., 2009
nAg, nAu, nC_{60}	ICP-OES (nAg, nAu), HPLC (nC_{60})	Kiser *et al*., 2012
nAg	spICP-MS[b]	Tuoriniemi *et al*., 2012
nAg	GFAAS[a]	Li *et al*., 2013
nZnO	spICP-MS[b]	Hadioui *et al*., 2015
$nTiO_2$, nZnO	ICP-OES, SEM	Choi *et al*., 2017
nTi, nAg	ICPQQQ[c], STEM[d]	Polesel *et al*., 2018

[a] GFAAS = Graphite Furnace Atomic Adsorption Spectrometry.
[b] spICP-MS = Single Particle Inductively Coupled Plasma Mass Spectrometry.
[c] ICPQQQ = Inductively Coupled Plasma Triple Quadrupole Mass Spectrometry.
[d] STEM = Scanning Transmission Electron Microscopy.

In addition to studies on nanomaterials in wastewater systems, ICP-MS methods have been demonstrated to be sensitive enough to identify and quantify NPs in low quantities in the environment. They have been applied to determine the presence of copper nanoparticles (nCu) in soil (Navratilova *et al*. 2015). Another study monitored the discharge of nanosized titanium oxide, $nTiO_2$, originating from sunscreens into surface water (Gondikas *et al*. 2014). Two other research

efforts investigated the issue of $nTiO_2$ and nAg in the aquatic environment arising from outdoor coatings. It was reported that $nTiO_2$ and nAg nanoparticles were found to be released into the environment at 600 μg TiO_2/L (20–300 nm size range) and 145 μg Ag/L (< 15 nm in size) (Kaegi *et al.* 2008, 2010). These nanoparticles were directly identified at the source in high concentrations; therefore, dilution away from the source was expected. Questions remain on how these nanoparticles can be effectively removed from industrial and domestic wastewaters and what are the proper sample preparation techniques required for nanoparticles analysis (Brar and Verma 2011).

As seen in Table 1, previous studies used Single Particle Inductively Coupled Plasma Mass Spectrometry (spICP-MS) to investigate only one single element in wastewater and surface water, which included nAg, (Tuoriniemi *et al*., 2012) and nZnO (Hadioui *et al*., 2015). These studies focused on quantifying a single element per run, which will be a lengthy process in our study of a broader variety of nanoparticles in wastewater. As a result, the ability to identify several elements utilizing spICP-MS in a single run can drastically reduce total measurement time and provide a broader study of nanoparticles in wastewater.

In accordance with the prior discussion, the following hypotheses, and objectives were developed to navigate this research:

Hypotheses:

- There is a wide range of different types of nanoparticles based on multiple elements present in municipal wastewaters.

- Single Particle ICP-MS (spICP-MS) is a sensitive technique to detect and quantify multiple inorganic nanoparticles at once with low concentrations and small size distributions in wastewater.
- Inorganic nanoparticles are only partially removed in WWTPs which vary greatly with the WWTPs sizes and the wastewater sources.

Objectives:

- Develop techniques to identify, quantify, and characterize inorganic nanoparticles in wastewater primarily using single-particle ICP-MS.
- Investigate the nature and occurrence of the various inorganic nanoparticles in wastewater treatment plant (WWTP) influent and effluent streams.
- Investigate the effect of the WWTP size and the related wastewater source compositions on the occurrence of inorganic nanoparticles in municipal wastewaters.

The objectives of this research were met through the following activities:

1. A detailed literature review was performed to scan the related work to inorganic nanoparticles, synthesize the major findings, and develop a solid knowledge foundation.
2. Experimental sampling and analyses were performed in two phases on various wastewaters from four WWTPs in Massachusetts. Extraction and concentration protocols were developed to prepare samples for further analysis.
3. Several analytical methodologies were used to identify and quantify inorganic nanoparticles in wastewater samples, including Single Particle Inductively Coupled Plasma Mass Spectrometry (spICP-MS), Scanning Electron Microscopy (SEM), Dynamic Light Scattering (DLS), and Atomic Force Microscopy (AFM).

4. Collecting, evaluating, and analyzing data and results, and formulating major conclusions and suggestions.

This rest of the thesis is organized as follows: First, a background section is developed to provide an overview of the sources, fate and toxicity of inorganic nanoparticles (section II). Second, a Materials and Methods section is provided, where the overall methodology used in this study is introduced, including the spICP-MS analysis along with other analytical techniques (section III). The research timeline and study phases (Phase I and Phase II) conducted to have a broad identification and quantification of INPs, are also explained). Third, Results and Discussion sections for both Phases I and II are in developed in detail (section IV and section V). Finally, Conclusions section is provided with key results summary and future recommendations (section VI). Appendixes are provided at the end.

II. BACKGROUND

The background section includes an overview of the sources of inorganic nanoparticles (section II.1), the fate of inorganic nanoparticles (section II.2), and the toxicity of inorganic nanoparticles (section II.3).

II.1 Sources of Inorganic Nanoparticles

Figure 1 summarizes some of the important sources of inorganic nanoparticles, including their engineered and natural origins. A detailed explanation of each source, its importance, and some application examples are developed in the following subsections.

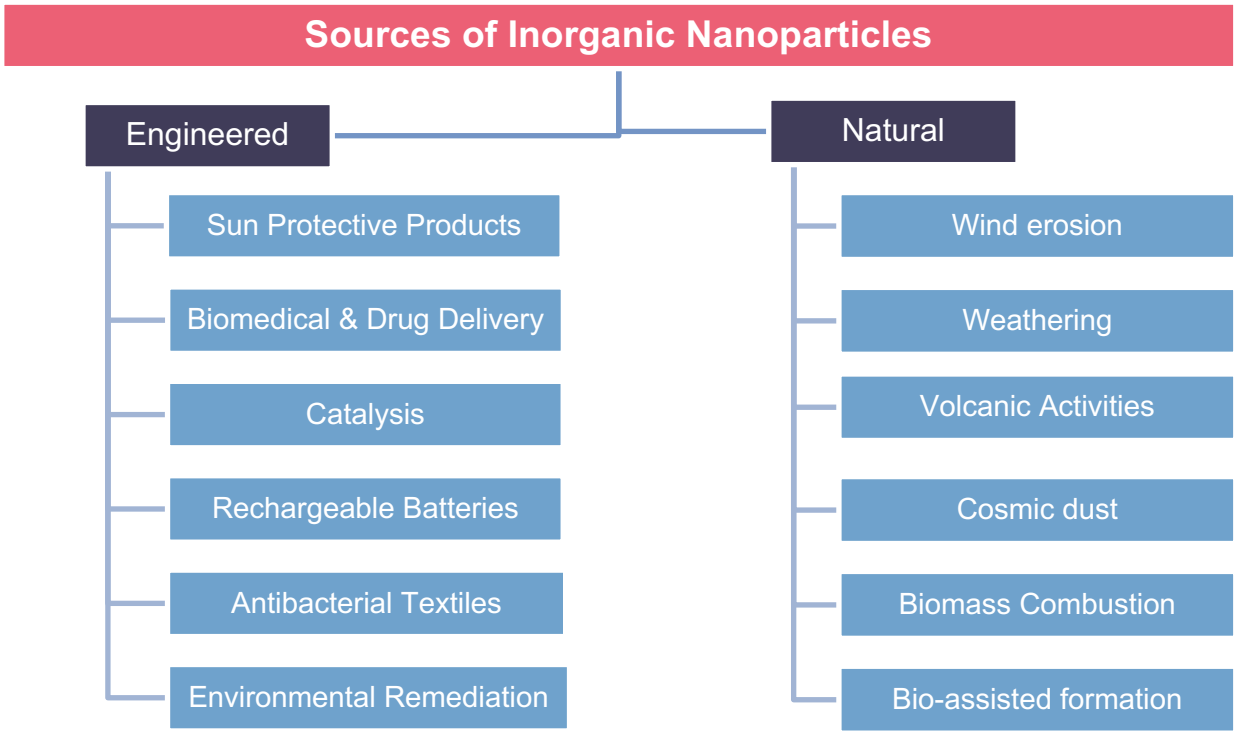

Figure 1. Overview of key sources of inorganic nanoparticles.

II.1.1 Engineered Inorganic Nanoparticles

II.1.1.1 Sun Protective Products

Sunscreen is an integral part of our routine for protecting our skin from ultraviolet (UV) rays. UV rays can cause dimerization of thymine bases and, in some instances, breakdown of the sugar-phosphate backbone of DNA if you don't wear sunscreen. Most photodamage to the skin is caused by UV radiation with wavelengths between 280 and 400 nm. UV light is divided into three categories: UVA (320–400 nm) is the most extended wavelength component; it can penetrate the dermis, where melanoma is found. UVB (280–320 nm) rays are primarily blocked by the epidermis, resulting in inflammation known as "sunburn cell development"; and UVC (200–280 nm), often known as germicidal rays, is the most energetic and, as a result, has the most significant potential for harm (Hidaka et al. 1997). Fortunately, the stratospheric ozone layer filters it out most of the time, so it isn't a ground-level problem. However, as long as chlorofluoro hydrocarbons (CFC) are used, this barrier will be depleted, allowing this beam to reach our skin. Nonetheless, prolonged sun exposure causes photocarcinogenesis, which causes the immune system to be suppressed as well as photoaging of the skin, eventually leading to the formation of basal cell carcinoma (Matsumura and Ananthaswamy 2004).

The organic molecules used in sunscreens are primarily advanced aromatic compounds that have been functionalized to delocalize electrons and absorb light in the 280–400 nm wavelength range. Unfortunately, UV light can aid in the disintegration of these molecules, and the resulting subunits are readily absorbed via the skin, posing a risk of allergic responses (Perugini et al. 2002). Inorganic particles like TiO_2 and zinc oxide were then incorporated into sunscreen

formulations to reflect UV radiation and lower the quantity of organic molecules needed to reach the appropriate sun protection factors (SPFs) for increased protection.

When TiO_2 is irradiated with UV light, the energy is larger than the bandgap, causing electrons to move from the valence to the conduction band. These electrons then swiftly travel to the particle's surface, where they combine with oxygen to create superoxide and hydroxyl radicals (Miriam 2017). The penetration of nanosized particles is another challenge with inorganic materials. Cosmetic companies use nanosized (100 nm) inorganic materials such as TiO_2 and zinc oxide because their tiny sizes allow maximum coverage without opacity. The health risks posed by nanoparticles, on the other hand, might be a concern in a variety of topical applications.

II.1.1.2 Biomedical/Drug Delivery

The systemic distribution of molecular medicines (i.e., drug delivery) is now used as a conventional therapeutic approach for the treatment of several disorders. The most popular medications are chemical substances that function quickly and are taken orally (in tablet or liquid form) or injected. As a result, medication development must advance with controlled drug release and delivery system targeting. Diagnostic and therapeutic inorganic nanoparticles (e.g., Carbon NPs, Gold NPs), have been extensively researched as novel platforms for various biomedical applications throughout the last few decades (Figure 2).

The use of magnetic nanoparticles managed by an external magnetic field is an intriguing method with enormous promise for remotely controlling the delivery of medication or genes. Lübbe et al. (1996) provided the first findings on magnetic medication targeting in human patients in 1996, after a prior investigation on animals. A ferrofluid, a colloidal dispersion of multidomain iron oxide (Fe_3O_4) with a 50-150 nm size range, was employed and generated using a wet chemical

process. Anhydro-glucose polymers were used to enclose the particles in order to increase stability under diverse physiological circumstances as well as drug chemisorption. Desorption of the drug that had been attached to the surface happened according to the physiological environment (pH, osmolality, and temperature) because the interaction between the coatings of the drug and magnetic particles was reversible (Lübbe et al. 1996).

The adaptability of diverse synthesis processes currently allows for the exact engineering of the essential properties of a broad range of nanoparticles, which is one of the main benefits of adopting nanotechnology for biological reasons. Various magnetic nanoparticles (MNPs) have been suggested and tested for biomedical applications to utilize nanoscale magnetic phenomena. Magnetite (Fe_3O_4), maghemite (γ-Fe_2O_3), ferrite of general formula MFe_2O_4 (M = Co, Ni, Zn), iron, and iron-based alloys such as iron-platinum (FePt) have all been identified as prospective possibilities for biomedical uses (Claudia 2017). Figure 2 shows more detailed representation of a multifunctional magnetic nanoparticle used for biomedical application.

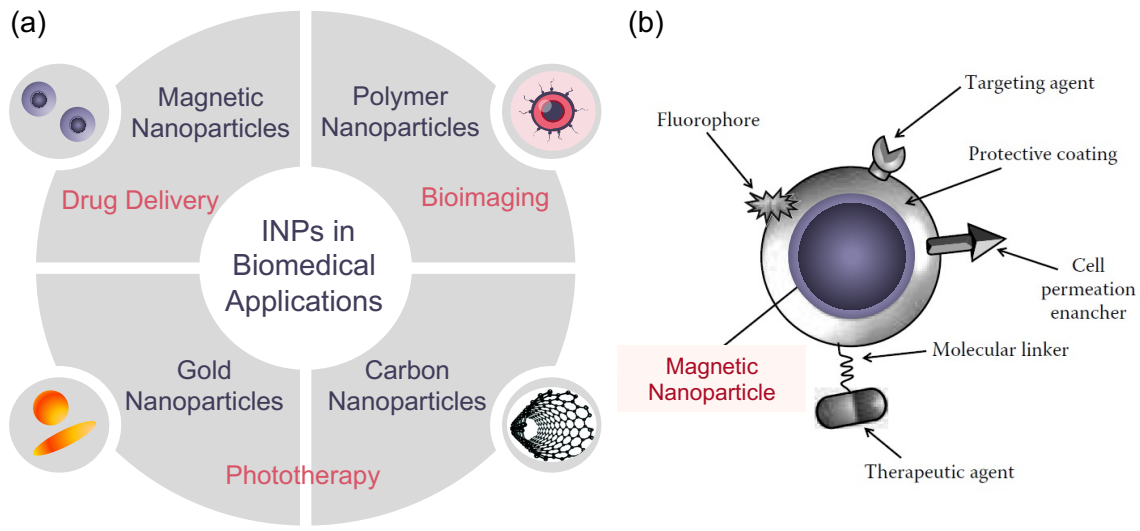

Figure 2. An overview of using nanoparticles in biomedical applications: (a) various INPs and their potential uses in biomedical applications; (a) an example of multifunctional hybrid magnetic nanoparticle for biomedical purposes, adapted from Claudia (2017).

II.1.1.3 Catalysis

A catalyst is a chemical reactant that is necessary to speed up a chemical reaction without being consumed in the process. The effects of catalysts appear in the rate law but doesn't influence the overall stoichiometry of the chemical reaction. The main types of catalyst materials used are metals, metal oxides, metal complexes, and biocatalysts. The catalytic function (i.e., activity and selectivity) is determined by the structure and content of the catalyst. One of the elements impacting catalytic characteristics is particle size. Because the catalytic reactions occur exclusively on the catalyst's surface, small particle sizes are preferred to increase specific surface area (Toshima 2011).

The reactive nature of nanoparticles makes them a natural choice for catalysts. Catalysts are divided into two groups based on the reaction phase in which they are utilized: homogeneous catalysts and heterogeneous catalysts (Figure 3). Metal complex catalysts and biocatalysts, for

example, are commonly utilized in solution, where other catalysts and reactants can be dissolved. On the other hand, metal catalysts are frequently used in heterogeneous phases such as gas/solid and liquid/solid. Small metal particles, such as alumina (Al_2O_3) and silica (SiO_2), are immobilized on inorganic oxide substrates for this purpose. Solid supports are advantageous not only for separating catalysts from reactants and products in a heterogeneous phase but also for improving catalytic functions such as lifetime through metal particle dispersion and dilution, tuning the electronic state of catalytic sites through interactions between metal particles and the support (Toshima 2011).

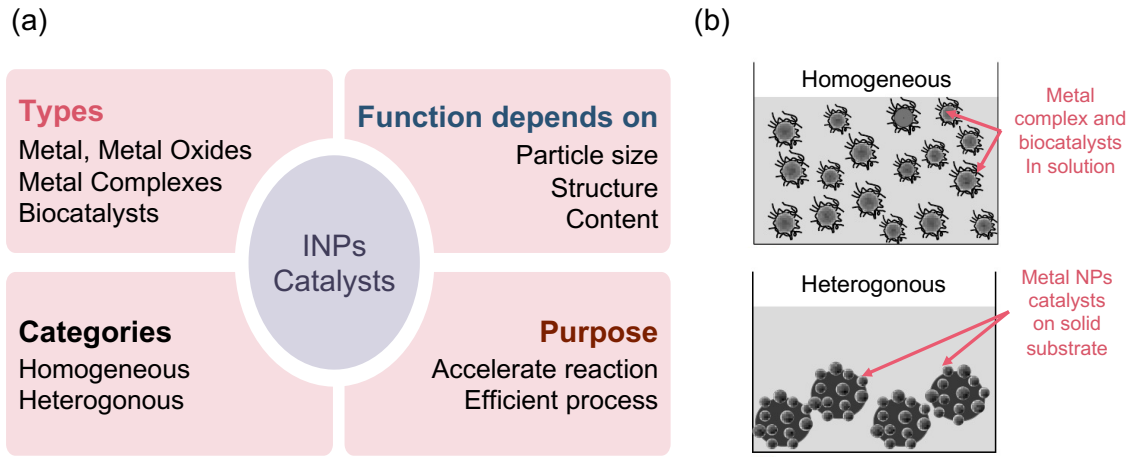

Figure 3. Nanoparticles as catalysts (a) Overview of types, classification, factors influencing the catalytic function and purposes; (b) Schematic representation of homogeneous and heterogeneous catalysts of NPs, adapted from Toshima (2011).

II.1.1.4 Rechargeable Batteries

Batteries are a common product that is used by many on a daily basis. Without batteries, which are portable energy storage devices, modern life would be hard to fathom. In recent years, much effort has been put into synthesizing and exploring nanomaterials in relation to batteries and

energy storage (e.g., fuel cells and photovoltaic solar cells). Inorganic nanoparticles (INPs) are being investigated as battery electrode materials. There has been impressive work on the development of new electrolyte systems in which inorganic nanoparticles play an important role in enhanced ionic conductivity. In addition, nanoparticles are critically important as catalysts for the reduction of oxygen and the oxidation of fuels (e.g., H_2, CH_3OH, CH_3CH_2OH,) in fuel cells. Furthermore, the use of nanoparticles significantly improves the performance of photovoltaic solar cells in terms due to the large surface area that enhances sunlight gathering, and therefore energy density.

The first aqueous batteries were introduced to the market. These systems are lead-acid, Ni-Cd, Ni–MH, and Zn–based batteries. All forms of lithium and lithium-ion batteries are included in the nonaqueous systems. Due to passivation processes, reactive electrodes (Li, Li–C, Li–M, Mg, Na, low redox potential, LiMOx) are stable in nonaqueous environments. Rechargeable systems are the focus of most attempts to integrate nanomaterials into batteries and associated devices, including Zinc Anode Batteries, Lithium-Liquid Cathode,Lithium Batteries with Solid Cathodes, Lead-Acid Batteries, Ni-Cd Batteries, Ni-Metal Hydride Batteries, Li (Metal)-MX2 Batteries, Li-Ion Batteries. (Doron and Ortal 2017). Figure 4 summarize some key primary and secondary battery systems and related devices (i.e., fuel cells) that uses nanoparticles.

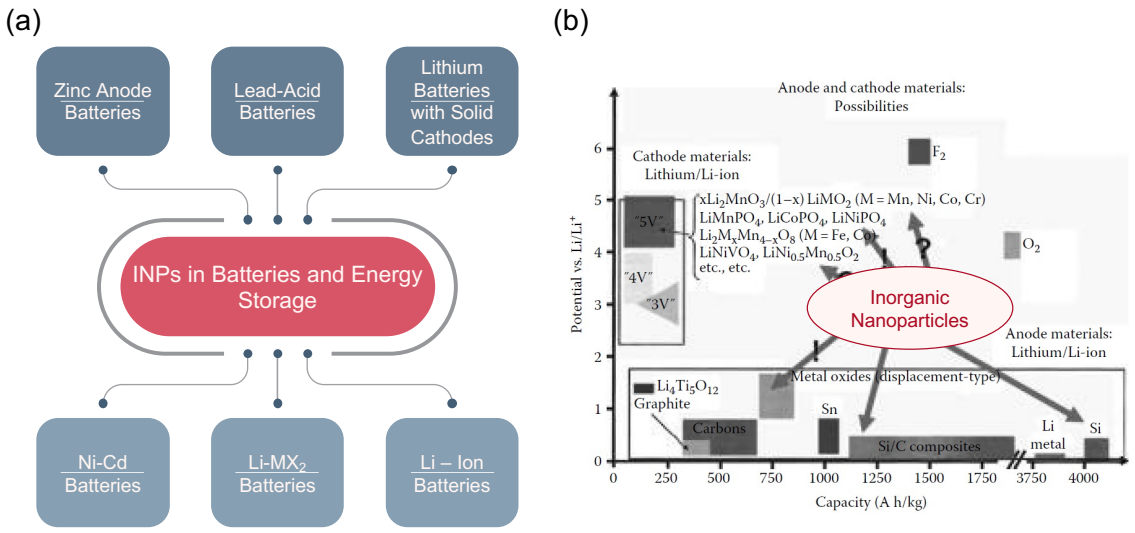

Figure 4. Nanoparticles in batteries and energy storage (a) A schematic review of INPs used in batteries and energy storage (b) Capacity of electrode materials for advanced rechargeable Li batteries. The arrows point to materials that are or could be used as nanoparticles, adapted from Doron and Ortal (2017).

II.1.1.5 Antibacterial Textiles Applications

The substantial specific surface area of nanomaterials and their novel size-dependent physical and chemical characteristics compared to bulk structures are driving interest in their creation and uses in various applications. The deposition of nanoparticles (NPs) on various substrates might increase their possible applications considerably (Figure 5). The possibility of combining the properties of the substrate and the coated NPs layer has piqued interest in coating different types of substrates with metal oxides. There is a considerable emphasis on the fact that one of the materials will determine the surface properties of the composite. At the same time, the other can be responsible for other system properties (e.g., optical, catalytic, magnetic, antibacterial) (Nina et al. 2017).

There is an increasing demand for high-quality fabrics with antibacterial qualities for sanitary clothes, athletic wear, and wound healing. Both synthetic and natural fibers are known to be susceptible to bacteria and harmful fungus. Microorganism control spans from medical facilities to everyday houses. Antibacterial fabrics have seen a considerable increase in manufacturing due to consumer demand (Figure 5). Likewise, the wound-care output is predicted to rise at a breakneck pace (Nina et al. 2017).

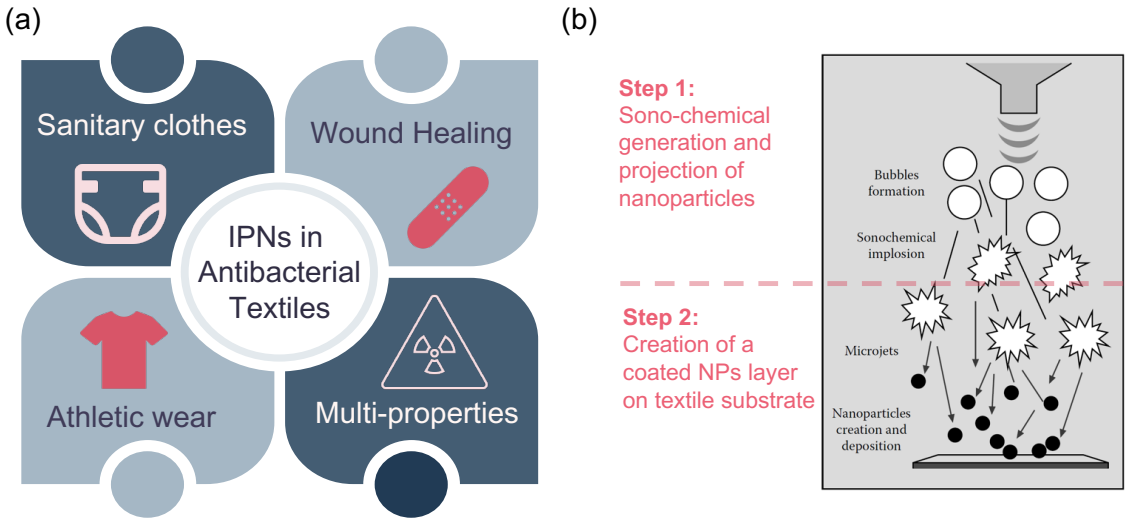

Figure 5. Inorganic nanoparticles in antibacterial textiles. (a) Examples of antibacterial uses of INPs in textiles (b) Illustration of the adhesion of nanoparticles to a given substrate, adapted from Nina et al (2017).

Nanosilver is a common antibacterial ingredient in general fabrics and wound dressings. More emphasis has recently been made on using inorganic metal oxides in textile antibacterial finishes. The Food and Drug Administration (FDA) has determined that several metal oxides, such as TiO_2, ZnO, MgO, and CuO, are harmless to human skin when used in fabrics. Photocatalytic activity, UV absorption, and protoxidizing capacity of nanosized TiO_2, ZnO, and MgO particles are promising against chemical and biological species. Metal oxide NPs have been the subject of

increased study in the previous decade, with an emphasis on the development of antibacterial, self-decontaminating, and UV-blocking textiles (Nina et al. 2017).

II.1.1.6 Environmental Remediation

Although the number of accessible environmental nanotechnologies is rapidly increasing, nanoscale iron particles and their derivatives are the most commonly employed nanomaterials for the rehabilitation of polluted soil in routine commercial applications. Over the last 40 years, the use of iron-based reagents to remove or degrade pollutants or toxicants in industrial waste streams has been extensively researched. Metallic iron, sometimes known as "zero-valent iron" (ZVI), has been used for land restoration since the mid-1990s (Scott 2011).

Previous studies show that iron nanoparticles (INPs) may be utilized to successfully remove or eliminate pollutants from groundwater in both in situ and ex situ approaches. An overview of using nanoparticles in environmental remediation, and a schematic view of using nanoparticles to clean up contaminated sediments are shown in Figure 6. Some INP remediation applications include remediation of chlorinated solvents such as trichloroethylene (TCE), a common groundwater contaminant. TCE exposure has been associated with liver damage, birth abnormalities, and cancer in humans. INPs have been shown in several studies to be exceptionally efficient at rapidly degrading TCE and other chlorinated hydrocarbons via reduction processes. INPs have also been applied to the remediation of uranium since its mining is one of the most well-known forms of heavy metal contamination (Scott 2011).

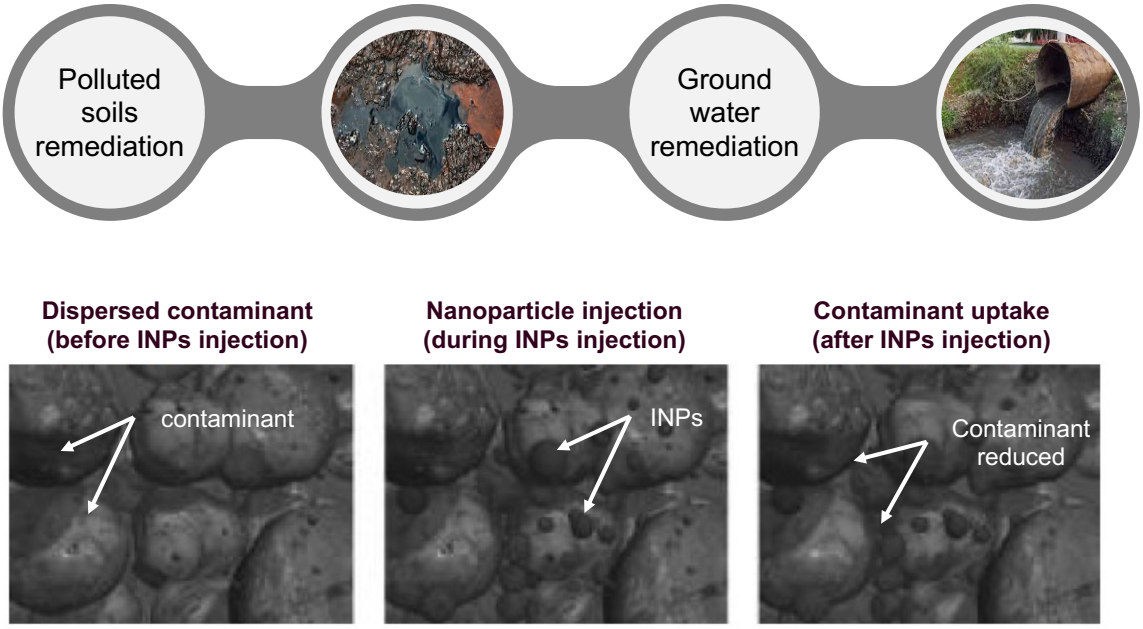

Figure 6. Nanopartciles uses for environrmntal remediation (top) ; schematic of using nanoparticles to clean up contaminated sediments. Particles are injected into the polluted region, where they quickly sequester contaminating species in the groundwater, immobilizing or killing them (bottom); adapted from Scott (2011).

II.1.2 Natural Inorganic Nanoparticles

Natural inorganic nanoparticles (NINPs) can be created by various mechanisms shown in Figure 7. These mechanisms can be classified into three major categories:

- Mechanical processes such as wind erosion and weathering (i.e., mechanical processes mixed with dissolution/precipitation). Inorganic nanoparticles can be generated by desert wind aeolian erosion, deforested fields and un-vegetated farmlands, and can be ejected from events triggered by mechanical grinding of the Earth's crust during earthquakes (Sharma et al. 2015).

- Nucleation and growth processes such as volcanic activity (i.e., fast cooling of fumes and explosions expelling tephra) and cosmic dust. Various inorganic phases nucleate and grow in the atmosphere, hydrosphere (including black smokers and other hydrothermal vents), and lithosphere (melts), due to purely inorganic reactions, or with contributions from organic matter. These processes produce NINPs containing Mn, Cr, Cu, Ba, and Pb (Sharma et al. 2015).
- Thermal processes including bio-assisted thermal reactions (i.e., biological) and biomass combustion. These processes can produce NINPs such as Fe- and Si-based nano-minerals, calcium carbonate, and calcium phosphate (Sharma et al. 2015).

In many circumstances, the production of NINPs is the result of a mixture of all the above-mentioned processes. An example includes a combination of weathering, the production of colloids in rivers, and volcanic activity. In addition, NINPs are mostly produced at phase transitions (e.g., solid–gas–wind erosion, liquid–gas–sea spray evaporation, solid–liquid–rock/mineral weathering, and so on). NINPs are generated in various forms including colloids, aerosols, dust (including cosmic dust), elements of soils and sediments, hydrothermal/chemical deposits (including evaporites), mineral nuclei, reaction rims, and lamellae. These nanoparticles can contain a broad range of elements most commonly as a part of the following chemical groups: metal oxides/hydroxides, metals or alloys, silicates, sulfides, sulfates, halides, and carbonates (Sharma et al. 2015).

Inorganic sulfide (H_2S and HS) is a key element of the worldwide biogeochemical sulfur cycle, which includes hydrothermal vents, mining water, sediments, and wastewater treatment plants (WWTPs). Figure 7(b) depicts the probable creation of noble metal NPs and associated sulfides through direct formation or transition mechanisms.

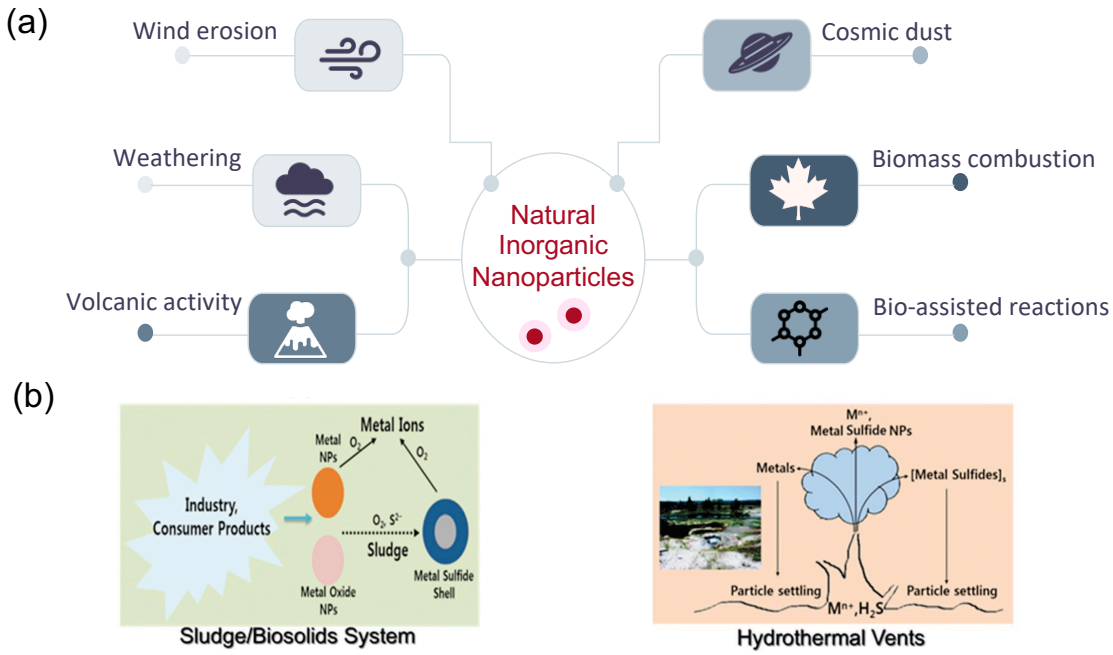

Figure 7. Formation of Natural Nanoparticles. (a) An overview of the natural environmental mechanisms that contribute significantly to the formation of nanoparticles. (b) The potential mechanisms of creating inorganic nanoparticles in the environment in the deep ocean and WWTP. Adapted from Sharma et al (2015).

II.2 Fate of Inorganic Nanoparticles in the Environment

II.2.1 Engineered Inorganic Nanoparticles

The stability of engineered nanoparticles (ENPs) is controlled by saccharides, surfactants, and polymers, which may result in a change in surface properties, transformation and environmental fate (Sharma et al. 2015). The properties of both the environment and the ENPs are crucial in determining how the released ENPs behave. In physicochemical, macromolecular interaction, and physiologically induced processes, the kind and degree of change may be seen.

In physicochemical transformation, the processes of ENP aggregation, stability, dissolution, and deposition are all interconnected. The natural pathways of photochemical reactions triggered by sunlight are important in managing photo transformations. Adsorption of molecules in the surrounding matrix of a natural system exhibiting macromolecular changes is a common occurrence. The aerobic and anaerobic environments can also influence ENP activity by affecting ligand affinity, such as sulfidation under O_2-limiting circumstances (Dwivedi et al. 2015).

The colloidal stability and aggregation of ENPs is explained by Derjaguin–Landau–Verwey–Overbeek (DLVO) theory through the interactions between colloid particles and adhering surfaces (Adamczyk and Weroński 1999). It has been shown that the DLVO explanation of ENP aggregation and stability is affected by the core–shell structure, surface properties (i.e., hydrophobic to hydrophilic coatings), and the degree of transformation (Hotze, Phenrat, and Lowry 2010). The key factors regarding aggregation kinetics and stability include ionic strength effects (e.g., capping agents and preparation methods, cation valence and salt type), and pH effects (Dwivedi et al. 2015).

ENPs can be classified in two types, (1) dissolvable (e.g., Ag, Zn, CuO, ZnO) and (2) non-dissolvable (e.g., graphene, CNTs). The dissolution behaviour of ZnO and CuO determine their toxicity to algae and bacteria. ENPs will last longer in the environment as a result of their dissolution. The metal speciation and its transport in the environment are highly influenced by oxidative and reductive dissolution processes (Stumm 1987). Metal ions tend to participate in redox and complexation processes, based on their rate of dissolution. It has also been shown that the increase of ionic strength will increase the dissolution of nanoparticles. Ultimately, several studies suggest that the dissolution of ENPs in the aquatic environment is a regulatory mechanism for particle/ion partitioning (Dwivedi et al. 2015).

Deposition refers to the process of molecules attaching to a solid surface from a solution, as opposed to detachment and/or dissolution. Surface coatings have been examined for their impact on ENPs mobility in porous media, but their impact on ENPs deposition and environmental fate has received less attention (Wang et al. 2014). The initial surface deposition of ENPs onto polysaccharide-coated surfaces was governed by electrostatic interactions, according to ENP deposition parameters. Furthermore, the distribution and heterogeneity of charges throughout the surface may have a role in ENP deposition, which requires further investigation for a more accurate prediction of ENP attachment to environmental surfaces (Ikuma et al. 2014).

Macromolecular interactions (i.e., interactions of Natural Organic Matter (NOM) and bio-macromolecules) take place in soil and water matrices and have the ability to speed up ENPs transformation in the environment. Several investigations have shown that NOM stabilized ENPs via electrostatic and steric interactions (Fernández-Nieves and de las Nieves 1999; Mylon, Chen, and Elimelech 2004). (Bio)macromolecules can be controlling variables in changes in stability and transformation (King and Jarvie 2012). The current data indicate that the interaction of ENPs with biological matter is an important aspect in their transformation and bioavailability studies (Dwivedi et al. 2015).

Photo transformation is an important mechanism in the regulation of the fate and the behaviour of ENPs. They are connected to reactive transients of various excited states as well as reactive oxygen species (ROS) of source and sink that can influence photoreactions. In addition, the environmental setting of aerobic and anaerobic conditions might have an impact on transformation routes (Dwivedi et al. 2015).

II.2.2 Natural Inorganic Nanoparticles

Several environmental parameters influence the fate (i.e., aggregation and dissolution) of natural inorganic nanoparticles (NINPs), including ionic strength, ionic components, pH, redox conditions, NOM content and nature, and the kind of individual nanoparticles. The potential for NINPs to be altered and transported in the complex environment will be determined by the cumulative influence of these physicochemical parameters (Sharma et al. 2015).

The influence of ionic strength and background electrolytes on the stability of manufactured NINPs has been investigated in a large number of research efforts. It has been shown that the presence of iron species, such as Fe^{3+} ions, has been found to have no effect on NINPs stability. However, the presence of Mg^{2+} and Ca^{2+} has an influence on the stability of NINPs. Furthermore, as NINPs are transported from freshwater to river water and then to seawater, the number of ions increase, and the stabilized NPs may become less stable (Sharma et al. 2015).

Several studies showed that the stability of naturally formed NPs is increased by NOM. The surface composition of NPs, as well as the binding manner of NOM, have an impact on their stability. Whether particles are generated at room temperature (RT) or at a higher temperature, this phenomenon may be observed. The size and shape of the particles also have an impact on their stability. Furthermore, NNPs in the environment may dissolve or ionize, for example, they can readily dissolve in physiological circumstances to generate ionic forms (Sharma et al. 2015).

II.3 Toxicity of Inorganic Nanoparticles

II.3.1 Engineered Inorganic Nanoparticles

The toxicity of engineered nanoparticles can affect ecosystems and creatures from different trophic levels, including bacteria, plants, and multicellular aquatic/terrestrial organisms as shown

in Figure 8. Several studies have been conducted to investigate the genotoxicity, cytotoxicity, and ecotoxicity of engineered AgNPs and AuNPs against a variety of food chain members, including bacteria, plants, aquatic and terrestrial organisms, as well as the toxicity of engineered AgNPs to marine organisms and algae (Sharma et al. 2015). It has been found that the toxicity of NPs is influenced by their surface chemistry, charge, and organic coating.

Bacteria are essential components of the food chain and perform important environmental activities. They are common ecosystem components who play an important role in global nutrient cycle. Because of its ecological importance, as well as the relative simplicity of culture, bacteria have been a key focus of eco-nanotoxicity research to date, including the use of a diverse variety of model organisms and toxicity tests to assess the effects of nanoparticles. While there is a considerable amount of data indicating nanoparticles are absorbed by a variety of mammalian cells, the absorption of nanomaterials by bacterial cells is yet unknown. There have been few systematic studies that have measured the rates and internal locations of nanoparticles in bacteria (Maurer-Jones et al. 2013).

Plants are particularly significant in eco-nanotoxicity concerns because to their interaction with air, soil, and water, all of which may include manufactured nanoparticles. Furthermore, because plants are fed by lower trophic level creatures, animals, and humans, they provide a large potential to enable nanoparticle transmission among many species in the food chain. Because many plant species have vast surface area leaf and root systems, they have plenty of opportunities to interact with nanoparticles. Several studies investigated the exposure of plant seeds to various nanoparticle solutions and then monitoring germination and root extension from the seed. They showed that the nanoparticles themselves (rather than the ions created during nanoparticle

dissolution) have an influence on the initial stages of plant growth, and that differences in nanoparticles effects exist (Maurer-Jones et al. 2013).

The paths of nanomaterial exposure to live creatures are determined by the organism's environment. As previously discussed, entrance through the roots is a major concern for plant uptake. Nanoparticles that are present in the aqueous or soil phases give a way for entrance into the animal (gills, mouth, to the stomach) that might be substantially influenced by the characteristics of the nanoparticle surface for fish in water or worms in soil. The noble metals are also becoming an increasing area of research on possible fish contamination, possibly as a result of increased market awareness of "antimicrobial nano-silver" products (Maurer-Jones et al. 2013).

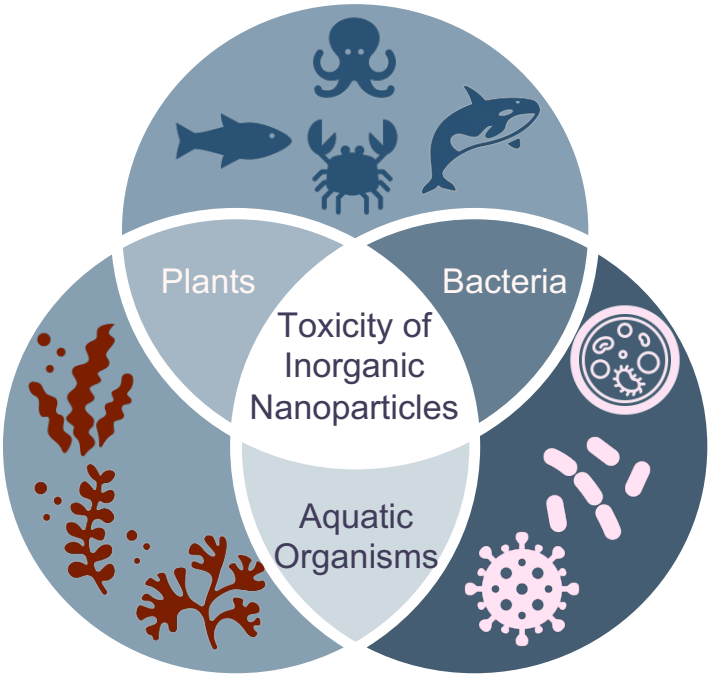

Figure 8. Schematic view of toxicity of engineered nanoparticles in the environment.

II.3.2 Natural Inorganic Nanoparticles

Few investigations on the toxic consequences of NNPs (e.g., natural Ag and Au) have been carried, due to their low concentrations. Recent research investigated the toxicity of natural Ag-based NPs by measuring the minimum inhibitory concentrations (MIC) of particles generated from the reduction of Ag+ by organic matter against Gram-positive (GP) and Gram-negative (GN) bacteria (Adegboyega et al. 2014). More crucially, natural noble metal NPs showed lower MIC values than ENPs, implying that natural noble metal NPs were less harmful than man-made nanoparticles. For GP species, the difference in toxicity between ENPs and natural AgNPs was substantially greater than for GN species. The organic coating produced in the natural environment appears to build complex structures, which may be responsible for the decreased toxicity. Another theory is that natural organic materials are less hazardous by nature than the polymers and surfactants employed in ENP manufacturing or post-processing treatment. The variations in toxicity of NNPs and ENPs might potentially be attributed to the surface coating compounds used to cover them (Sharma et al. 2015).

The presence of natural organic matter functional groups encasing naturally generated noble metal NPs would have a significant impact on their toxicity. The interaction of these NPs with aquatic creatures is poorly understood. Significantly, depending on the functioning of the organic matter and the formation of reactive oxygen species, these NPs may have varied toxicity (Sharma et al. 2015).

Having a better understanding of the sources, fate and toxicity of various engineered and natural inorganic nanoparticles, is essential to understand the presence of INPs in wastewater. Next, we will introduce the methodology used in this research to monitor and quantify INPs in wastewater, as an important step to evaluate their potential implications and risks on the environment.

III. MATERIALS AND METHODS

The materials and methods section includes methodology for sample collection (section III.1), sample preparation (section III.2), overall analysis methodology using Inductively Coupled Plasma Mass Spectrometer (ICP-MS) (section III.3), and other analytical methods used for nanoparticles characterization including SEM (section III.4), DLS (section III.5) and AFM (section III.6). These methods were used to validate and confirm the occurrence of the INPs detected by spICP-MS.

I.1 Sample collection

I.1.1 Sample collection for Phase I: UB WWTP

Wastewater samples were collected at monthly intervals over a twelve-month sampling duration from the influent stream to the UB wastewater treatment facility serving approximately 250,000 people in the Northeast U.S. Samples from the effluent were also obtained. The treatment facility treats an average daily flow rate of about 30 million gallons per day (MGD), influent Carbonaceous Biochemical Oxygen Demand (CBOD) averaging approximately 150 mg/L, and influent Total suspended solids (TSS) averaging around 160 TSS. The UB treatment facility utilizes screening, grit removal, primary clarification, activated sludge, chlorine disinfection, and dechlorination prior to discharge. See the detailed treatment flow diagram in Appendix C.3. One-liter wastewater samples were collected and stored in capped, high-density polyethylene containers at 4°C until analysis was performed within three days of sampling.

I.1.2 Sample collection for Phase II: AC, SB, UB, and DI WWTPs

Wastewater samples were collected from four WWTPs in Massachusetts: AC, SB, UB, and DI. Descriptions regarding these WWTPs are shown in Table 2. For each WWTP, one-liter samples were collected from both influent and effluent wastewater. Afterward, wastewater samples were stored in polyethylene containers at 4°C. Then, analysis was performed within three days of sampling.

The AC WWTP treats an average daily flow rate of about 0.5 million MGD. Raw wastewater from the nearby domestic community is pumped to the treatment facility and it is first strained and aerated. The AC treatment facility then utilizes coagulation, flocculation, equalization, membrane filtration, disinfection, and fluoridation prior to discharge. See the detailed treatment flow diagram in Appendix C.1.

The SB WWTP treats an average daily flow rate of about 5 MGD. The influent wastewater consists of both domestic and industrial sources from the surrounding areas. The SB treatment facility utilizes screening, grit removal, primary clarification, activated bio-filter, chlorine disinfection, and dechlorination prior to discharge. See the detailed treatment flow diagram in Appendix C.2.

The DI WWTP treats an average daily flow rate of about 360 MGD. The facility eliminates human, domestic, commercial, and industrial contaminants from wastewater that originates in homes and companies in 43 towns around the greater Boston area. The DI treatment facility utilizes screening, grit removal, primary clarification, activated sludge, chlorine disinfection, and dechlorination prior to discharge which are similar to the processes used by UB and SB WWTPs. See the detailed treatment flow diagram in Appendix C.4.

The major differences among these four WWTPs are the design flow rates and the wastewater sources, which include industrial and domestic sources (Table 2). The sizes of WWTPs with mixed sources (SB, UB, and DI) are three orders of magnitude larger than the purely domestic AC WWTP. These comparisons will help us to determine both the effect of the size and sources of WWTPs on the presence of INPs.

Table 2 Information about AC, SB, UB, and DI wastewater treatment plants.

WWTP	Design flow rate (mgd)	Wastewater type
AC	0.05	domestic
SB	5	domestic + industrial
UB	30	domestic + industrial
DI	360	domestic + industrial

I.2 Sample preparation

I.2.1 Removal of dissolved constituents from the samples with dialysis

The procedure used to remove the dissolved inorganic and organic constituents from the wastewater samples with dialysis was adapted from Choi *et al.* (2017) and Choi *et al*. (2018). Samples were transferred to 24 mm diameter, 1 kDa molecular weight cut off dialysis tubes (Spectrum Chemical Manufacturing Corporation, 25 cm in length), sealed on both ends by plastic clips, and immersed in purified water in a 2 L conical glass flask subjected to constant stirring for 72 hours. The ionic strength was continuously monitored with a conductivity meter (Model 150,

Orion Thermo Scientific). Results showed substantial removal of the dissolved constituents over time as the conductivity dropped from 45-50 to 1.4-1.8 μS/cm after 72 h with the purified rinse water changed every 24 hours. Purified water was produced with a Thermo Scientific Barnstead Nanopure Life Science UV/UF system (Waltham MA, USA).

I.2.2 Further removal of organics from the samples

To further remove dissolved organic material from the samples subsequent to dialysis, the deionized samples were transferred from the dialysis tubes to 150 mL glass beakers. Ten mL of hydrogen peroxide, H_2O_2 (30%, Macron Fine Chemicals), was added to each beaker, and the beakers were held at 100°C for 2 h on a hot plate. This technique was adapted from Choi *et al.* (2017). To evaluate the possible particle size changes due to the redox conditions of H_2O_2, standard Au nanoparticles of known size were subjected to the same method above. The detected size of Au nanoparticles was within the manufacturing range.

I.2.3 Removal of coarse particles from the samples

The prepared samples were subjected to ultrasonication at an intensity of 24 W for 10 minutes (Marshall Scientific, Model 1510R-MT). The samples were transferred to 50 mL polypropylene tubes (VWR North American) after sonication, and centrifuged (Eppendorf, Model 5804) for the separation of coarse particles from the samples. The centrifugation process was conducted at a speed of 1000 g (2794 rpm) for 3 min, which was adequate to separate particles at sizes larger than 200 nm when composed of metallic oxides with a density in the range of 2.6–3.0 g/cm^3 (Choi et al. 2017).

I.2.4 Filtration of samples

The samples were then transferred to 50 mL polypropylene tubes (VWR North American) using syringes equipped with 0.45 μm filters (polyvinylidene fluoride, Fisher Scientific). The filtered samples were subjected to subsequent analysis as described below. Filtration is an essential step in all ICP-MS analysis to protect the equipment from clogging by large particles.

I.3 Inductively Coupled Plasma Mass Spectrometer (ICP-MS) analysis

ICP-MS analysis was conducted with a PerkinElmer NexION 300x Inductively Coupled Plasma Mass Spectrometer. A schematic showing the two modes of ICP-MS analysis, conventional ICP-MS and single-particle ICP-MS, employed in this research is illustrated in Figure 9.

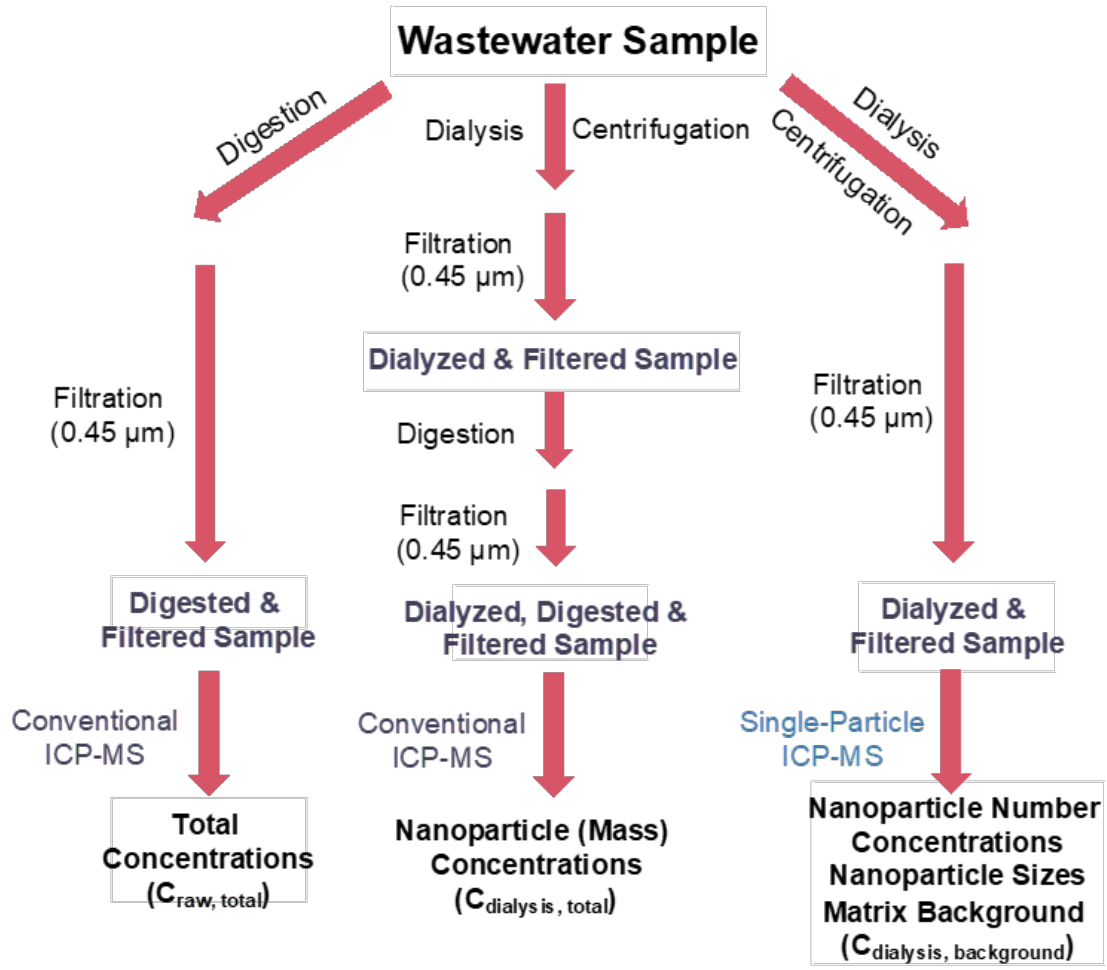

Figure 9. Schematic of the characterization approach for the inorganic nanoparticles by conventional and spICP-MS.

Conventional ICP-MS analysis is typically designed for samples that contain dissolved metals or inorganic elements. In this mode, constant streams of charged ions are generated in plasma, resulting in a constant concentration signal in the instrument. However, single-particle ICP-MS analysis is intended for samples with metal or inorganic nanoparticles. In single-particle mode, pulses of charged ions are created in plasma instead of a continuous flow of charged ions (as in conventional mode), providing spikes of signal that can be converted to nanoparticle size and concentration.

I.3.1 Conventional ICP-MS analysis

50 mL of filtered samples and 50 mL of raw wastewater samples were digested in nitric acid (HNO_3) solution (67-70% purity, Fisher Scientific) and heated with a hot plate. After heating, samples were cooled to room temperature and diluted with purified water to 50 mL. The acid-digested wastewater samples were filtered with 0.45 μm syringe filters prior to analysis.

I.3.2 Single Particle ICP-MS analysis

Based on the ionic standard for each element, nanoparticle calibration curves were generated and used for converting the intensities of single-particle events to the equivalent mass of each element. Particle number concentrations in the single-particle mode were determined from the number of "events" (detected particles) and the transport efficiency in the ICP. The determination of the transport efficiency of the ICP-MS included the use of an aqueous suspension containing 60 nm diameter Au nanoparticles. Particle diameters in the samples were determined from the known density of each type of nanoparticle, the mass fraction of each element, and its anticipated form. Ionic standards were obtained from ICP-MS multi-element standard solutions (Instrument Calibration Standard, 100 μg/mL, PerkinElmer).

I.4 Scanning Electron Microscopy (SEM) analysis

Scanning Electron Microscopy (SEM) can be used to characterize particles from 50 nm to 1cm. It can also offer information about the element's composition using EDS. The prepared nanoparticle samples were filtered with 0.015 μm Nuclepore membranes (GE Healthcare Whatman™, polycarbonate hydrophilic membranes) to isolate the nanoparticles for SEM analysis. After filtration of the samples, the nanoparticle-loaded membranes were freeze-dried for 72 hours,

followed by resuspension with ethanol (90.5%, Fisher Scientific) in an ultrasonic bath for 2 hr. Subsequently, the nanoparticles in ethanol solution were deposited drop-wise onto SEM stubs, dried, and coated with Pt/Au prior to SEM imaging with a JSM-7000F SEM (JEOL Ltd.).

I.5 Dynamic Light Scattering (DLS) characterization

Dynamic Light Scattering (DLS) relies on Brownian motion of particles in a liquid medium to determine particle size in the range of 50nm to 1 micron. The prepared samples were subjected to an ultrasonic bath for 15 minutes in order to disaggregate the nanoparticles. The samples were then transferred to 12 mm glass cells (Malvern Panalytical Inc, PCS1115) followed by dynamic light scattering measurements conducted with a Zetasizer Nano ZS (Malvern, Model ZEN3600) instrument.

I.6 Atomic Force Microscopy (AFM) analysis

Atomic Force Microscopy (AFM) is used for characterizing particles from 0.1 nm to 10 micrometers. It offers information on many physical properties including size, morphology, surface texture and roughness. Fifty μL volume samples were loaded on a glass slide using a pipette (Thermo Scientific, Catalog No. 14-386-318) and allowed to air dry. AFM images were acquired over a 5 μm scan range at a fast scan speed in phase-contrast mode. All images were obtained using a Nanosurf Company AFM (NaioAFM) and were analyzed using Gwyddion software. A stiff cantilever (MIKROMASCH USA, Model NSC16/Cr-Au) and phase-contrast mode were chosen to avoid the possible dragging of nanoparticles by the cantilever tip.

An additional round of AFM analysis was conducted with concentrated samples. The samples were concentrated by evaporating approximately 95% of the water using a hot plate at

110°C. 50 µL of the concentrated samples were loaded on slides and allowed to dry. Images were obtained with a scan range of 1 µm at a fast scan speed in phase-contrast mode.

Next, the outcomes of using all the above methods to quantify INPs in samples from different WWTPs in MA are discussed: (1) in phase I, where we focused on UB WWTP for influent and effluent sample collection in a monthly time interval, and analysis using sp-ICP-MS and other analytical methods; (2) in phase II, where we performed sample collection from four different WWTPs AC, SB, UB and DI followed by spICP-MS analysis and statistical analysis.

IV. RESULTS AND DISCUSSION PHASE I

The results and discussion phase I section includes results of nanoparticles analysis using ICP-MS in UB WWTP (section IV.1), SEM results (section IV.2), AFM results (section IV.3), DLS results (section IV.4), a discussion on the potential for nanoparticle release to the environment (section IV.5), and limitations of spICP-MS on detecting nanoparticles composed of multiple elements (section IV.6).

IV.1 Nanoparticles Analysis using ICP-MS

IV.1.1 Identification and concentration of inorganic nanoparticles in the wastewater samples

After sample preparation (described above), the targeted fourteen different types of inorganic nanoparticles (i.e., Mg, Al, Ti, Mn, Fe, Cu, Zn, Sr, Zr, Mo, Ag, Sn, Ba, Pb) were identified through single-particle ICP-MS analysis of the wastewater samples. Figure 10 shows the average particle number concentrations using single-particle ICP-MS analysis over the 12-month sampling duration. These results indicated that the techniques developed in this study successfully identified multiple types of inorganic nanoparticles in the wastewater samples. In addition, many different

types of inorganic nanoparticles were present at concentrations over 10^6 particles/mL, based on their elemental composition.

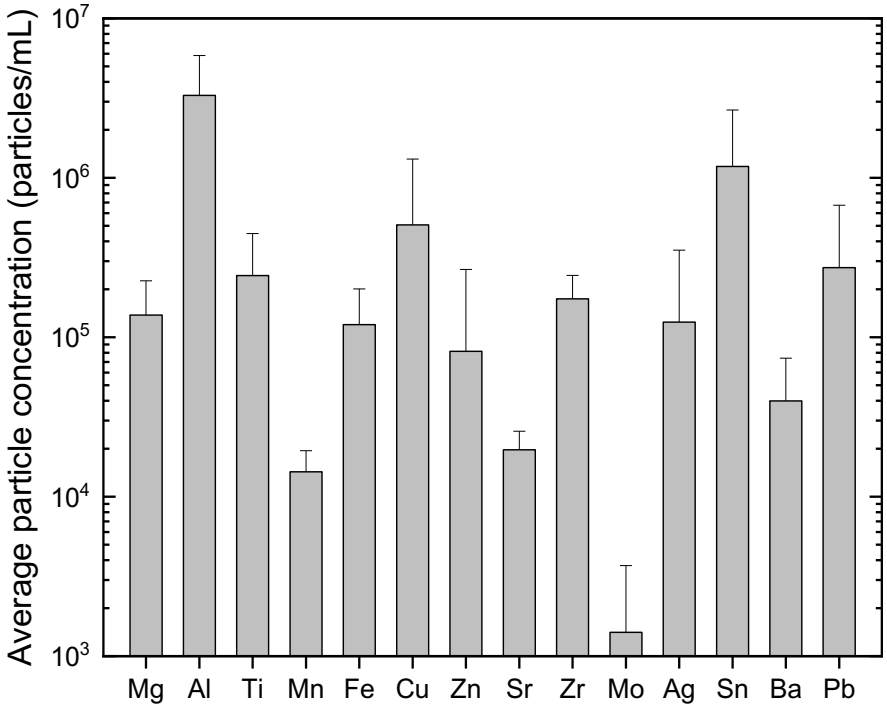

Figure 10. Average nanoparticle concentrations in wastewater samples from UB WWTP over a 12-month sampling period. Error bars show standard deviation.

The presence of different types of nanoparticles in community wastewater with multiple wastewater sources, domestic and industrial, should be expected, as various nanoparticles are used in many industrial and consumer applications and materials (see Table 3). The detection of many different nanoparticle types in the analyzed samples is anticipated due to the multitude of nanoparticle applications in communities. In particular, for the studied UB WWTP samples, the

detection of all nanoparticles identified here should be expected as many of the sources listed in Table 3 are present in this municipality.

Table 3 A summary of industrial and consumer uses of various nanoparticles.

Nanoparticles	Industrial and consumer uses	References
$BaSO_4$	Fillers in coatings (e.g., in motor vehicles) Orthopedic medicine Diagnostic imaging	*Gomoll et al*., 2008 *Mohn et al*., 2010 *Villalobos-Hernández and Müller-Goymann*, 2005
TiO_2	Ultraviolet protective cosmetics Self-cleaning coated glass Construction and building materials Biomedical applications Toothpastes Photocatalysts	*Egerton and Tooley*, 2012 *Faure et al*., 2013 *F. Li et al*., 2013 *Shandilya et al*., 2015 *Fei Yin et al*., 2013 *Rompelberg et al*., 2016 *Chowdhury et al*., 2017
MoO_x	Electronics, catalysis, sensors, energy-storage units, field emission devices, lubricants, superconductors, thermal materials, biosystems, chromogenic and electrochromic systems.	*de Castro et al.*, 2017
ZrO_2	Abrasives Piezoelectric, electro-optic, and dielectric material Catalysts	*Heuer*, 1987 *Somiya*, 1988 *Yamaguchi*, 1994
$SrCO_3$	Ceramics, paints, dryers, pigments, fireworks Nanocarriers for drug delivery	*Shi and Du*, 2007 *Qian et al*., 2012
Cr	Catalysts and pigments	*Bvrith and Reddy*, 2013

Over the 12-month testing duration, the particle concentrations for some nanoparticle types varied over large concentration ranges (over an order of magnitude) dependent on the nanoparticle type, ranging from 32 particles/mL (Mo in December) to 8.2 x10^6 particles/mL (Al in May) (data not shown). The concentration of Al-based NPs was the highest in influent sample of UB wastewater and Mo nanoparticles was the lowest. Aluminum nanoparticles are used usually in household appliances, the manufacture of cans for beverage, medicines, and as a base for making pigments and cosmetic. Also, the largest consumers of Al include the fields of transportation and construction as well as production of electrical equipment.

The concentrations of titanium and zirconium nanoparticles in wastewater samples from UB WWTP over the 12-month sampling period are shown in Figure 11. The significant variation in concentration for these two nanoparticle types with time can be seen in these data. Titanium concentrations range over almost two orders of magnitude, while zirconium ranges in concentration from ~10^5 to 3×10^5 particles/mL. Note that there are many uses for these nanoparticles; for titanium, this includes cosmetics, glass coatings, building materials, biomedical applications, toothpaste, and photocatalysts; and zirconium uses include abrasives, piezoelectrics, dielectrics, and catalysts (See Table 3). In addition, the samples collected at different months exhibited similar particles concentration with high values in June, Sep for Ti, perhaps due to an industrial source (e.g., paint, polishers, semiconductor wastes) discharged into the sewers during these months. For example, TiO_2 is extensively used in consumer products, including paints, paper, plastics, sunscreens, and even food

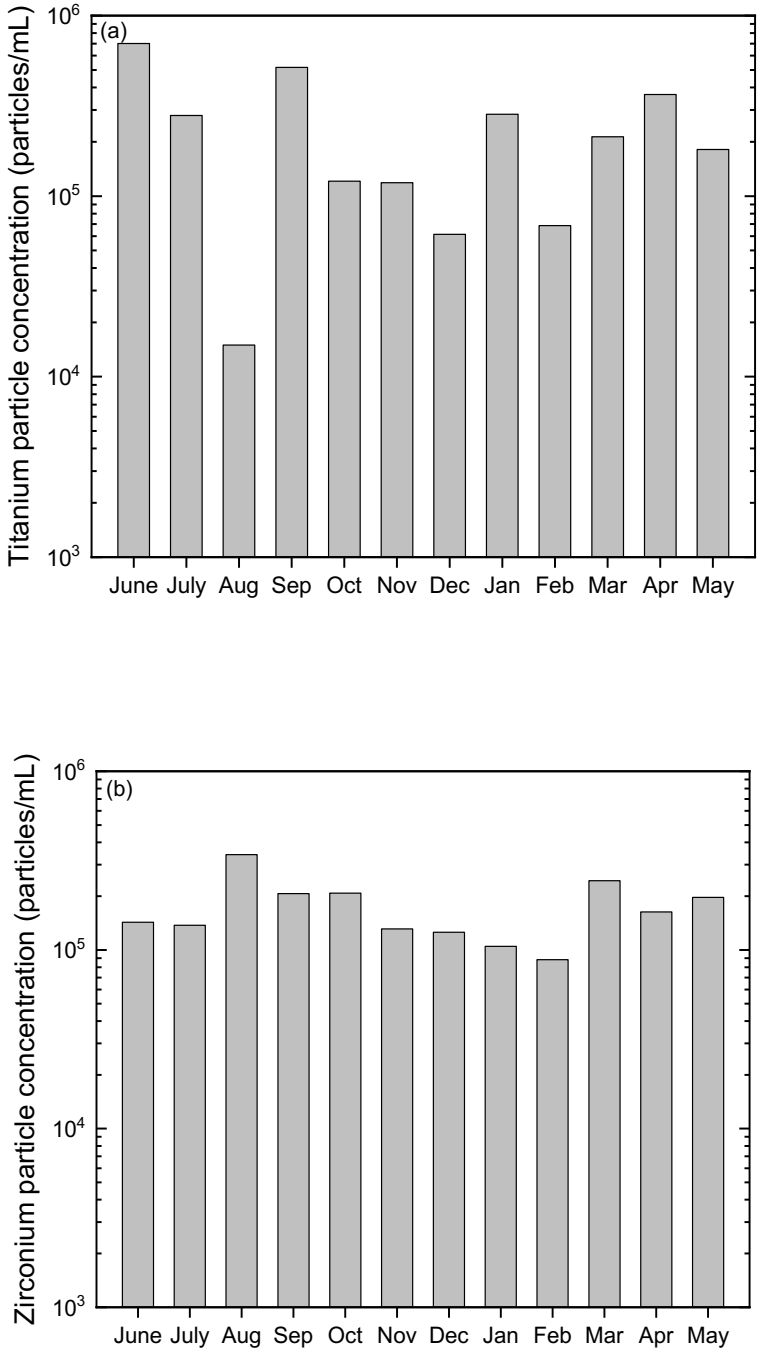

Figure 11. Variation in concentration of titanium and zirconium nanoparticles in wastewater samples collected every month from UB WWTP over a 12-month sampling period. (a) Concentration of titanium nanoparticles. (b) Concentration of zirconium nanoparticles.

The concentrations of nanoparticles in the influent wastewater samples found from our research were comparable with the data published by Huang *et al.* (2021). For example, Ti nanoparticles detected in the wastewater samples studied here ranged in concentration from 10^4 to 10^6 particles/mL. By assuming a spherical shape and estimating density, a concentration range from 60 to 6500 ng/L was calculated; whereas Huang *et al.* found approximately 2000 ng/L Ti in their samples. Possible reasons for the variations include differing degrees of agglomeration, sample pretreatment methods, and sampling periods (i.e., the samples in this work were taken over a 12-month period). And indeed, different sources of wastewater must be considered as a reason for variations in sizes and concentrations from location to location.

IV.1.2 Most frequent sizes of nanoparticles in the wastewater samples

Figure 12 shows the most frequent size distributions of detected nanoparticles in the studied wastewater samples, averaged over the 12-month sampling duration. The most frequent sizes of detected inorganic nanoparticles in these samples varied from 16 nm (Pb) to 139 nm (Ti). The most frequent size found for Ti in these samples differed from that found by Huang *et al.* , who measured a Ti nanoparticle size of around 255 nm, whereas 139 nm was found in this work.

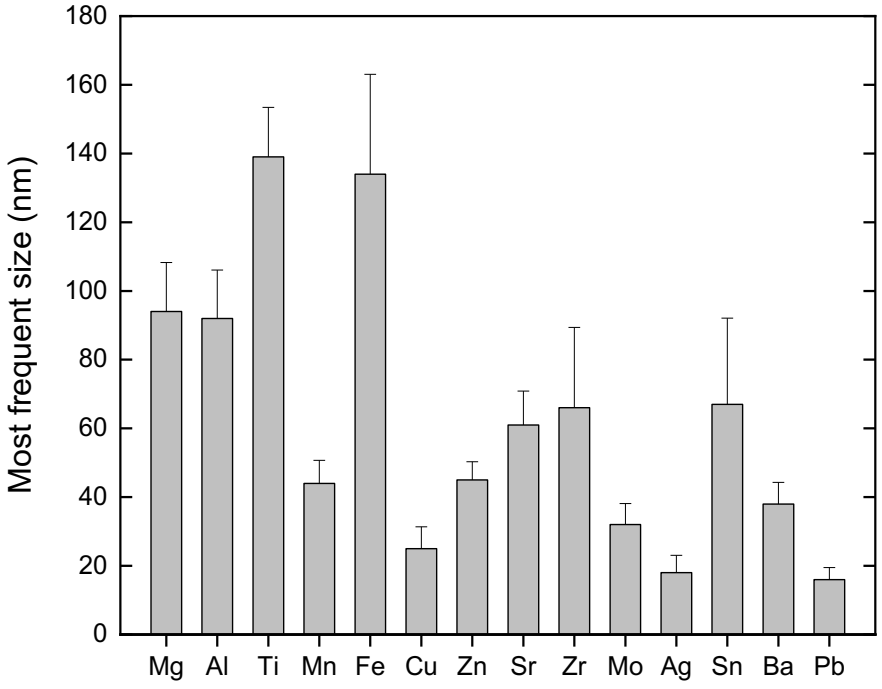

Figure 12. Most frequent sizes of nanoparticles detected in wastewater samples averaged over a 12-month sampling period. Error bars indicate standard deviations.

IV.1.3 Effectiveness of the sample preparatory techniques for removing dissolved (background) constituents in the samples

With a high dissolved ion concentration background in the samples, the corresponding signal of dissolved ions in the ICP-MS analysis overlaps that of the nanoparticles and may lead to erroneous discrimination between the forms (dissolved versus nano-particulate) (Hadioui, Peyrot, and Wilkinson 2014). Based on the total mass concentration results of the raw wastewater samples, five elements with high total dissolved mass concentrations (Mg, Mn, Sr, Mo, and Zn) were selected for further evaluation of preparatory procedures used in this research. The effectiveness of the sample preparatory techniques in removing dissolved background concentrations that

interfere with the single-particle analysis can be quantified by the dissolved mass removal efficiency (θ_d) as expressed in Equation 1.

$$\theta_d = 1 - \frac{C_{dialysis,background}}{C_{raw,dissolved}} \quad (1)$$

$$C_{raw,dissolved} = C_{raw,total} - \left(C_{dialysis,total} - C_{dialysis,background}\right) \quad (2)$$

Where $C_{dialysis,background}$ is the background concentration, as prepared with this methodology, reported by the sp-ICP-MS analysis, and $C_{raw,dissolved}$ is a measure of the dissolved concentration in the raw samples, calculated using Equation 2.

As shown in Figure 13, the analytical method developed in our study achieved greater than 90% removal efficiencies for Mg, Mn, and Sn for all samples. Zn and Mo showed somewhat lower removal efficiencies than for Mg, Mn, and Sn. Removing dissolved background by our preparatory method results in a more accurate measurement of INP concentration and sizes even in the presence of high content of organic matter in the influent.

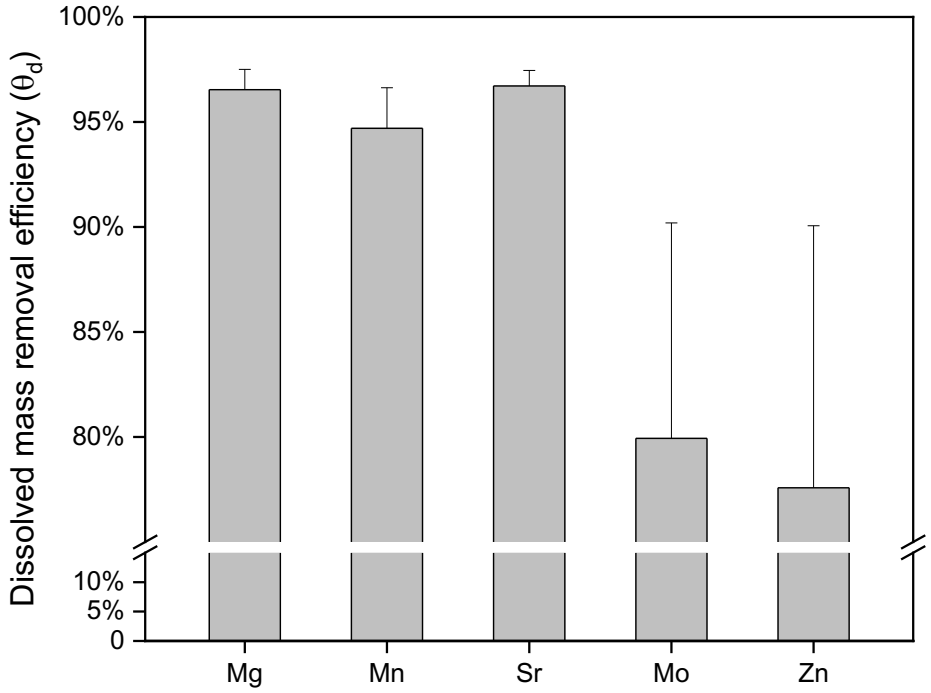

Figure 13. Removal of background dissolved constituents using sample preparatory techniques as quantified by dissolved mass removal efficiency for Mg, Mn, Sr, Mo, Zn. Error bars indicate standard deviations.

IV.2 Scanning Electron Microscopy (SEM) results

Scanning Electron Microscopy (SEM) images of the nanoparticles prepared from the wastewater samples are shown in Figure 14. From these images, individual particle sizes were estimated and ranged from approximately 50 nm to 200 nm in the samples, somewhat larger than the size ranges found with ICP-MS. As the techniques used to prepare the samples for SEM

included drying, it is possible that the drying step promoted some degree of agglomeration, as found by others (Polesel et al. 2018; Smeraldi et al. 2017).

SEM and EDS results revealed that elemental O, Fe, Al, Ti, Mo, Ba, Mg, Zn, and Si were frequently present as elements in the particles (Figure 14c). It should be noted that size information determined from SEM analysis does not differentiate between the different elemental forms of nanoparticles as ICP-MS does. Also, agglomerates of particles greater than 1 μm in size were detected (Figure 14(a-b). Elemental O and Si were frequently detected in association with Fe, Al, Mg, and Zn in the samples (Figure 14(c)), indicating a possibility that metallic oxide particles were associated with SiO_2 nanoparticles in wastewater. Ti, Mo, and Ba showed both elemental and oxidized forms of particles (Figure 14(c)). Elemental Au and Pd were also detected, but because the coating materials used in SEM sample preparation contained Au and Pd, it is unclear if these elements were initially present in the samples. Other elements that were found in the ICP-MS analysis were not detected with SEM/EDS, possibly because of low concentrations (Polesel et al. 2018).

The SEM results demonstrated that the nanoparticles agglomerated in aggregates of sizes from approximately ~ 1-3 μm. In addition, the EDS elemental analysis confirmed that these aggregates of nanoparticles are based on Al, Ti, Mg, Fe, Zn, Ba, Sn and Mo, which is in good agreement with the elements detected with spICP-MS analysis.

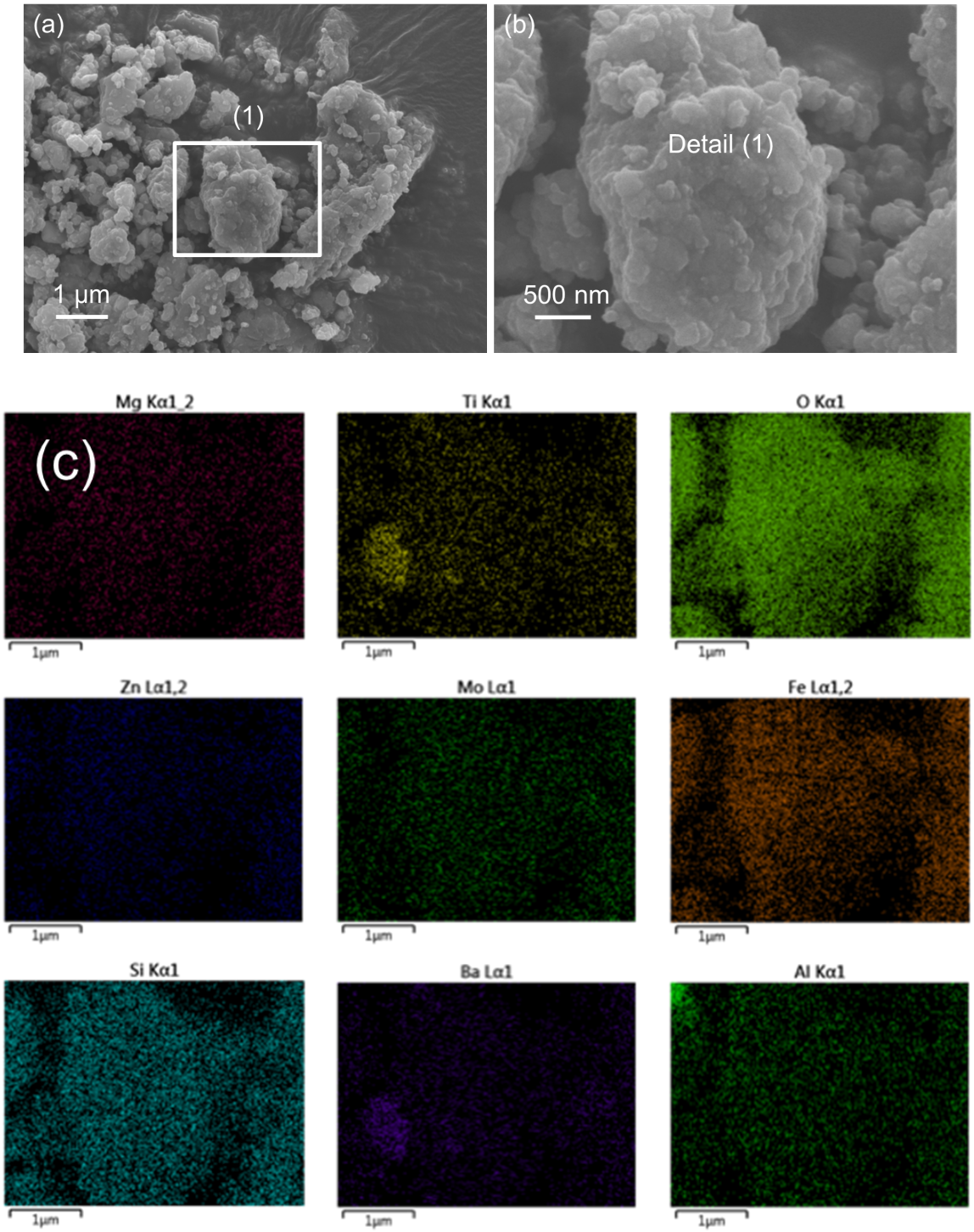

Figure 14. SEM images and elemental analysis (EDS) of inorganic nanoparticles in the wastewater samples. (a) 10,000 magnification, (b) 30,000 magnification, (c) Elements O, Fe, Al, Ti, Mo, Ba, Mg, Zn, Si analyzed by EDS.

IV.3 Dynamic Light Scattering (DLS) results

The average size of the nanoparticles, as well as the size range, was determined by DLS, and found to be 261 ± 22 nm. The average sizes found from DLS analysis were observed to be significantly larger than indicated by ICP-MS and SEM. And, similar to SEM size analysis, DLS does not differentiate between nanoparticles of different compositions as ICP-MS does. Since the size difference between the upper and lower limit of the NP size distribution in ICP-MS is 9:1, it was expected that the DLS would be unable to confirm the size of all the nanoparticles accurately. Previous research has shown that particle mixtures with a size difference greater than 2:1, result in statistical data that not representative of the mixture. The large 260 nm value could be due to agglomeration or impurities (Hoo et al. 2008). The sizes of the different nanoparticle types may be considered necessary in fate and transport studies, and spICP-MS can provide that information in actual samples such as wastewater.

IV.4 Atomic Force Microscopy (AFM) results

Figure 15 shows the AFM image obtained from the influent wastewater sample. Detected particle sizes ranged from approximately 50 nm to 200 nm. This result suggests that the sizes of INPs are closer to the upper limit obtained values with ICP-MS analysis. The larger sizes found with AFM analysis compared to the results from ICP-MS and SEM could be attributed to aggregation and agglomeration of the nanoparticles during the sample preparation, including drying. The possible presence of SiO_2 nanoparticles could also be playing an important role in the size increase, as discussed in the DLS results.

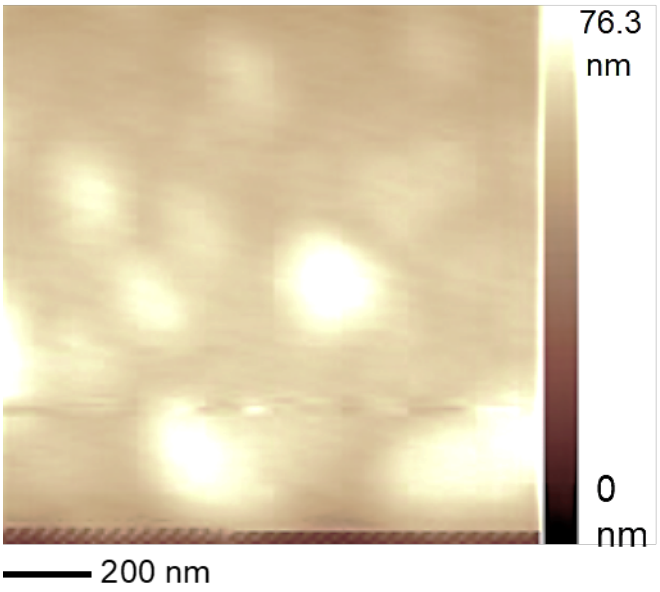

Figure 15. Z-axis forward image of concentrated wastewater samples with a scan range of 1 µm at a fast scan speed in phase-contrast mode. Height range of approximately 76 nm. The dark strip at the bottom does not represent the nanoparticles.

IV.5 Potential for nanoparticle release to the environment

The results show the presence of a significant amount of many different types of inorganic nanoparticles in community wastewaters. While wastewater may be directly discharged to a receiving water source in some locations, it should be expected that many communities would subject their wastewater to treatment to certain standards before discharge, through the utilization of specific treatment process levels (e.g., primary, secondary, tertiary). The many processes in a wastewater treatment facility can impose significant water quality changes. Yet sampling of effluent from a wastewater treatment facility with conventional processes shows that a significant inorganic nanoparticle mass remains in the effluent; data is shown in Figure 16 (nanoparticle sizes range from 20 nm to 120 nm). Future work needs to address the potential release of this material from wastewater treatment facilities in water discharge and the potential impact on the receiving

water sources. Nanoparticulate material may also be an unanticipated source of contamination in water directed for reuse applications and biosolids utilized in land applications.

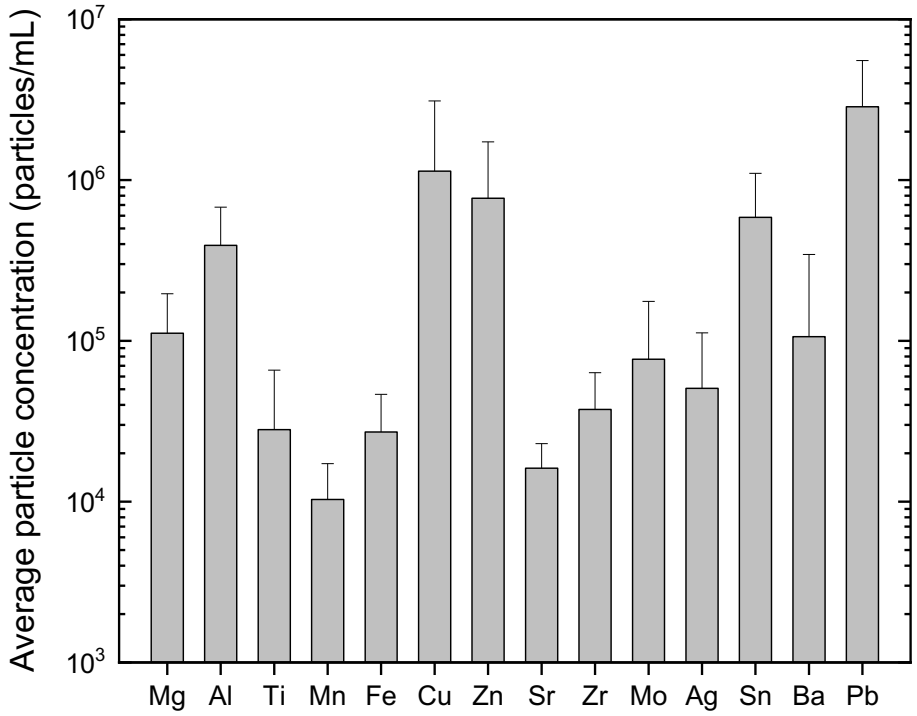

Figure 16. Average nanoparticle concentrations in effluent from a wastewater treatment facility over a 12-month sampling duration. Error bars show standard deviation.

IV.6 Limitations of spICP-MS on detecting nanoparticles composed of multiple metal elements

In spICP-MS, only one nanoparticle will enter the Inductively Coupled Plasma (ICP) at a time. When a nanoparticle enters the plasma, it is vaporized, atomized, and ionized, resulting in a cloud of elemental ions. The generated ions produced by the ICP are directed toward the mass analyzer. This cloud of elemental ions will produce an extremely rapid transient signal (i.e., signal spike) with a total duration of a fraction of a millisecond. The mass analyzer must be able to do a quick measurement to identify these ions. However, the mass spectrometer/analyzer used in our ICP-MS (i.e., quadrupole) can only capture one or two elements (oxide particles) from this transient signal. The mass spectrometer will not be able to capture all the metal elements within this nanoparticle even if a nanoparticle contains more than one metal element.

Our study uses spICP-MS to analyze nanoparticles in wastewater samples, assuming that these nanoparticles are mostly engineered and contain only a single metal element or oxide-particles. A recent study showed that this assumption is valid when spICP-MS is used to analyze engineered nanoparticles in wastewater samples, even though other nanoparticles (i.e., natural INPs) may contain more than one metal element (Cervantes-Avilés and Keller 2021). This assumption applies to our study since we focused mainly on engineered nanoparticles (ENPs) that come from industrial and domestic wastewater sources. ENPs usually contain a single metal element versus natural nanoparticles, which often contain multiple elements. (Azimzada et al. 2020).

To sum up, a reliable analysis of more than one metal element in a single particle is not practical for the current spICP-MS, especially if the samples contain multiple elements (e.g. wastewater samples) measured in a single run. But it may be feasible for samples containing only two metal elements (e.g., Au-Ag Core−Shell Nanoparticles sample) (Merrifield, Stephan, and Lead 2017). In this case, it is necessary to run the sample twice, once for each target metal element, to detect both accurately. In addition, time-of-flight (TOF) mass spectrometry can possibly address this challenge by allowing detection of multiple metal elements per nanoparticle in a single measurement (Naasz et al. 2018).

In the next section, the outcomes of phase II are discussed. In phase II, samples were collected from four different WWTPs AC, SB, UB and DI followed by spICP-MS analysis and statistical analysis. The major differences among these four WWTPs are the design flow rates and the wastewater sources, which include industrial and domestic sources. These comparisons will help to determine both the effect of the size and sources of WWTPs on the presence of INPs.

V. RESULTS AND DISCUSSION PHASE II

The results and discussion phase II section includes results of identification of inorganic nanoparticles in four different WWTPs AC, SB, UB and DI, and investigate the effect of wastewater (WW) sources on INPs presence in influent streams (section V.1), effect of WWTP sizes on INPs presence in influent streams (section V.2) Nanoparticle Mass Proportion Comparison (section V.3), Effect of WWTP Size in INPs Removal Efficiency (section V.4), and Particle Size Comparison for WWTPs with Mixed Sources (section V.5),

V.1 Effect of WW sources on INPs presence in influent streams

Figure. 17 shows the detected particle number concentrations of 14 elements (Mg, Al, Ti, Mn, Fe, Cu, Zn, Sr, Zr, Mo, Ag, Sn, Ba, Pb) of four WWTPs (AC, SB, UB, and DI). Overall, particle number concentrations range from 7×10^2 to 2×10^6 particles/mL. Trends of our results indicated relatively similar concentrations of 6 elements (Ti, Zn, Mo, Ag, Ba, and Pb) shown in Figure 17(a) and different concentrations of 8 elements (Mg, Al, Mn, Fe, Cu, Sr, Zr, and Sn) shown in Figure. 17(b). Due to the potential presence of various inorganic engineered nanoparticles in industrial wastewater and the differences in designed treatment processes between domestic and industrial wastewater, particle concentrations from the AC WWTP were expected to differ from those in the other WWTPs (SB, UB, DI). To understand the statistical difference between AC data and other WWTPs (SB, UB, DI) data, t-tests were conducted for the detected elements. The student t-test is generally designed for two populations with equal variances. The Welch t-test is used for populations with unequal variances (Nuzzo 2014). In this study, the variances specifically refer to standard deviations; H_0 (null hypothesis) represents that there is no statistical significance between the particle number concentrations of each element. Student's t-tests and Welch's t-tests were

selectively conducted based on standard deviations of data that were compared. Generally, a p-value measures if an observed result can be attributed to chance (Nuzzo 2014). A 95% confidence level has been applied in the present study meaning p values above 0.05 were considered no significant differences between the data.

Based on our analysis we classified the 14 INPs into two groups: the first group (Figure 18(a)) includes Ti, Zn, Mo, Ag, Ba, Pb that showed similar concentration trends in both AC WWTP which receives only domestic WW and SB, UB and DI WWTPs that have mixed WW. This highlights that the major sources of this group of INPs are both domestic and industrial activities. As shown in Figure 18(a), elements with similar concentrations have most p values above 0.05, indicating most of these elements (Ti, Zn, Mo, Ag, Ba, Pb) have no significant differences between WWTP AC and other WWTPs (SB, UB, DI). Only elements that showed significant differences were Zn from AC/UB, Ag from AC/SB, and Pb from AC/UB. This result further confirms that these INPs come from both domestic and industrial sources. The second group (Figure 18(b)) of INPs include Mg, Al, Mn, Fe, Cu, Sr, Zr, Sn that showed variable concentration trends in both AC WWTP which receive only domestic WW and SB, UB and DI WWTPs with mixed sources. This highlights that the major sources of this group of INPs are related mainly to industrial activities. In Figure 18(b), we can see that most p values are within the range of 0.05, meaning that there are significant differences between WWTP AC and other WWTPs (SB, UB, DI) for elements Mg, Al, Mn, Fe, Cu, Sr, Zr, and Sn according to a 95% confidence level.

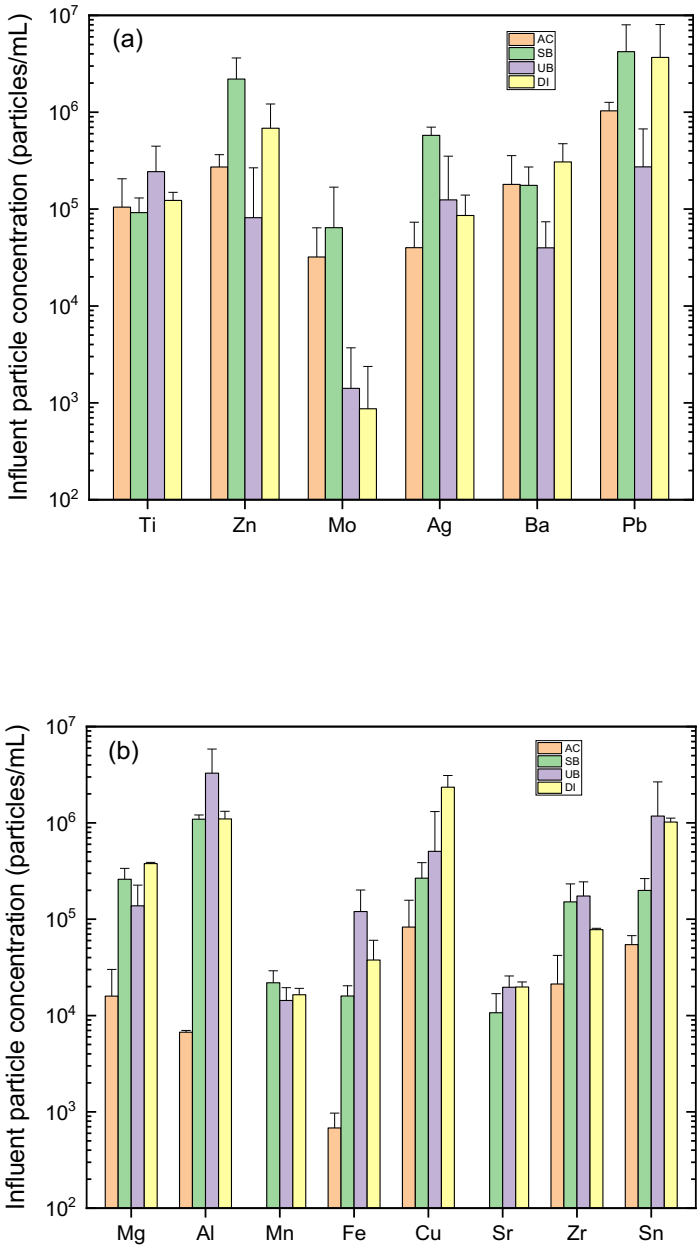

Figure 17. Influent number concentrations of detected elements (Mg, Al, Ti, Mn, Fe, Cu, Zn, Sr, Zr, Mo, Ag, Sn, Ba, Pb) of four WWTPs (AC, SB, UB and DI). (a) Elements with similar concentrations; (b) Elements with different concentrations.

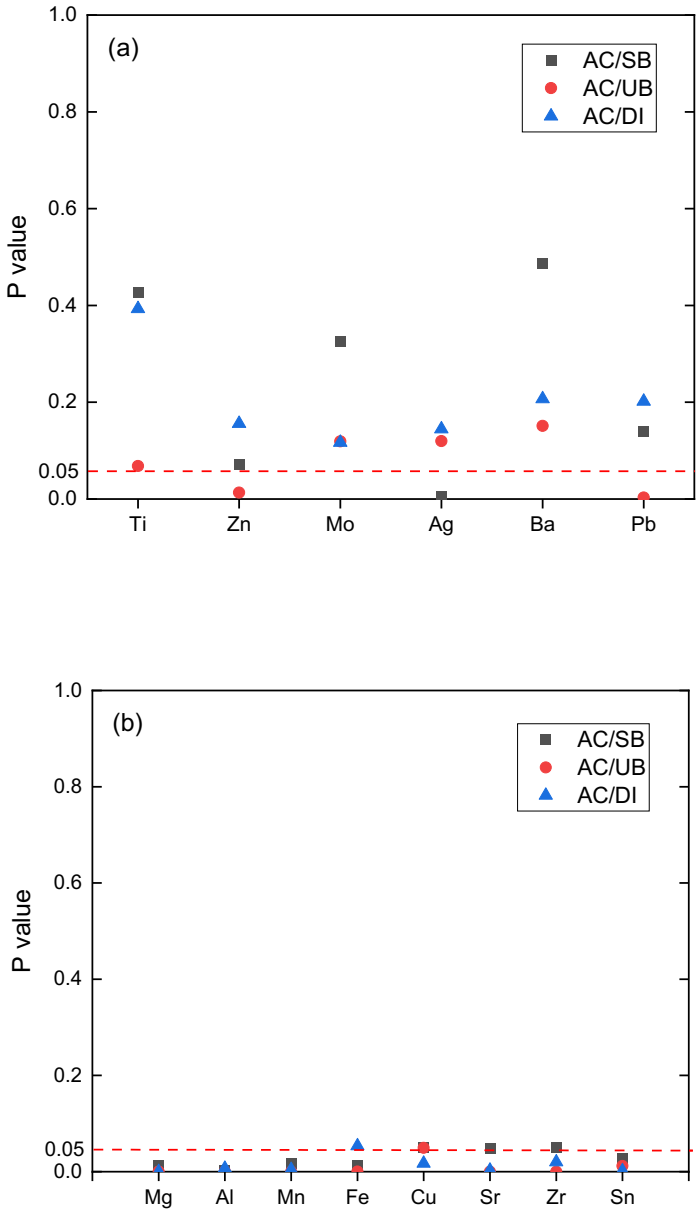

Figure 18. P values regarding different comparison groups between AC and other three WWTPs. (a) Elements with similar concentrations; (b) Elements with different concentrations.

V.2 Effect of WWTP sizes on INPs presence in influent streams

To understand the relationship between the WWTP size and the presence of INPs elements, the samples concentration data from three WWTPs mixed domestic and Industrial WW sources, were compared. As seen in Figure 19(a), the variation with size of the average particle concentrations of all the 14 elements is highly dependent on the element. For example, the concentration of Cu increases when the WWTP size increases. This can be explained by the larger the WWTP, the larger the industrial activities that discharges WW containing Cu. The opposite behavior was seen for Ag, where its concentration increases when the WWTP size decreases.

Moreover, to estimate the statistical significance of comparative data among WWTPs (SB, UB, and DI) with mixed wastewater sources (domestic and industrial), t-tests were conducted as well. Results for p values related to different groups of comparisons of each element are shown in Figure 19(b). As we can see from Figure 19(b), 24 out of 42 p-values are below or approximately close to the 0.05 line, meaning that 57% of the data from different WWTPs are statistically different, and 43% of the other data has no statistical differences based on a 95% confidence level. There are several possible explanations for this result. First, nanoparticle concentrations are highly dynamic due to different sampling times and various components of wastewater sources. Second, sample sizes for three WWTPs are relatively small. Twelve samples were collected for UB WWTPs; meanwhile, three samples were collected for both SB and DI WWTPs. In large samples, the estimate will be closer to the population standard deviation so that the test statistic will be approximately standard normal.

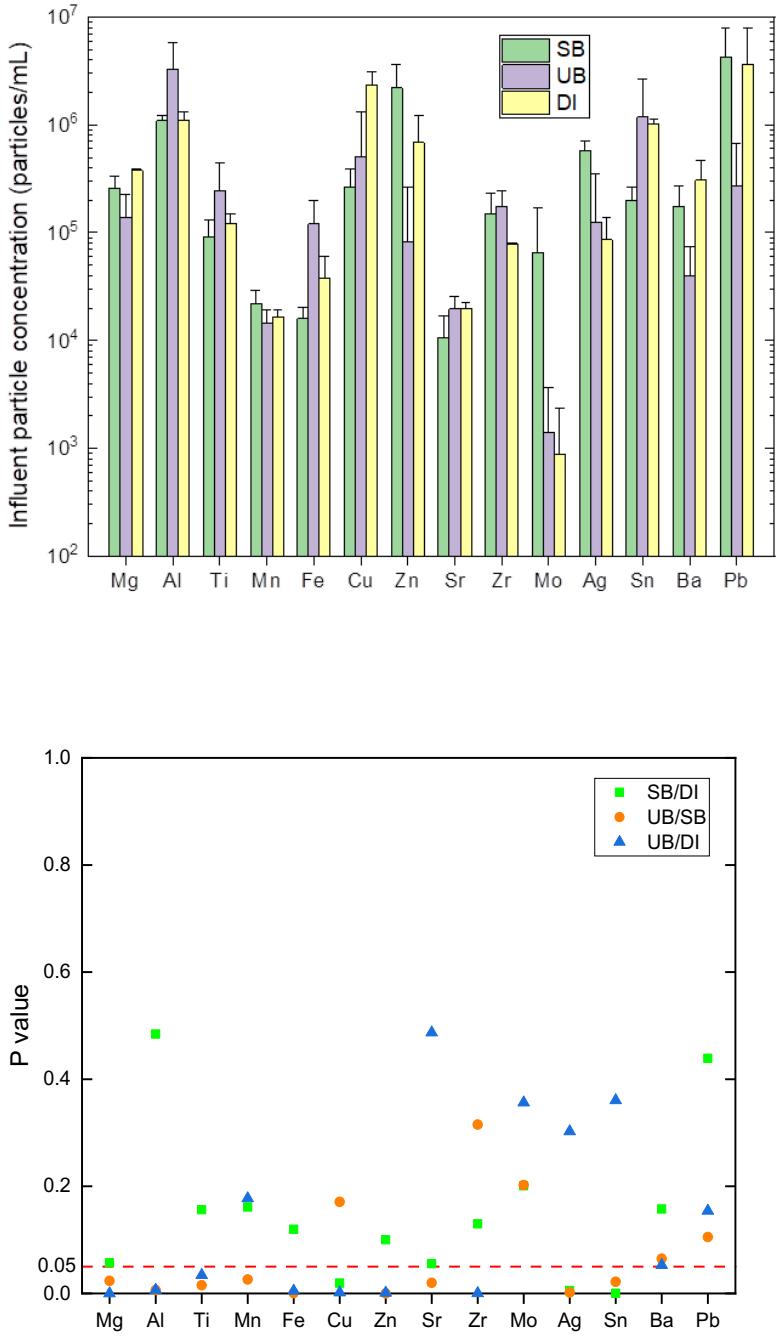

Figure 19. (a) Influent number concentrations of detected elements with of three WWTPs with mixed sources (SB, UB and DI). (b) P values regarding different groups among SB, UB, and DI WWTPs.

V.3 Nanoparticle Mass Proportion Comparison

To further understand the relations among WWTPs (SB, UB, DI) with mixed wastewater sources, the nano mass to total mass ratio calculation has been developed. Nano mass to total mass ratio (θ_p) was derived from C_T (mg/L), C_1 (mg/L) and C_R (mg/L), i.e., $\theta_p = (C_T - C_1)/C_R$, where C_T (mg/L) is the total dissolved mass concentrations of samples treated by the analytical method (including particle and dissolved concentrations), C_1 (mg/L) is the dissolved mass concentration in treated samples, and C_R (mg/L) is the total dissolved mass concentration of raw wastewater samples (nanoparticle + dissolved concentrations).

Figure 20(a) presents the influent nanoparticle mass to total mass ratio for SB, UB, and DI WWTPs. The graph shows that the ratios of elements Mg, Ti, Mn, Zn, Sr, and Ba decrease as design flow rates increase from SB to DI WWTP. A possible explanation for this might be that the larger the design flow rate, the more nanoparticle concentration is diluted. As can be seen from Figure 20(b), elements Mg, Mn, Fe, and Sr are in the nano mass ratio range of 0 to 10%; elements Al, Ti, Zn, Mo, Ag, Ba, and Pb are in the range of 10% - 30%; elements Cu, Zr, and Sn are in the range of 40% - 60%.

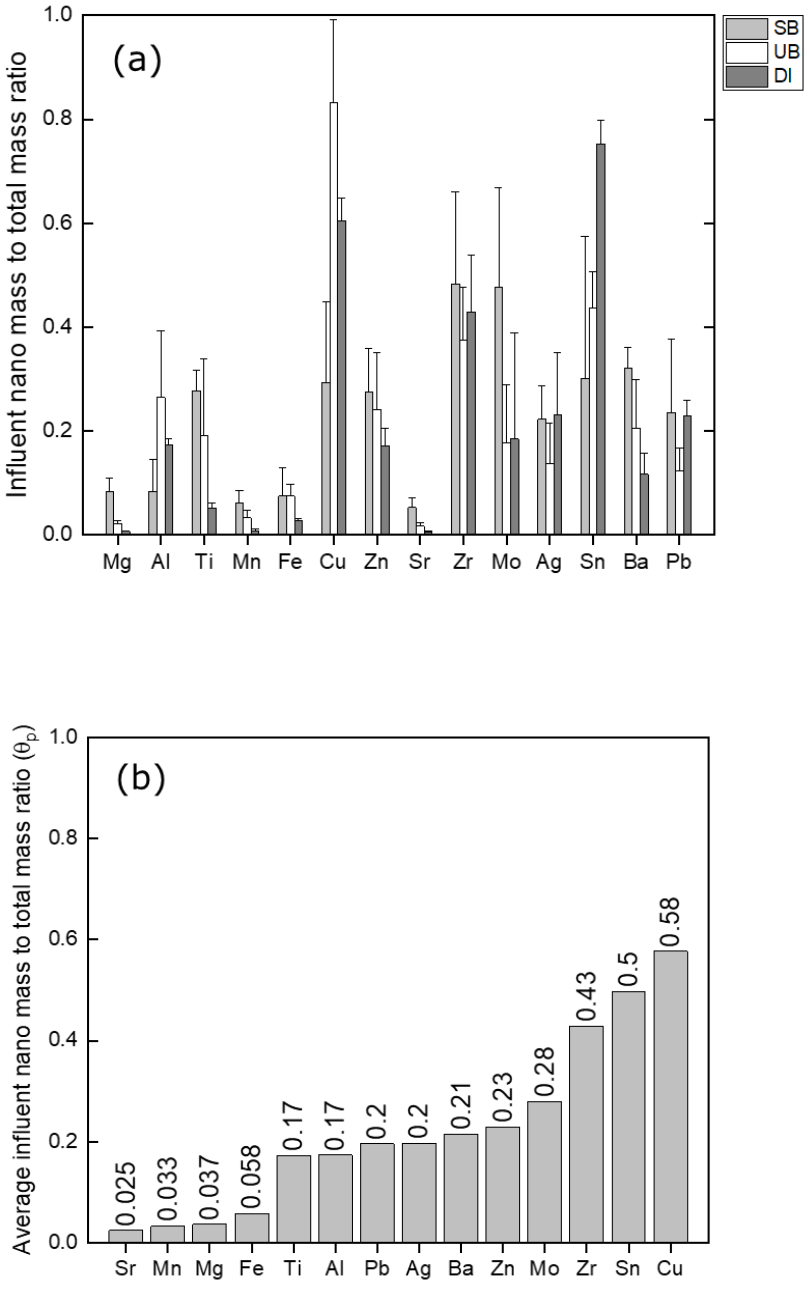

Figure 20. (a) Nanoparticle mass to total mass ratios of detected elements (Mg, Al, Ti, Mn, Fe, Cu, Zn, Sr, Zr, Mo, Ag, Sn, Ba, Pb). (b) Average nanoparticle mass to total mass ratios.

V.4 Effect of WWTP Size in INPs Removal Efficiency

The removal efficiencies were calculated from the influent nanoparticle concentrations and effluent nanoparticle concentrations. Figure 21(a) provides information on removal efficiencies related to nanoparticles (Mg, Al, Ti, Mn, Fe, Sr, Zr) that were removed during treatment processes. As can be seen in Figure. 21(a), removal efficiencies of elements Mg, Ti, Mn, and Sr decrease as the flow rate increases from SB to DI WWTP. Therefore, it is possible that smaller-sized WWTPs have relatively higher nanoparticle removal efficiencies. It can be seen from the data in Figure 21(b) that the average removal efficiencies of elements Mg, Mn, and Sr were within the range of 0 – 50%. Elements Al, Ti, Fe, and Zr were in the range of 50 – 100% average removal efficiency. These findings suggest that with various sizes of WWTPs and treatment processes utilized in WWTPs, the removal effects of nanoparticles are very much different. In addition, SB treatment is able to remove more than 30% of almost all INPs especially those that are originated from industrial sources, compared to UB and DI. This indicates that the smaller the size, the better the removal for most INPs.

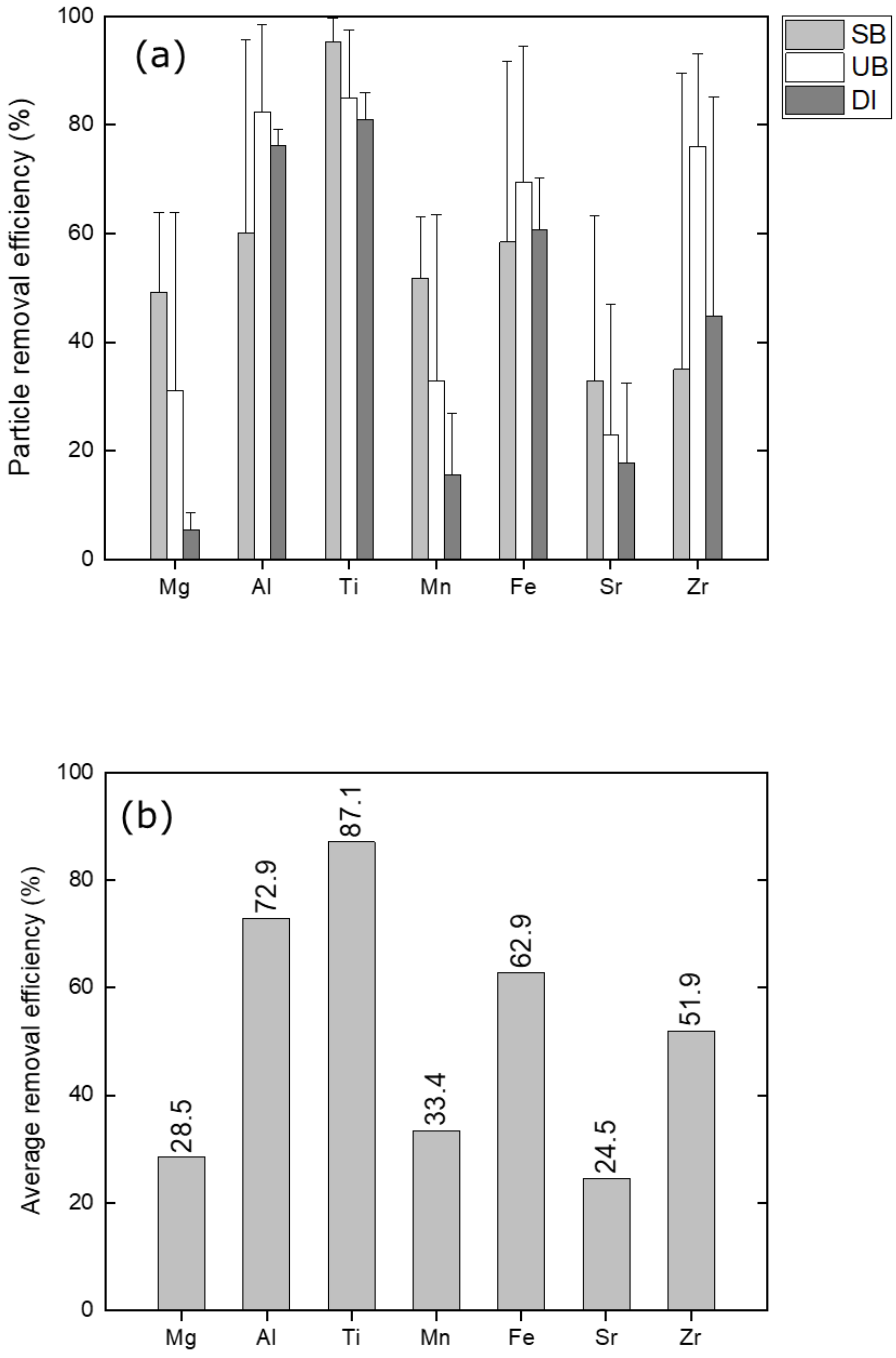

Figure 21. (a) Nanoparticle removal efficiencies of Mg, Al, Ti, Mn, Fe, Sr, Zr. (b) Average removal efficiencies.

V.5 Particle Size Comparison for WWTPs with Mixed Sources

The overall average size changes of nanoparticles that were removed during treatment processes are shown in Figure 22. Most of the elements (Al, Ti, Sr, Zr) showed size decreases from influent to effluent in three WWTPs, due to the partial solubility of some NPs, or their transformation to more stable forms. Elements Mg in UB and DI WWTPs, Mn in SB WWTP, and Fe in SB WWTP showed size increases in the treatment systems, which can be explained by the aggregation and agglomeration. If the nanoparticulate concentration decreased during the treatment system, an increase in particle size would offset the effect of the decrease in nanoparticulate concentration. This behavior indicates that the nanoparticulate mass might remain the same with nanoparticle size increases.

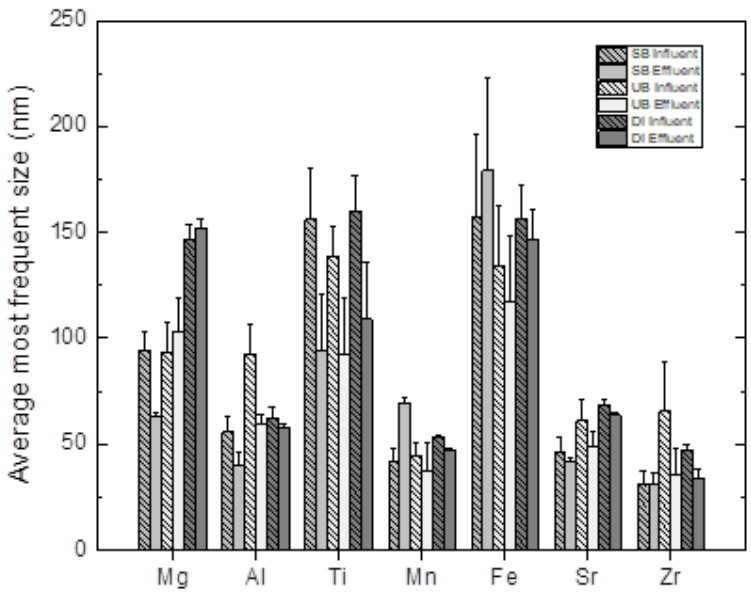

Figure 22. Average sizes of nanoparticles removed during wastewater treatment processes (Mg, Al, Ti, Mn, Fe, Sr, Zr).

V.6 Fate and transport of inorganic nanoparticles in wastewater streams

Based on the results, the studied WWTPs treatment systems removed between 10% to 100% of the INPs. This value varies with the element type and the size of the WWTP. The size change of nanoparticles from influent to effluent is related to their transport mechanisms. A size decrease is due to the partial solubility of some NPs, or their transformation to more stable forms. A size increase can be explained by the aggregation and agglomeration. There are other factors that were not included but can significantly affect the fate and transport of INPs, such as the treatment processes steps, addition of compounds that can lead to INPs formation and WWTP location. For example, Mg compounds can be added in the biological process to increase the influent alkalinity and control the pH value. Fe compounds can also be added for phosphorous removal during the wastewater treatment process. The treatment steps involved could also influence the transformation of INPs. For example, the anerobic treatment allows the aggregation, settling, accumulation, and potential transformation of INPs due to the anaerobic conditions (Cervantes-Avilés and Keller 2021). Thus, the fate and transformation of nanoparticles in wastewater treatment processes could be very complex and could include formation (e.g., during oxidation conditions) and dissolution (under reducing conditions).

In the next section, the outcomes of phases I and II are summarized. Major research findings and conclusions are developed. A discussion of the research implications and future perspectives is provided.

VI. CONCLUSIONS

The work in Phase I developed and improved techniques to identify, quantify, and characterize inorganic nanoparticles in wastewater, and investigated the nature of inorganic nanoparticles in wastewater from a community. This information is useful for those determining the impact of discharged wastewater on receiving streams. Based on the results, the following conclusions were obtained.

a) Results indicated the presence of detectable quantities of inorganic nanoparticles in wastewater for elements evaluated in this work (Mg, Al, Mn, Fe, Cu, Sr, Mo, Ag, Sn, Ba, Pb, Zr, Ti, Zn) examined by the analytical methods in this study. This further developed analytical method can serve as a means to study inorganic nanoparticles in various environmental systems.
b) Both nanoparticle sizes and concentrations were highly dynamic over time in wastewater, and it is recommended that nanoparticle variations with time in wastewater be further investigated. The temporal fluctuation of the data may result from the complexity of wastewater sources and the sampling period applied in this study. Furthermore, research regarding wastewater composed of different sources and sampling periods (i.e., weekly, daily, hourly sampling) can be conducted to gain a better understanding of the origin, fate, and transport of inorganic nanoparticles in wastewater.
c) The dissolved mass removal efficiency (θ_d) was defined and discussed in this research. Results revealed that the preparatory method developed in this work achieved acceptable removal efficiencies of dissolved materials to minimize matrix effects in single-particle ICP-MS analysis.

d) Both elemental and oxidized forms of inorganic nanoparticles were detected in the wastewater samples. The nanoparticle size ranges obtained from ICP-MS, SEM, DLS, and AFM showed significant differences between the instrumental techniques. ICP-MS can provide more detailed size information on specific nanoparticle types (elemental composition) that may assist fate and transport studies.

Phase II research was designed to examine the effects of the WWTP size and wastewater sources on the presence of inorganic nanoparticles in wastewater. It also investigated the nature of inorganic nanoparticles from four different WWTPs. Based on the findings, the following conclusions were acquired.

a) Results showed the presence of detectable quantities of inorganic nanoparticles in this work (Mg, Al, Mn, Fe, Cu, Sr, Mo, Ag, Sn, Ba, Pb, Zr, Ti, and Zn). The analytical methods developed in previous research (Chen and Bergendahl 2021) were shown to be applicable for studying inorganic nanoparticles in different environments.
b) Results indicated the presence of significant differences between WWTP AC and other WWTPs (SB, UB, DI) for elements Mg, Al, Mn, Fe, Cu, Sr, Zr, and Sn according to a 95% confidence level. Elements Ti, Zn, Mo, Ag, Ba, and Pb, have no significant differences between WWTP AC and other WWTPs (SB, UB, DI) due to the differences in wastewater sources.
c) Nanoparticle mass proportion ranges from 0 – 60% among WWTP SB, UB, and DI. Further research regarding wastewater composed of different sizes can be conducted to understand better the nature of inorganic nanoparticles in mixed wastewater (industrial and domestic).
d) The effectiveness of treatment processes was compared among WWTP SB, UB, and DI. Results indicated that there are no clear correlations between the size of WWTP and the

removal efficiency of inorganic nanoparticles, possibly because of how different the treatment processes are applied.

As treated municipal wastewater is frequently discharged to the environment, research on nanoparticles in wastewater contributes to the knowledge of the effects on public health and the environment. In particular, the findings of this research: (1) provided a framework/protocol to collect wastewater samples & analyze various inorganic nanoparticles in complex wastewater systems; (2) explored factors affecting the nature of nanoparticles which are of importance to those determining environmental impacts; and (3) provided valuable information on the concentrations and size of these different INPs in wastewater for realistic risk assessment.

For future perspectives, we recommend that: (1) research on wastewater composed of different sources and sampling periods can be conducted to gain a better understanding of the origin, fate, and transport of INPs in wastewater; (2) an improvement in the spICP-MS sensitivity is needed to detect the smaller INPs than the current cut off point; (3) a development of new analytical techniques and novel approaches to detect, quantify and differentiate natural from engineered INPs; and (4) studies in organisms exposed to treated effluents could consider these measurements, in order to obtain a realistic scenario for organisms exposed to INPs.

APPENDIX A. ICP-MS MONTHLY DATA (UB WWTP)

A.1 Monthly nanoparticle data

Monthly nanoparticle concentration data in particles/mL													
Element	**Type**	**June**	**July**	**August**	**September**	**October**	**November**	**December**	**January**	**February**	**March**	**April**	**May**
Mg	Influent	2256.59	143812	68007.24	562.04	119395.9	104160.9167	197090.3424	153228.5	202380.7	260743.9	126294	275334.5
	Effluent	141.04	132845.2	40654.47	53019.42	100849	331.1952838	170993.0834	73881.41	183921.4	189565.4	109331.5	282718.2
Al	Influent	2310752	1003921	115968.3	3428839.068	2608660	6268698.734	701423.875	6036790	1017106	2910633	4857155	8209710
	Effluent	609421.3	97149.58	31661.77	186973.0844	275554.5	267108.9964	444934.2499	806099	73165.82	784427.3	372713.9	755858.4
Ti	Influent	700860.9	279716.3	14950.35	516199.338	121101.6	118750.069	61464.64862	284141.9	68685.25	213370.8	365481.7	181211.7

	Effluent	142876.4	7832.113	3578.343	9667.145444	6855.742	28813.98969	29363.41901	21127.82	6695.679	24775.24	21881.71	33459.85
Mn	Influent	8242.87	20209.99	8411.92	7699.994	14589.15	16659.12	22558.92	19940.44	11914.62	17748.88	10501.37	13348.96
	Effluent	4931.26	20842.05	7418.97	9236.246	10382.97	10995.68	11671.72	22145.58	4916.877	17895.26	1357.006	2079.096
Fe	Influent	115650.4	90787.08	64822.33	332542.3094	204347.5	80149.25867	85176.32995	104225.6	52525	134671.9	141714.6	33420.99
	Effluent	28912.6	50601.46	60700.68	28102.16699	8114.284	13744.60428	14729.74127	7915.866	25003.92	59101.94	17579.39	11269.87
Cu	Influent	35964.46	72234.94	889339.9	101167.8012	23846.06	106810.479	1345850.056	54280.22	618217.6	144369.8	6785.028	2680480
	Effluent	3808.002	1540533	4612315	5806844.439	13247.81	8942.272662	21614.29425	434430.2	459803.5	4391.476	418204.4	314973.4
Zn	Influent	423.1113	131.5755	N/A	N/A	11260.64	331.1952838	N/A	556372.3	153211.9	4208.498	4780.36	3303.237
	Effluent	423.1113	490193.5	3559.608	349590.9573	2087855	2649.56227	255528.9898	456293.1	N/A	360832.9	1686542	2787738

Sr	Influent	10889.27	21828.37	21826.02	20889.28	16427.29	17106.24	26305.4	24539.18	14549.26	21792.7	10054.18	30059.46
	Effluent	27707.61	11297.07	7587.59	11596.83	7981.806	17669.27	21662.33	24595.73	14180.07	22030.57	9529.88	17876.34
Zr	Influent	142800.1	137378	341216.5	206700.8056	208106.6	131219.5714	125667.1078	104772.1	88184.95	244074.6	163041.1	196736.9
	Effluent	27050.91	22764.12	28308.25	41535.00281	13711.48	21792.64967	37368.71318	75445.74	20892.53	102101.8	37841.95	20577.22
Mo	Influent	187.9953	171.0481	N/A	2660.338475	198.7172	1043.265144	32.02117667	603.1136	2684.984	36.59563	246.7283	7636.307
	Effluent	43.38353	21861.92	N/A	156810.0918	10399.53	312780.826	51826.27444	94.2365	50.34345	86658.45	34387.75	170932.8
Ag	Influent	706.0669	192205.5	396146.9	743264.8473	15284.66	960.466323	8565.66476	2996.721	60915.58	567.2323	53987.23	17021.39
	Effluent	52.30126	32139.12	199694	4290.26416	138274	11095.04201	61736.82862	4033.322	35710.29	74911.26	6214.469	39949.74
Sn	Influent	468807.3	195258	4303004	313245.488	574955	832459.3458	2380134.062	50887.71	3848757	679397.9	181653.7	305063.7

	Effluent	1476235	291448.7	931305.8	844563.7919	1567547	494805.754	473112.8853	240680	288300.2	339607.5	58443.76	31477.91
Ba	Influent	17065.49	5657.746	81121.59	103416	75181.33	54481.62	60199.81	33548.19	4698.722	9514.864	6322.412	27591.75
	Effluent	7757.04	77667.36	52457.38	45525.51	53819.23	48520.11	86297.07	857175.2	335.623	1280.847	7401.848	36141.3
Pb	Influent	88853.37	282097.8	156435.4	1119215.637	89257.13	95053.04644	60680.12979	29590.26	47322.85	177305.8	1112436	20790.96
	Effluent	150345.5	4683447	5344283	4951789.171	4750168	247568.4746	6959642.644	940103.3	649094.9	5404809	23593.39	219762.4

Monthly nanoparticle size data in nanometer													
Element	**Type**	**June**	**July**	**August**	**September**	**October**	**November**	**December**	**January**	**February**	**March**	**April**	**May**
Mg	Influent	95	120	66	74	89	104	102	100	83	97	93	100
	Effluent	107	117	74	85	104	103	127	124	99	109	100	86
Al	Influent	108	100	62	99	102	93	82	75	86	94	97	111
	Effluent	53	67	56	58	60	63	64	55	59	64	61	59
Ti	Influent	170	155	128	156	141	133	126	130	132	133	137	122
	Effluent	135	122	69	70	58	56	110	95	122	97	94	83
Mn	Influent	56	48	31	45	42	49	46	47	35	43	49	40

	Effluent	46	75	31	28	32	40	31	32	30	43	31	29
Fe	Influent	184	149	86	107	126	94	137	157	116	156	156	138
	Effluent	157	115	71	75	87	99	140	162	108	119	155	121
Cu	Influent	35	34	30	31	23	25	17	17	27	23	24	17
	Effluent	21	18	15	14	17	17	18	15	14	21	14	15
Zn	Influent	47	46	N/A	N/A	45	49	N/A	34	42	51	48	46
	Effluent	35	43	34	33	31	39	38	38	N/A	39	35	33
Sr	Influent	82	66	43	64	58	61	71	63	51	55	57	64
	Effluent	59	49	36	39	47	51	64	51	44	47	45	52

Zr	Influent	107	103	25	71	65	36	52	63	55	72	68	69
	Effluent	38	42	26	26	31	30	36	31	26	32	41	71
Mo	Influent	36	27	32	40	28	28	36	28	23	36	27	32
	Effluent	15	21	20	22	23	33	19	18	19	15	21	20
Ag	Influent	30	18	13	12	15	22	20	16	14	22	15	16
	Effluent	45	16	11	12	13	13	15	12	12	13	12	12
Sn	Influent	81	91	32	47	64	54	75	122	32	64	72	68
	Effluent	72	79	49	48	46	77	112	122	41	87	91	85
Ba	Influent	38	36	38	38	44	36	40	25	27	45	45	40

	Effluent	28	25	37	35	37	38	40	16	37	35	42	36
Pb	Influent	25	14	13	13	15	12	14	18	17	17	15	18
	Effluent	13	13	31	30	10	39	12	14	13	18	16	16

A.2 Monthly total concentration data

Monthly total concentration of raw wastewater data in parts per billion (ppb)													
Element	**Type**	**June**	**July**	**August**	**September**	**October**	**November**	**December**	**January**	**February**	**March**	**April**	**May**
Mg	Influent	5535.291	5432.785	6030.36	4866.696	5566.1	5906.217	5484.038	5666.145	5466.283	5486.246	5556.242	5545.927
	Effluent	11952.687	14435.302	18317.716	15391.521	17692.934	20884.628	13193.995	14901.902	15024.307	15558.032	16445.798	15981.255
Al	Influent	629.163	249.436	419.295	1192.43	889.155	311.017	439.300	432.631	622.581	675.896	615.083	589.971
	Effluent	38.332	42.045	47.06	293.235	24.412	44.32	40.189	42.479	105.168	89.017	81.567	75.656
Ti	Influent	16.403	12.507	24.06	34.228	42.453	14.865	14.455	17.657	21.800	25.930	24.086	22.710
	Effluent	2.9	2.629	2.978	4.562	1.411	1.63	2.765	2.836	3.267	2.896	2.685	2.696

Mn	Influent	168.884	183.665	166.685	175.652	148.389	168.425	176.275	173.078	173.722	168.655	168.617	169.711
	Effluent	15.298	71.602	46.036	82.222	20.626	32.645	43.450	44.312	53.790	47.157	44.738	44.554
Fe	Influent	1138.528	1004.797	1852.162	2356.903	2576.789	1687.104	1071.663	1331.829	1588.098	1785.836	1769.381	1669.707
	Effluent	222.676	277.256	245.793	192.265	162.593	187.385	249.966	248.575	234.498	220.117	214.661	219.705
Cu	Influent	29.218	26.492	49.617	34.02	49.62	38.427	27.855	35.109	34.837	37.793	37.899	36.464
	Effluent	5.778	8.851	8.46	5.257	6.812	8.264	7.315	7.696	7.087	7.032	7.237	7.248
Zn	Influent	69.569	51.011	107.766	82.155	94.133	187.149	60.290	76.115	77.625	80.927	98.631	93.153
	Effluent	26.889	61.94	44.322	24.077	26.497	41.889	44.415	44.384	39.307	36.745	37.602	38.576
Sr	Influent	220.443	231.575	212.531	206.02	180.629	255.281	226.009	221.516	217.642	210.240	217.747	218.927

	Effluent	188.784	181.186	200.205	193.336	181.346	235.733	184.985	190.058	190.878	188.971	196.765	195.082
Zr	Influent	3.023	0.151	2.513	0.667	2.717	3.857	1.587	1.896	1.589	1.814	2.155	2.074
	Effluent	0.288	0.335	0.282	1.32	0.189	0.274	0.312	0.302	0.556	0.483	0.448	0.429
Mo	Influent	2.734	5.167	4.311	4.159	8.605	3.778	3.951	4.071	4.093	4.995	4.792	4.672
	Effluent	1.621	2.266	4.004	2.349	3.271	2.245	1.944	2.630	2.560	2.702	2.626	2.529
Ag	Influent	0.326	0.077	0.105	0.214	0.261	0.253	0.202	0.169	0.181	0.197	0.206	0.205
	Effluent	0.045	0.02	0.028	0.035	0.027	0.032	0.033	0.031	0.032	0.031	0.031	0.031
Sn	Influent	5.718	2.049	4.092	0.84	2.963	4.674	3.884	3.953	3.175	3.132	3.389	3.460
	Effluent	0.76	0.496	1.794	0.638	0.795	1.983	0.628	1.017	0.922	0.897	1.078	1.013

Ba	Influent	44.054	38.314	52.194	67.32	61.679	59.629	41.184	44.854	50.471	52.712	53.865	52.053
	Effluent	23.405	21.181	22.563	37.111	21.353	27.865	22.293	22.383	26.065	25.123	25.580	25.110
Pb	Influent	4.242	1.374	3.081	47.902	13.977	2.844	2.808	2.899	14.150	14.115	12.237	10.890
	Effluent	0.275	0.581	0.359	12.396	0.307	0.241	0.428	0.405	3.403	2.784	2.360	2.084

Monthly total concentration of treated samples (nanoparticle + dissolved) data in parts per billion (ppb)													
Element	**Type**	**June**	**July**	**August**	**September**	**October**	**November**	**December**	**January**	**February**	**March**	**April**	**May**
Mg	Influent	336.198	263.952	248.892	289.156	289.796	405.777	300.075	283.014	284.550	285.599	305.629	304.835
	Effluent	464.595	489.741	390.352	415.138	403.474	695.341	477.168	448.229	439.957	432.660	476.440	476.544
Al	Influent	174.191	68.223	259.877	521.978	168.453	171.603	121.207	167.430	256.067	238.544	227.388	212.219
	Effluent	118.31	31.525	130.333	392.065	43.051	35.635	74.918	93.389	168.058	143.057	125.153	117.977
Ti	Influent	3.583	4.299	8.178	20.065	7.616	8.082	3.941	5.353	9.031	8.748	8.637	7.966
	Effluent	0.882	1.456	4.102	4.686	1.105	1.788	1.169	2.147	2.782	2.446	2.337	2.170
Mn	Influent	12.346	10.737	8.045	15.988	19.866	16.142	11.542	10.376	11.779	13.396	13.854	13.524

	Effluent	3.116	4.064	4.486	15.024	2.726	3.497	3.590	3.889	6.673	5.883	5.486	5.215
Fe	Influent	86.242	258.639	573.477	403.996	360.007	385.673	172.441	306.119	330.589	336.472	344.672	320.068
	Effluent	47.469	66.352	116.588	64.297	44.932	98.908	56.911	76.803	73.677	67.928	73.091	70.780
Cu	Influent	17.488	22.243	87.923	26.809	31.232	35.57	19.866	42.551	38.616	37.139	36.878	34.447
	Effluent	4.707	8.103	11.061	4.683	7.032	15.637	6.405	7.957	7.139	7.117	8.537	8.233
Zn	Influent	32.778	20.567	34.067	68.254	40.077	51.555	26.673	29.137	38.917	39.149	41.216	39.139
	Effluent	10.288	14.991	14.024	28.362	15.548	19.882	12.640	13.101	16.916	16.643	17.183	16.534
Sr	Influent	11.255	9.683	6.48	10.463	9.231	17.665	10.469	9.139	9.470	9.422	10.796	10.749
	Effluent	7.512	6.592	4.624	7.784	5.791	10.022	7.052	6.243	6.628	6.461	7.054	7.054

Zr	Influent	1.102	1.769	2.078	6.174	1.944	2.305	1.436	1.650	2.781	2.613	2.562	2.401
	Effluent	0.699	0.639	0.641	2.291	0.358	0.82	0.669	0.660	1.068	0.926	0.908	0.874
Mo	Influent	2.319	0.96	2.255	1.956	1.136	1.236	1.640	1.845	1.873	1.725	1.644	1.643
	Effluent	0.489	0.402	1.388	0.643	0.446	0.4	0.446	0.760	0.731	0.674	0.628	0.602
Ag	Influent	0.414	0.123	0.339	0.254	0.162	0.179	0.269	0.292	0.283	0.258	0.245	0.249
	Effluent	0.047	0.03	0.096	0.041	0.037	0.048	0.039	0.058	0.054	0.050	0.050	0.048
Sn	Influent	12.562	20.373	10.972	13.24	26.372	24.518	16.468	14.636	14.287	16.704	18.006	17.786
	Effluent	1.185	33.337	9.034	33.381	53.199	58.647	17.261	14.519	19.234	26.027	31.464	29.435
Ba	Influent	35.121	5.329	7.593	46.467	42.055	45.959	20.225	16.014	23.628	27.313	30.421	28.964

	Effluent	32.392	1.85	5.027	40.109	44.536	37.773	17.121	13.090	19.845	24.783	26.948	25.544
Pb	Influent	0.769	0.967	2.287	459.143	3.313	1.662	0.868	1.341	115.792	93.296	78.024	67.001
	Effluent	0.651	0.349	1.833	8.319	0.428	0.385	0.500	0.944	2.788	2.316	1.994	1.781

Monthly total concentration of treated samples (dissolved) data in parts per billion (ppb)													
Element	**Type**	**June**	**July**	**August**	**September**	**October**	**November**	**December**	**January**	**February**	**March**	**April**	**May**
Mg	Influent	173.969	154.559	127.323	226.998	182.819	253.612	164.264	151.950	170.712	173.134	186.547	183.364
	Effluent	282.446	276.556	188.252	322.671	254.659	426.184	279.501	249.084	267.481	264.917	291.795	290.038
Al	Influent	61.615	14.879	66.236	100.177	72.825	87.051	38.247	47.577	60.727	63.146	67.131	63.004
	Effluent	0.000	0.000	27.892	0.944	2.852	1.804	0.000	9.297	7.209	6.338	5.582	4.785
Ti	Influent	2.447	2.919	4.689	5.270	4.435	3.401	2.683	3.352	3.831	3.952	3.860	3.692
	Effluent	0.665	0.553	1.649	0.335	0.303	0.618	0.609	0.956	0.801	0.701	0.687	0.676
Mn	Influent	8.005	8.273	4.734	8.932	12.362	8.728	8.139	7.004	7.486	8.461	8.506	8.453

	Effluent	2.250	2.844	2.510	9.558	1.482	1.663	2.547	2.535	4.291	3.729	3.385	3.265
Fe	Influent	214.519	743.939	127.799	486.945	461.392	413.074	479.229	362.086	393.301	406.919	407.945	418.128
	Effluent	9.210	34.076	0.000	2.855	0.000	0.000	21.643	14.429	11.535	9.228	7.690	9.683
Cu	Influent	1.447	0.843	12.637	4.719	2.026	1.641	1.145	4.976	4.911	4.334	3.885	3.494
	Effluent	0.578	0.000	0.000	0.269	0.404	0.866	0.289	0.193	0.212	0.250	0.353	0.344
Zn	Influent	20.716	0.000	26.129	39.750	21.458	28.696	10.358	15.615	21.649	21.611	22.791	21.015
	Effluent	1.803	0.000	11.105	12.400	2.819	2.991	0.901	4.303	6.327	5.625	5.186	4.574
Sr	Influent	7.978	7.373	4.125	6.700	5.989	10.360	7.676	6.492	6.544	6.433	7.087	7.171
	Effluent	5.894	4.683	2.939	4.581	3.621	5.401	5.289	4.506	4.524	4.344	4.520	4.630

Zr	Influent	1.356	5.418	2.610	3.724	5.487	3.905	3.387	3.128	3.277	3.719	3.750	3.698
	Effluent	0.469	0.457	0.419	0.491	0.444	1.477	0.463	0.448	0.459	0.456	0.626	0.603
Mo	Influent	0.643	0.833	1.277	0.681	0.632	0.517	0.738	0.918	0.859	0.813	0.764	0.760
	Effluent	0.235	0.263	3.866	0.096	0.116	0.121	0.249	1.455	1.115	0.915	0.783	0.707
Ag	Influent	0.498	0.251	0.302	0.174	0.087	0.154	0.375	0.351	0.307	0.263	0.245	0.263
	Effluent	0.290	0.234	0.285	0.003	0.050	0.097	0.262	0.270	0.203	0.172	0.160	0.174
Sn	Influent	55.044	394.027	3.254	49.570	80.783	82.033	224.536	150.775	125.474	116.536	110.785	127.035
	Effluent	288.635	591.771	1.157	126.576	183.814	182.974	440.203	293.854	252.035	238.391	229.155	259.304
Ba	Influent	23.229	0.709	4.421	30.702	26.312	28.374	11.969	9.453	14.765	17.074	18.958	17.959

	Effluent	19.799	0.000	2.780	22.910	25.305	19.176	9.899	7.526	11.372	14.159	14.995	14.267
Pb	Influent	2.620	3.511	2.196	0.941	2.916	1.628	3.066	2.776	2.317	2.437	2.302	2.411
	Effluent	2.482	3.040	1.902	0.595	1.761	1.246	2.761	2.475	2.005	1.956	1.838	1.970

APPENDIX B. ICP-MS DATA (AC, SB, AND DI WWTPS)

B.1 AC WWTP

Nanoparticle concentration data in particles/mL				
Element	**Type**	**Sample1**	**Sample2**	**Sample3**
Mg	Influent	1748.773	30117.751	15933.262
	Effluent	0.000	47216.861	23608.430
Al	Influent	6995.090	6412.166	6703.628
	Effluent	37307.149	76168.763	56737.956
Ti	Influent	205344.767	3925.023	104634.895
	Effluent	60488.102	83144.423	71816.262
Mn	Influent	N/A	N/A	N/A
	Effluent	58.292	58.292	58.292
Fe	Influent	388.616	971.540	680.078
	Effluent	3497.545	1360.156	2428.851
Cu	Influent	157195.228	8743.863	82969.545
	Effluent	2017306.372	353640.686	1185473.529
Zn	Influent	364521.937	180123.580	272322.759
	Effluent	961242.017	649960.491	805601.254
Sr	Influent	N/A	N/A	N/A
	Effluent	N/A	N/A	N/A
Zr	Influent	42087.128	485.770	21286.449
	Effluent	204684.120	196095.703	200389.912
Mo	Influent	64005.078	0.000	32002.539
	Effluent	66472.790	66841.976	66657.383
Ag	Influent	73293.004	6567.613	39930.308
	Effluent	17682.034	116409.964	67045.999
Sn	Influent	41193.311	67619.208	54406.259
	Effluent	301566.123	1078409.783	689987.953
Ba	Influent	3691.853	356555.307	180123.580
	Effluent	325077.399	860979.054	593028.226
Pb	Influent	1265917.069	801520.784	1033718.927
	Effluent	805406.946	852040.882	828723.914

Total concentration of raw wastewater data in parts per billion (ppb)				
Element	**Type**	**Sample1**	**Sample2**	**Sample3**
Mg	Influent	10350.373	10233.617	10008.309
	Effluent	7601.782	8043.669	7834.952
Al	Influent	381.784	382.394	346.117
	Effluent	1.826	9.956	10.179
Ti	Influent	22.927	24.002	25.296
	Effluent	14.752	15.727	15.641
Mn	Influent	40.85	39.483	36.264
	Effluent	6.324	6.234	4.582
Fe	Influent	347.781	347.597	334.029
	Effluent	141.396	190.328	172.332
Cu	Influent	40.234	50.856	63.637
	Effluent	8.993	12.971	17.11
Zn	Influent	148.431	147.349	148.739
	Effluent	18.993	72.251	58.241
Sr	Influent	204.019	204.185	192.924
	Effluent	161.149	177.193	170.351
Zr	Influent	212.085	167.553	136.196
	Effluent	7.619	29.571	23.78
Mo	Influent	2.608	1.402	1.202
	Effluent	0.572	0.13	0.107
Ag	Influent	0.463	0.189	0.183
	Effluent	N/A	0.021	0.016
Sn	Influent	24.994	12.38	8.567
	Effluent	0.885	4.35	2.118
Ba	Influent	60.183	61.826	62.284
	Effluent	21.866	29.31	25.458
Pb	Influent	1.962	0.868	1.192
	Effluent	0.142	0.166	0.14

Total concentration of treated samples (nanoparticle + dissolved) data in parts per billion (ppb)				
Element	**Type**	**Sample1**	**Sample2**	**Sample3**
Mg	Influent	737.409	754.519	739.72
	Effluent	240.517	271.117	280.216
Al	Influent	160.787	194.119	209.983
	Effluent	18.67	15.924	21.807
Ti	Influent	9.012	9.007	8.272
	Effluent	1.997	2.596	2.602
Mn	Influent	4.286	4.752	4.122
	Effluent	1.395	1.126	1.042
Fe	Influent	108.098	128.699	122.482
	Effluent	44.623	18.897	21.746
Cu	Influent	73.413	102.086	101.124
	Effluent	50.03	21.392	36.129
Zn	Influent	100.466	115.066	100.146
	Effluent	139.928	62.816	53.844
Sr	Influent	9.541	9.791	9.53
	Effluent	6.577	6.944	7.675
Zr	Influent	257.249	326.429	308.726
	Effluent	62.899	65.275	56.099
Mo	Influent	0.907	0.804	0.72
	Effluent	0.252	0.432	0.449
Ag	Influent	0.136	0.145	0.15
	Effluent	0.047	0.049	0.059
Sn	Influent	20.435	20.669	22.54
	Effluent	3.806	4.467	4.372
Ba	Influent	33.727	33.666	30.695
	Effluent	36.159	44.344	43.231
Pb	Influent	1.173	1.929	6.622
	Effluent	1.714	0.158	0.174

Total concentration of treated samples (dissolved) data in parts per billion (ppb)				
Element	**Type**	**Sample1**	**Sample2**	**Sample3**
Mg	Influent	468.044	467.905	467.975
	Effluent	165.325	174.798	170.062
Al	Influent	78.858	85.007	81.933
	Effluent	N/A	N/A	N/A
Ti	Influent	27.212	17.780	22.496
	Effluent	2.556	2.070	2.313
Mn	Influent	5.023	5.042	5.033
	Effluent	1.048	0.741	0.894
Fe	Influent	314.528	297.436	305.982
	Effluent	0.691	N/A	0.346
Cu	Influent	13.365	12.473	12.919
	Effluent	0.833	0.717	0.775
Zn	Influent	78.849	71.810	75.330
	Effluent	13.606	18.164	15.885
Sr	Influent	10.571	9.961	10.266
	Effluent	5.979	6.462	6.220
Zr	Influent	8.474	5.426	6.950
	Effluent	0.710	0.511	0.611
Mo	Influent	1.137	0.603	0.870
	Effluent	0.150	0.121	0.135
Ag	Influent	0.191	0.182	0.186
	Effluent	0.174	0.172	0.173
Sn	Influent	40.589	30.745	35.667
	Effluent	1.794	1.901	1.847
Ba	Influent	18.949	13.463	16.206
	Effluent	23.107	12.337	17.722
Pb	Influent	2.943	2.898	2.921
	Effluent	2.899	2.905	2.902

B.2 SB WWTP

Nanoparticle concentration data in particles/mL				
Element	**Type**	**Sample1**	**Sample2**	**Sample3**
Mg	Influent	177062.263	276192.192	327822.237
	Effluent	113677.298	147759.705	114554.982
Al	Influent	1070270.720	988597.634	1217654.466
	Effluent	229224.972	799689.656	210829.914
Ti	Influent	111827.704	116399.734	48178.088
	Effluent	3013.384	1932.722	4630.946
Mn	Influent	23005.625	28575.189	14177.195
	Effluent	10661.143	10827.399	8551.001
Fe	Influent	18080.301	18911.580	10968.030
	Effluent	4572.030	1662.556	9952.472
Cu	Influent	198467.677	404832.497	197221.432
	Effluent	32004.212	43018.648	86728.683
Zn	Influent	1960985.342	3742206.767	903034.488
	Effluent	838967.552	622419.574	10968.030
Sr	Influent	4904.542	10016.903	17203.559
	Effluent	15586.467	6109.895	6926.108
Zr	Influent	88697.387	121491.313	243530.893
	Effluent	220829.061	112804.456	5484.015
Mo	Influent	N/A	8458.256	184770.687
	Effluent	80675.552	49980.604	54819.840
Ag	Influent	715314.916	540143.811	476439.046
	Effluent	479252.681	395459.835	355993.825
Sn	Influent	274529.635	157527.224	165129.788
	Effluent	578154.008	739006.345	511638.299
Ba	Influent	226731.137	65255.341	236218.873
	Effluent	174152.789	60059.852	424503.392
Pb	Influent	8118471.002	609742.581	3931023.277
	Effluent	2195613.622	2108952.867	1418938.132

Nanoparticle size data in nanometer				
Element	**Type**	**Sample1**	**Sample2**	**Sample3**
Mg	Influent	84	100	99
	Effluent	63	65	62
Al	Influent	57	62	48
	Effluent	46	35	40
Ti	Influent	141	184	143
	Effluent	88	123	72
Mn	Influent	35	42	48
	Effluent	71	67	71
Fe	Influent	142	202	128
	Effluent	149	229	159
Cu	Influent	20	21	21
	Effluent	24	21	23
Zn	Influent	41	40	42
	Effluent	41	44	44
Sr	Influent	39	47	53
	Effluent	40	44	41
Zr	Influent	38	28	28
	Effluent	28	28	37
Mo	Influent	N/A	28	26
	Effluent	26	26	26
Ag	Influent	47	53	36
	Effluent	40	12	32
Sn	Influent	45	48	45
	Effluent	50	50	48
Ba	Influent	35	32	30
	Effluent	42	41	42
Pb	Influent	19	23	16
	Effluent	19	19	16

Total concentration of raw wastewater data in parts per billion (ppb)				
Element	**Type**	**Sample1**	**Sample2**	**Sample3**
Mg	Influent	4130582.127	3980403.97	3745383.459
	Effluent	4155811.394	3712268.192	4029382.23
Al	Influent	2752754.002	2098055.255	1939800.887
	Effluent	88020.494	42626.754	67382.48
Ti	Influent	27372.776	20843.669	19646.81
	Effluent	4470.112	2649.089	3829.32
Mn	Influent	240415.601	182276.134	165009.887
	Effluent	248215.264	162574.974	203937.2334
Fe	Influent	16554549.84	14217525.68	13365770.41
	Effluent	1805076.017	1040882.683	1438293.234
Cu	Influent	87581.443	73978.059	74655.324
	Effluent	10463.147	9987.929	10383.64
Zn	Influent	89391.925	72294.779	70717.611
	Effluent	21357.685	16277.563	18394.56
Sr	Influent	89036.897	100734.622	101017.502
	Effluent	120250.232	119210.063	120345.869
Zr	Influent	702573.449	544701.969	456410.72
	Effluent	521232.248	164288.157	429495.958
Mo	Influent	4782.667	5211.393	3812.283
	Effluent	3479.192	3841.974	3792.483
Ag	Influent	805.872	238.779	391.844
	Effluent	144.934	90.181	120.42
Sn	Influent	26769.076	13459.288	6330.937
	Effluent	7336.03	1159.032	3948.058
Ba	Influent	35920.089	39083.521	28937.134
	Effluent	17394.013	13960.805	16483.289
Pb	Influent	5333.306	4076.148	3655.719
	Effluent	1154.568	737.823	974.293

Total concentration of treated samples (nanoparticle + dissolved) data in parts per billion (ppb)				
Element	**Type**	**Sample1**	**Sample2**	**Sample3**
Mg	Influent	219066.026	356205.878	390169.969
	Effluent	82941.314	96268.398	90532.79
Al	Influent	146247.216	324479.348	81002.92
	Effluent	164583.065	18443.921	103200.425
Ti	Influent	7047.096	6752.683	4960.395
	Effluent	2785.179	2662.403	2052.581
Mn	Influent	8600.729	14550.93	11332.972
	Effluent	48241.845	52151.677	45780.035
Fe	Influent	1604142.26	1612124.617	163127.818
	Effluent	1459869.222	59782.834	43459.734
Cu	Influent	17095.366	34895.613	15964.243
	Effluent	16918.917	6022.717	23396.735
Zn	Influent	16791.254	25665.653	20015.129
	Effluent	15690.478	12571.936	15597.44
Sr	Influent	2729.462	5943.7	6790.629
	Effluent	3088.349	3432.341	2883.958
Zr	Influent	614409.692	795296.103	55008.615
	Effluent	344962.099	89444.578	111926.216
Mo	Influent	3301.228	1664.498	1606.921
	Effluent	674.85	710.201	664.027
Ag	Influent	237.629	149.893	65.641
	Effluent	90.599	119.871	99.542
Sn	Influent	77717.55	77975.542	2053.766
	Effluent	71917.783	2960.37	1894.454
Ba	Influent	11505.843	14100.968	8106.567
	Effluent	41519.736	39177.907	30142.589
Pb	Influent	1817.375	1188.629	276.683
	Effluent	1287.277	63.306	134.503

Total concentration of treated samples (dissolved) data in parts per billion (ppb)				
Element	**Type**	**Sample1**	**Sample2**	**Sample3**
Mg	Influent	148.077	239.353	267.263
	Effluent	53.704	54.284	48.344
Al	Influent	11.728	16.072	N/A
	Effluent	N/A	N/A	N/A
Ti	Influent	10.871	6.315	4.693
	Effluent	1.626	1.430	0.686
Mn	Influent	2.839	6.578	9.962
	Effluent	23.037	21.651	26.542
Fe	Influent	355.753	653.229	307.908
	Effluent	N/A	6.184	N/A
Cu	Influent	2.357	3.595	1.403
	Effluent	1.611	1.760	1.036
Zn	Influent	N/A	N/A	N/A
	Effluent	N/A	N/A	N/A
Sr	Influent	1.804	4.489	6.219
	Effluent	2.214	2.310	2.370
Zr	Influent	1.030	0.352	1.678
	Effluent	0.372	0.225	1.763
Mo	Influent	1.235	1.258	1.480
	Effluent	0.295	0.308	0.322
Ag	Influent	0.001	N/A	0.145
	Effluent	N/A	N/A	0.144
Sn	Influent	7.211	5.830	5.382
	Effluent	4.995	5.776	4.129
Ba	Influent	7.591	1.731	1.840
	Effluent	24.243	18.679	16.603
Pb	Influent	2.332	2.362	3.246
	Effluent	2.048	2.046	3.178

B.3 DI WWTP

Nanoparticle concentration data in particles/mL				
Element	**Type**	**Sample1**	**Sample2**	**Sample3**
Mg	Influent	364131.5	388241.1471	379924.2125
	Effluent	335429.6357	381544.0351	355451.1723
Al	Influent	1327558.935	1081105.215	886358.2537
	Effluent	271711.3991	265014.2872	234467.514
Ti	Influent	131952.24	93549.08664	143305.4393
	Effluent	28147.0048	20952.3931	19025.81511
Mn	Influent	13681.24298	16647.10685	19025.81511
	Effluent	12781.91652	11939.99388	16756.138
Fe	Influent	59508.62333	13968.26207	39472.64546
	Effluent	18177.87529	6888.458006	14999.60527
Cu	Influent	2825415.859	2737588.019	1472329.676
	Effluent	1286993.571	420578.6305	93550.16973
Zn	Influent	616708.3376	1248915.706	187692.4291
	Effluent	5035080.11	1891647.107	5859122.128
Sr	Influent	17221.14501	22272.68089	19933.68596
	Effluent	15709.51117	14523.16563	18019.26265
Zr	Influent	75218.1345	78719.76732	79951.84337
	Effluent	16015.66486	34958.92438	180784.7162
Mo	Influent	N/A	N/A	2605.1946
	Effluent	430145.9333	121810.8991	577938.7385
Ag	Influent	30175.27299	90028.31922	137522.6968
	Effluent	546197.3161	367518.3692	383832.0044
Sn	Influent	1079000.408	1076130.217	903134.128
	Effluent	92611.49097	88401.87774	81511.01287
Ba	Influent	117103.7861	387284.4168	417620.5889
	Effluent	49367.28238	58551.89305	155522.2231
Pb	Influent	1067519.645	8699357.077	1258585.3
	Effluent	4226451.679	3026137.871	3718125.839

Nanoparticle size data in nanometer				
Element	**Type**	**Sample1**	**Sample2**	**Sample3**
Mg	Influent	146	154	141
	Effluent	156	148	152
Al	Influent	62	58	68
	Effluent	60	57	56
Ti	Influent	173	166	141
	Effluent	80	133	114
Mn	Influent	54	54	52
	Effluent	47	48	46
Fe	Influent	147	175	147
	Effluent	135	163	141
Cu	Influent	22	19	23
	Effluent	22	23	25
Zn	Influent	55	48	54
	Effluent	41	41	38
Sr	Influent	71	66	69
	Effluent	65	63	63
Zr	Influent	50	45	47
	Effluent	39	31	31
Mo	Influent	N/A	N/A	31
	Effluent	18	24	18
Ag	Influent	14	15	15
	Effluent	13	20	13
Sn	Influent	41	37	39
	Effluent	66	62	72
Ba	Influent	46	47	49
	Effluent	44	45	39
Pb	Influent	19	16	17
	Effluent	16	16	16

Total concentration of raw wastewater data in parts per billion (ppb)				
Element	**Type**	**Sample1**	**Sample2**	**Sample3**
Mg	Influent	21506	20839.967	21196.71
	Effluent	25663.472	25987.185	26766.754
Al	Influent	753.95	729.705	758.039
	Effluent	36.702	41.35	39.38
Ti	Influent	23.633	21.413	21.336
	Effluent	5.533	5.778	5.828
Mn	Influent	238.05	229.199	224.867
	Effluent	163.125	168.342	172.314
Fe	Influent	6449.559	6336.677	6144.159
	Effluent	477.171	477.323	485.074
Cu	Influent	61.358	61.431	63.839
	Effluent	10.789	13.696	13.373
Zn	Influent	124.238	131.063	131.111
	Effluent	24.96	25.822	24.052
Sr	Influent	234.286	224.965	229.592
	Effluent	235.844	232.192	235.668
Zr	Influent	1957.055	775.498	1156.351
	Effluent	540.536	625.255	529.286
Mo	Influent	5.778	4.409	4.466
	Effluent	7.201	7.414	7.563
Ag	Influent	0.399	0.33	0.342
	Effluent	0.077	0.071	0.083
Sn	Influent	11.62	3.203	2.409
	Effluent	0.833	0.637	0.749
Ba	Influent	97.473	93.342	94.493
	Effluent	34.608	35.054	34.777
Pb	Influent	6.975	10.222	6.781
	Effluent	0.351	0.359	0.362

Total concentration of treated samples (nanoparticle + dissolved) data in parts per billion (ppb)				
Element	**Type**	**Sample1**	**Sample2**	**Sample3**
Mg	Influent	799.802	750.639	794.673
	Effluent	808.028	825.01	873.166
Al	Influent	135.254	143.312	155.005
	Effluent	32.809	27.73	29.72
Ti	Influent	6.535	5.206	5.242
	Effluent	1.798	1.459	1.548
Mn	Influent	14.83	15.343	15.44
	Effluent	10.653	10.84	10.672
Fe	Influent	405.983	412.758	397.075
	Effluent	81.212	64.018	72.159
Cu	Influent	39.958	36.595	44.134
	Effluent	8.042	7.067	7.676
Zn	Influent	57.727	45.265	60.054
	Effluent	18.094	16.397	16.318
Sr	Influent	13.268	12.716	13.029
	Effluent	9.635	9.579	10.179
Zr	Influent	606.53	621.707	606.855
	Effluent	173.191	140.194	152.628
Mo	Influent	3.933	1.527	1.675
	Effluent	0.655	0.456	0.497
Ag	Influent	0.203	0.113	0.101
	Effluent	0.078	0.071	0.085
Sn	Influent	51.735	39.137	32.458
	Effluent	34.62	26.17	32.124
Ba	Influent	46.447	44.179	54.483
	Effluent	28.383	25.855	27.492
Pb	Influent	1.267	0.722	0.91
	Effluent	0.222	0.121	0.128

Total concentration of treated samples (dissolved) data in parts per billion (ppb)				
Element	**Type**	**Sample1**	**Sample2**	**Sample3**
Mg	Influent	651.400	607.364	651.556
	Effluent	680.911	655.491	678.392
Al	Influent	12.107	8.464	23.140
	Effluent	9.963	7.189	6.450
Ti	Influent	9.924	6.478	4.214
	Effluent	1.932	1.662	0.826
Mn	Influent	13.256	12.997	14.837
	Effluent	10.823	10.614	10.611
Fe	Influent	236.697	210.207	264.179
	Effluent	103.752	105.040	81.662
Cu	Influent	2.907	2.202	2.716
	Effluent	0.846	1.003	0.892
Zn	Influent	38.964	17.581	39.981
	Effluent	6.732	4.026	4.902
Sr	Influent	14.699	13.521	14.175
	Effluent	11.567	10.970	11.054
Zr	Influent	1.697	0.739	1.343
	Effluent	0.821	0.360	0.529
Mo	Influent	1.537	1.034	1.561
	Effluent	0.261	0.247	0.293
Ag	Influent	0.058	0.048	0.057
	Effluent	0.042	0.039	0.044
Sn	Influent	10.557	7.914	10.066
	Effluent	97.286	72.775	94.434
Ba	Influent	38.921	33.275	39.720
	Effluent	26.838	25.606	25.258
Pb	Influent	3.093	2.981	2.301
	Effluent	2.862	2.833	1.974

APPENDIX C. TREATMENT PROCESS FLOW DIAGRAM (AC, SB, UB, AND DI WWTPS)

C.1 AC WWTP

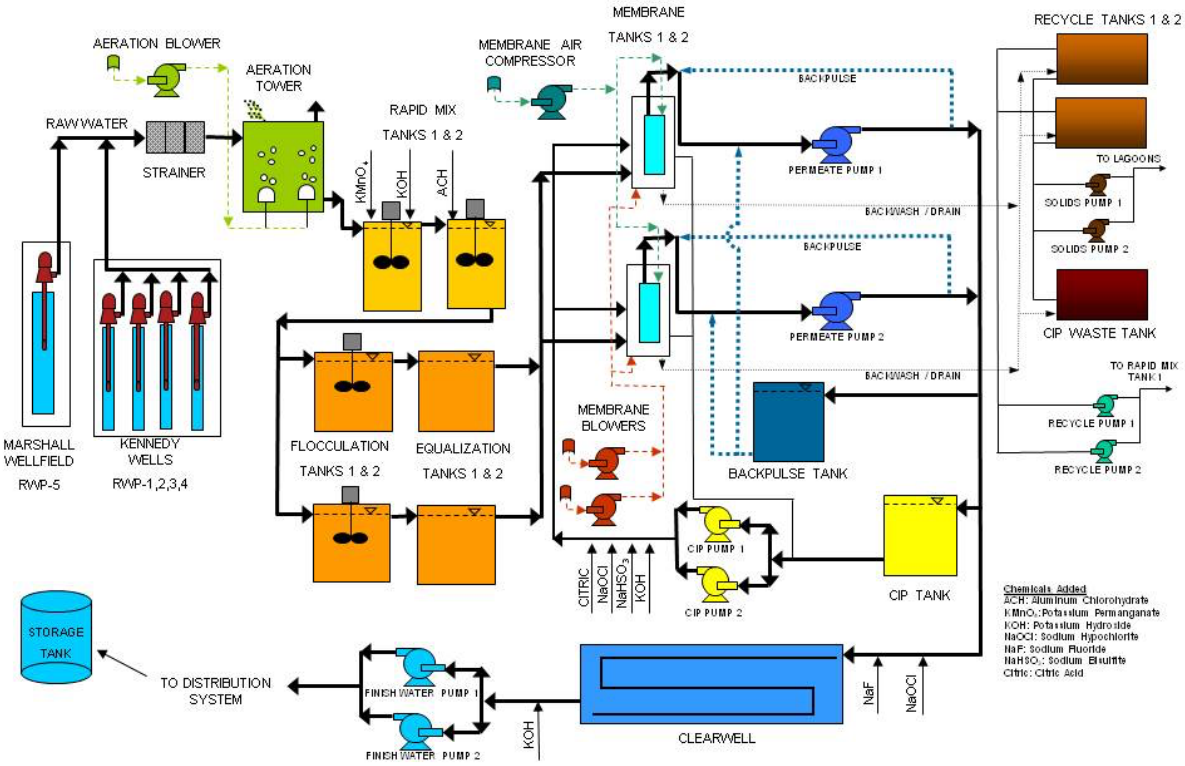

Figure C1. AC WWTP treatment flow diagram.

C.2 SB WWTP

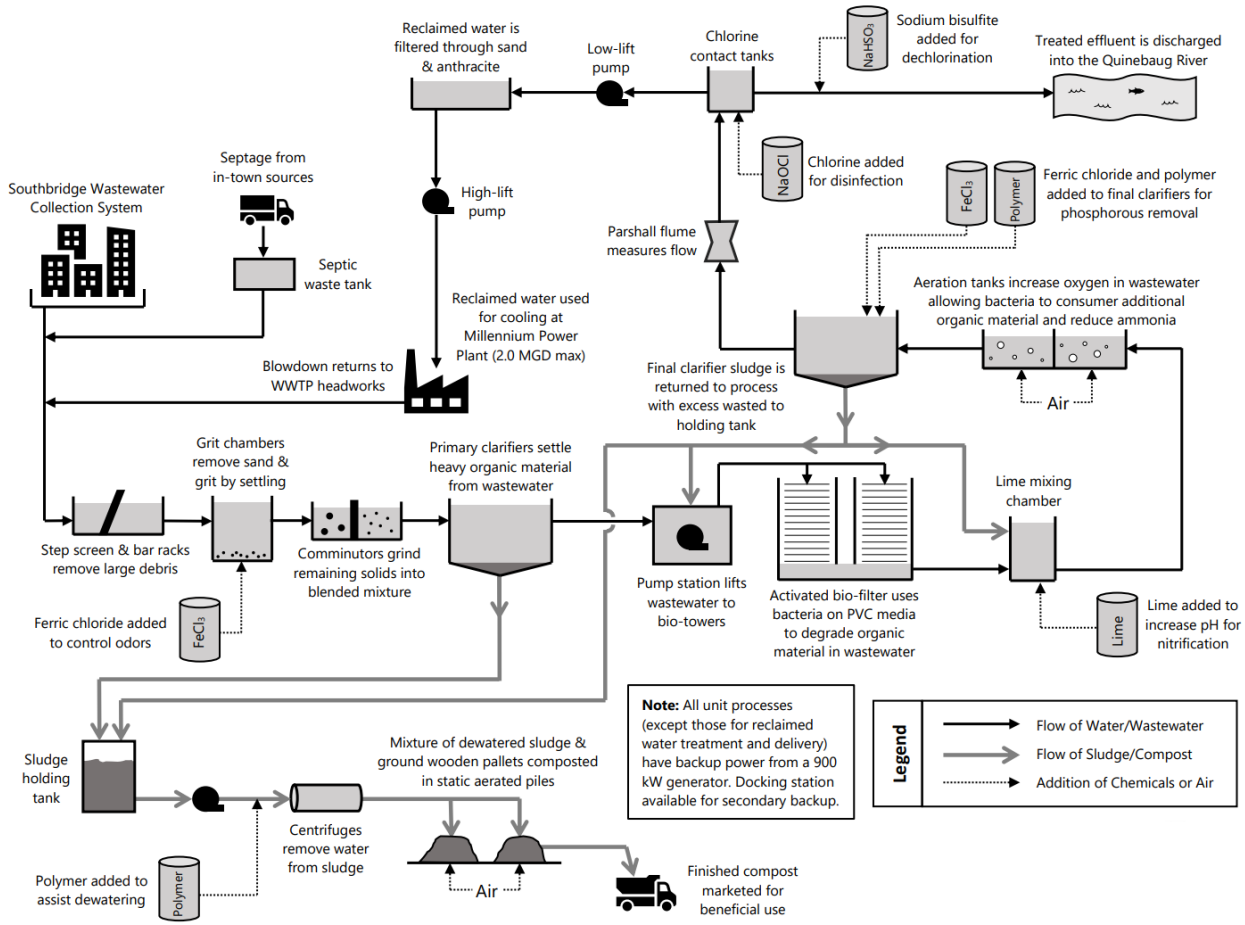

Figure C2. SB WWTP treatment flow diagram.

C.3 UB WWTP

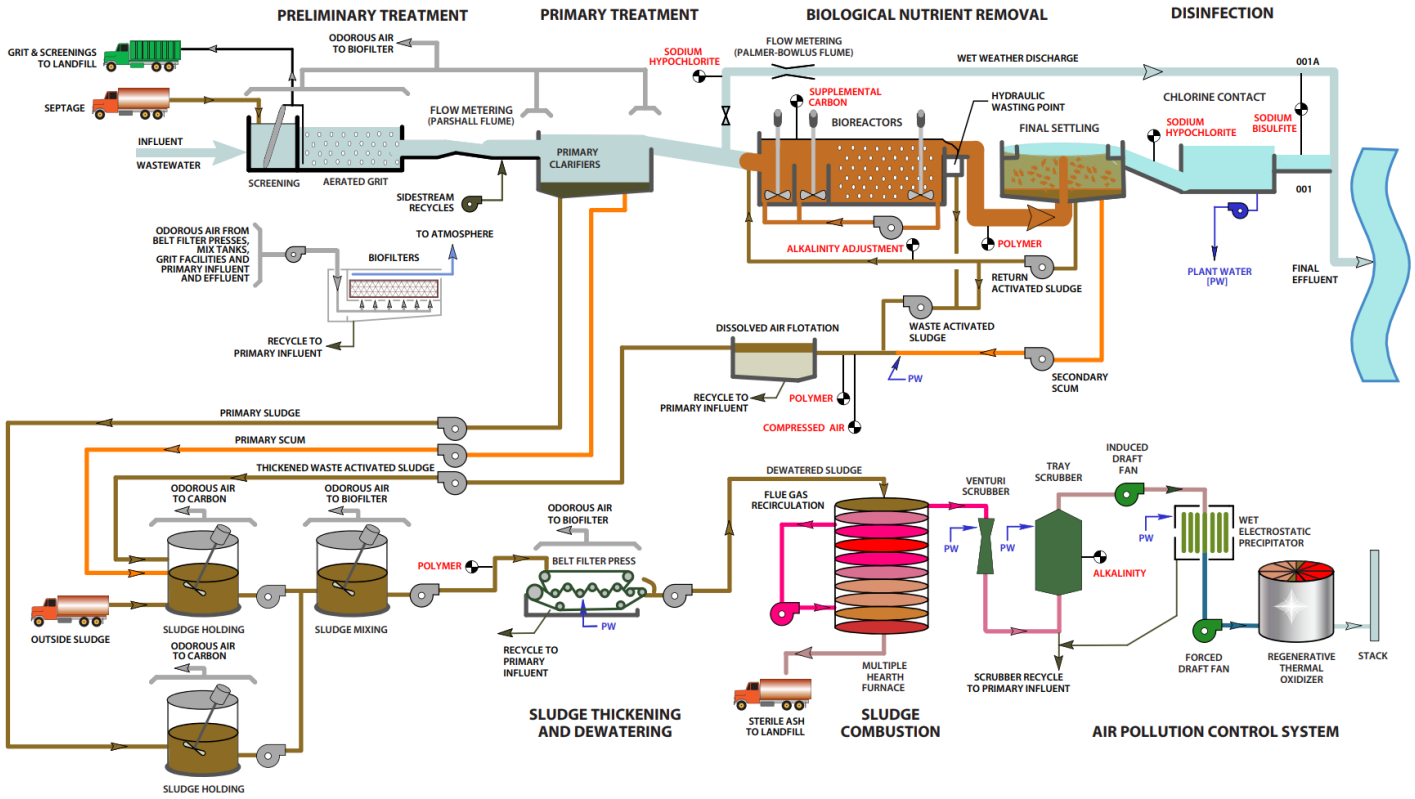

Figure C3. UB WWTP treatment flow diagram.

C.4 DI WWTP

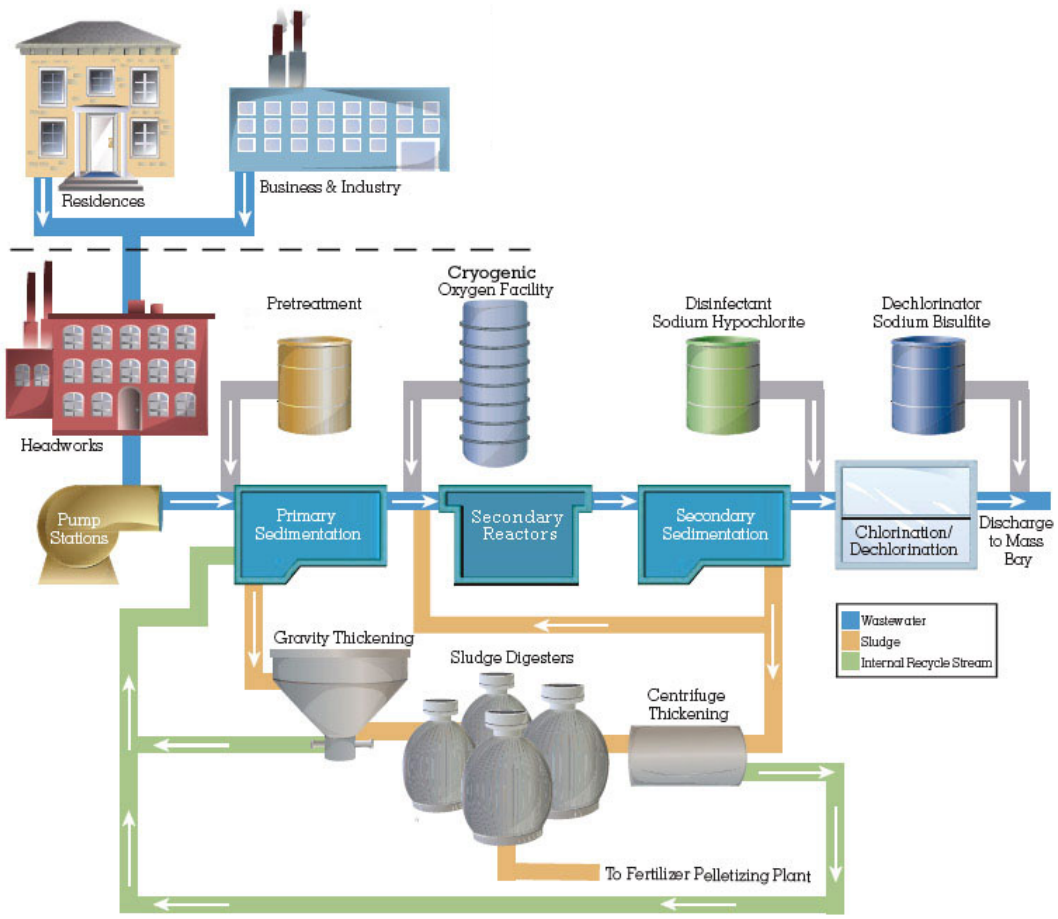

Figure C4. DI WWTP treatment flow diagram

APPENDIX D. SEM/EDS DATA

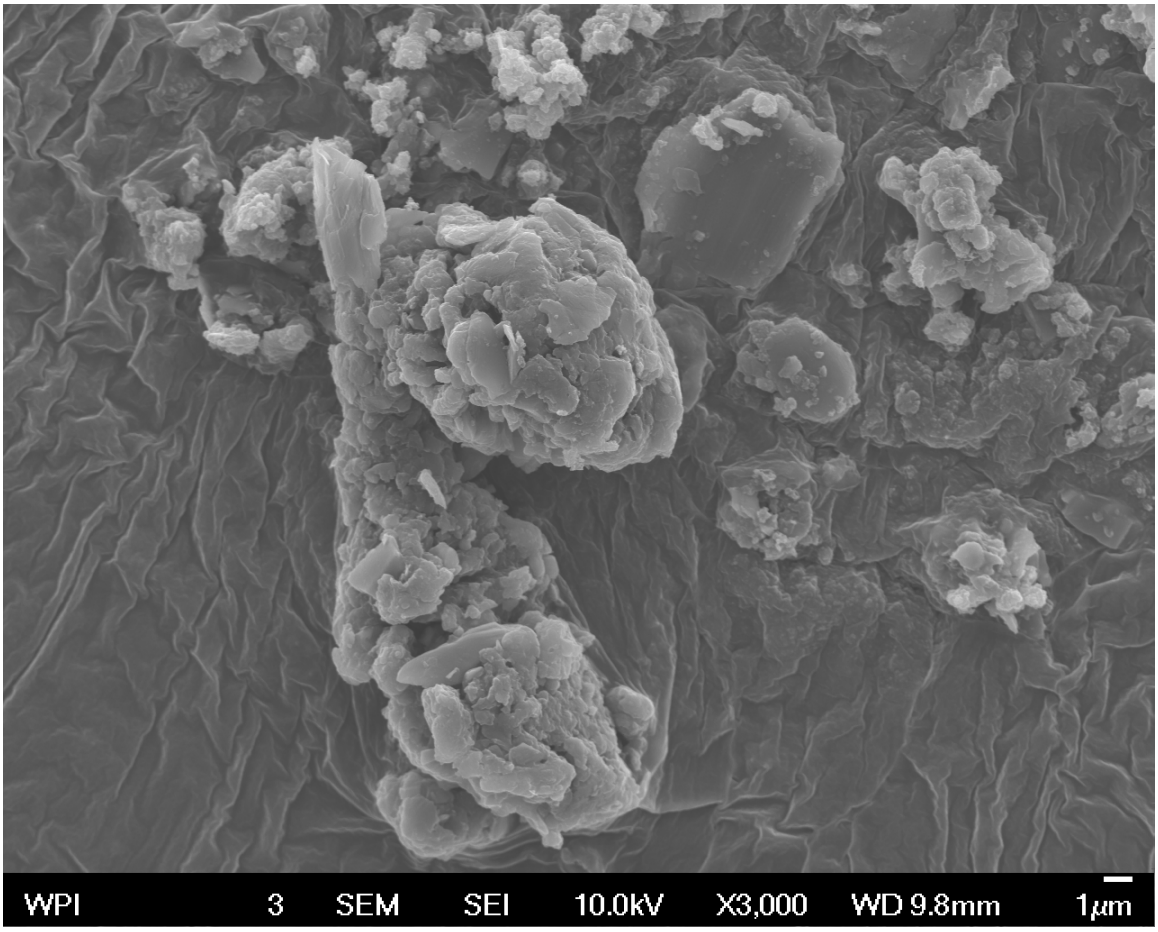

Figure D1. UB influent with 3000 magnifications.

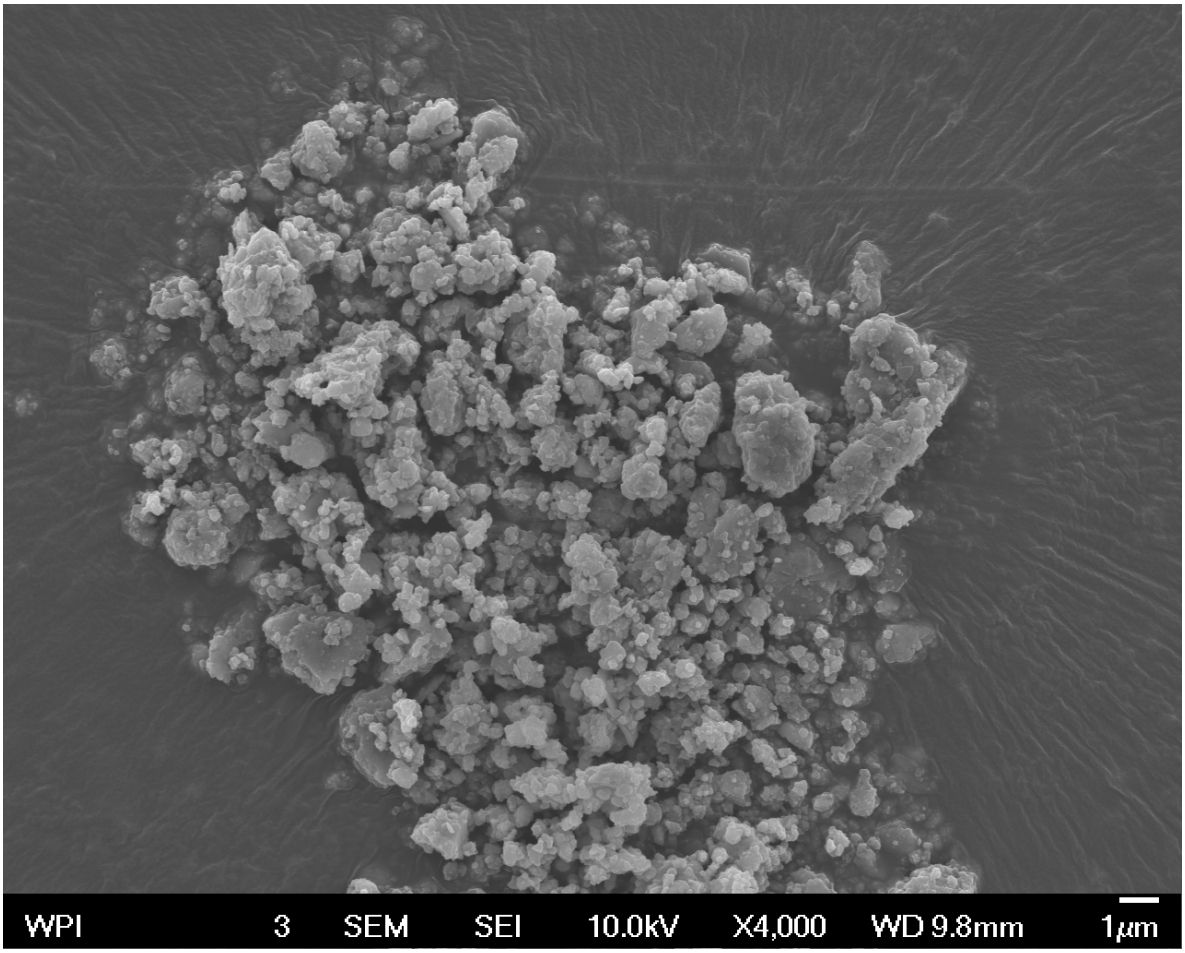

Figure D2. UB influent with 4000 magnifications.

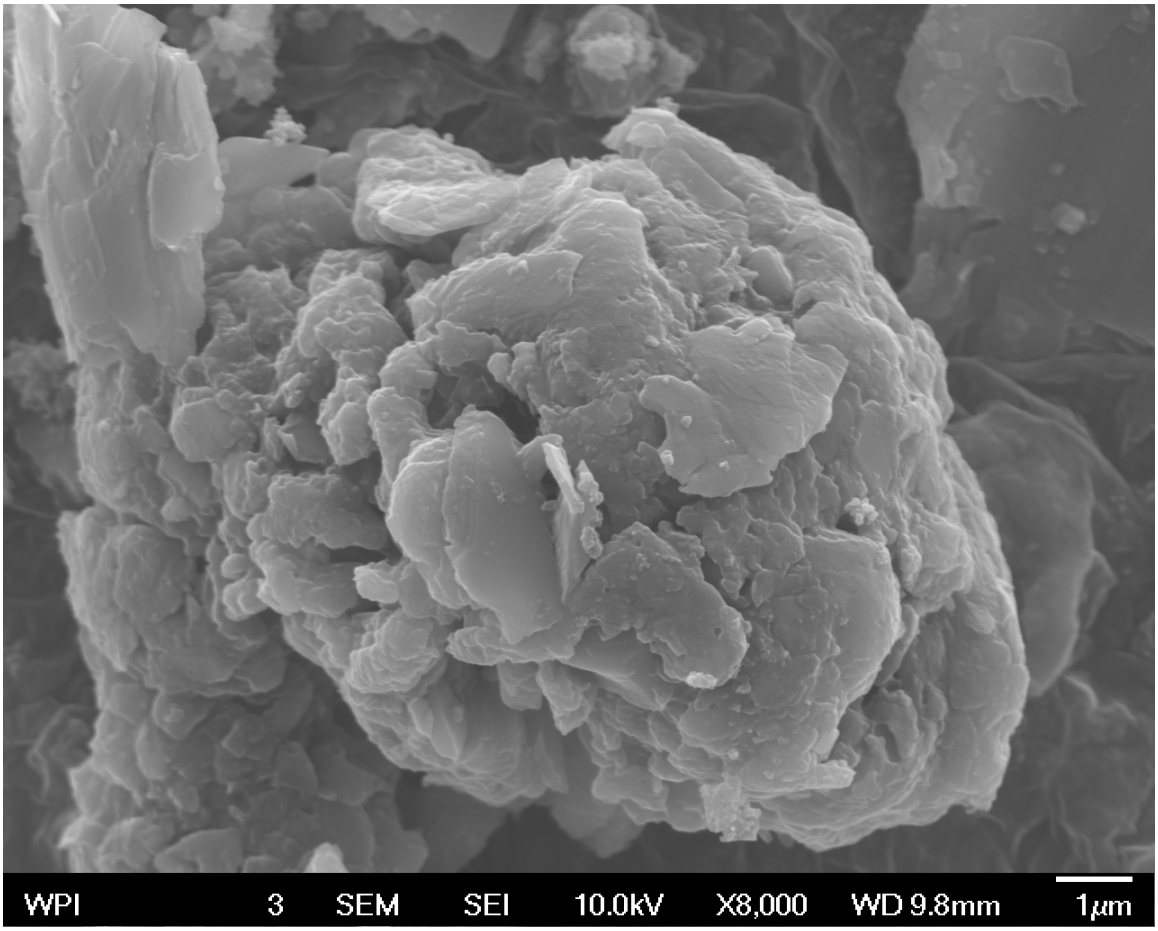

Figure D3. UB influent with 8000 magnifications.

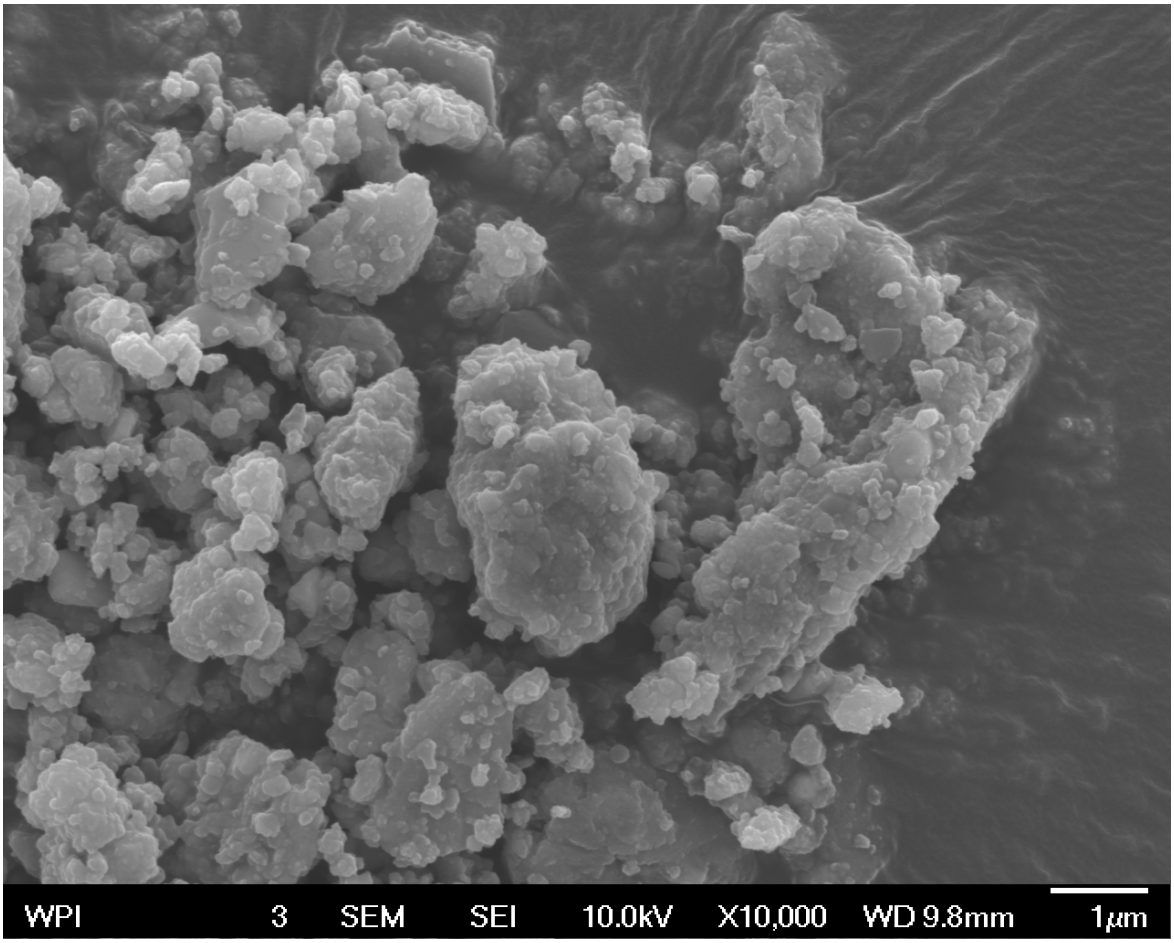

Figure D4. UB influent with 10,000 magnifications.

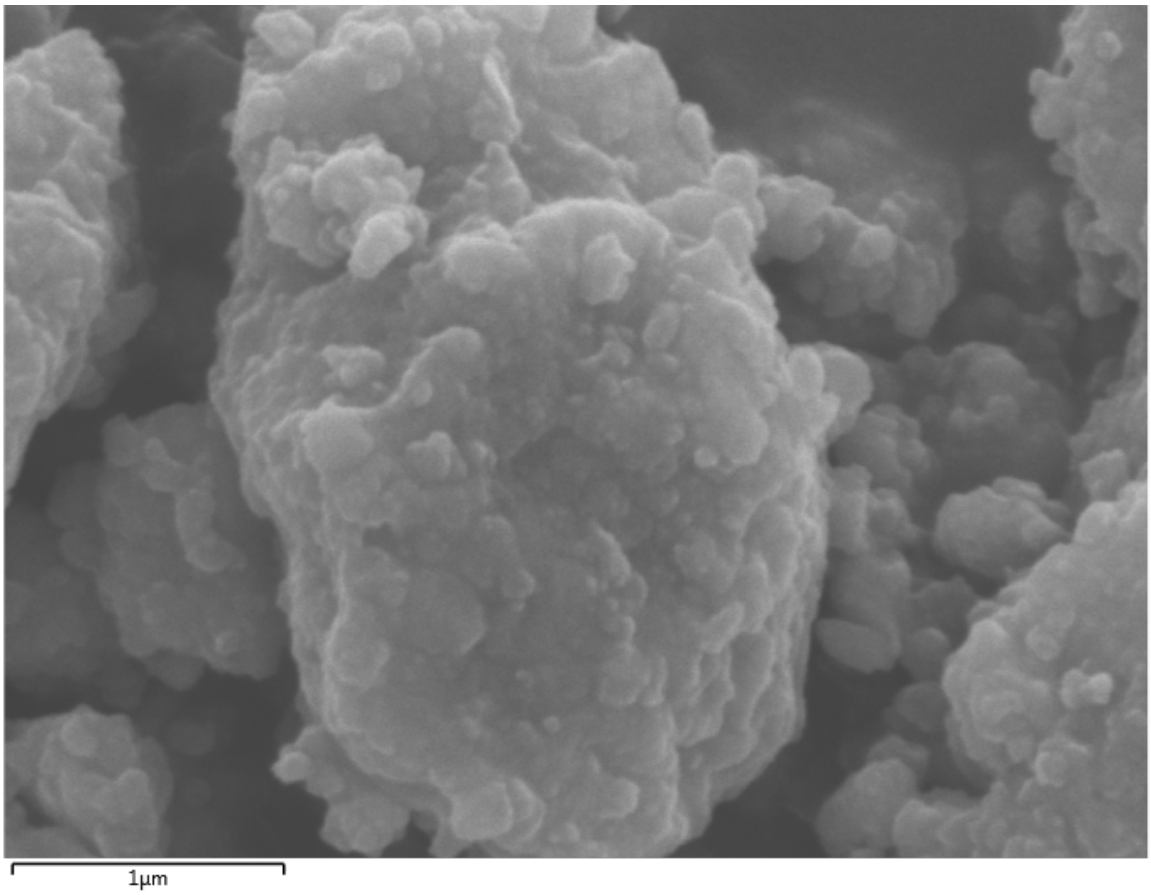

Figure D5. UB influent with 30,000 magnifications.

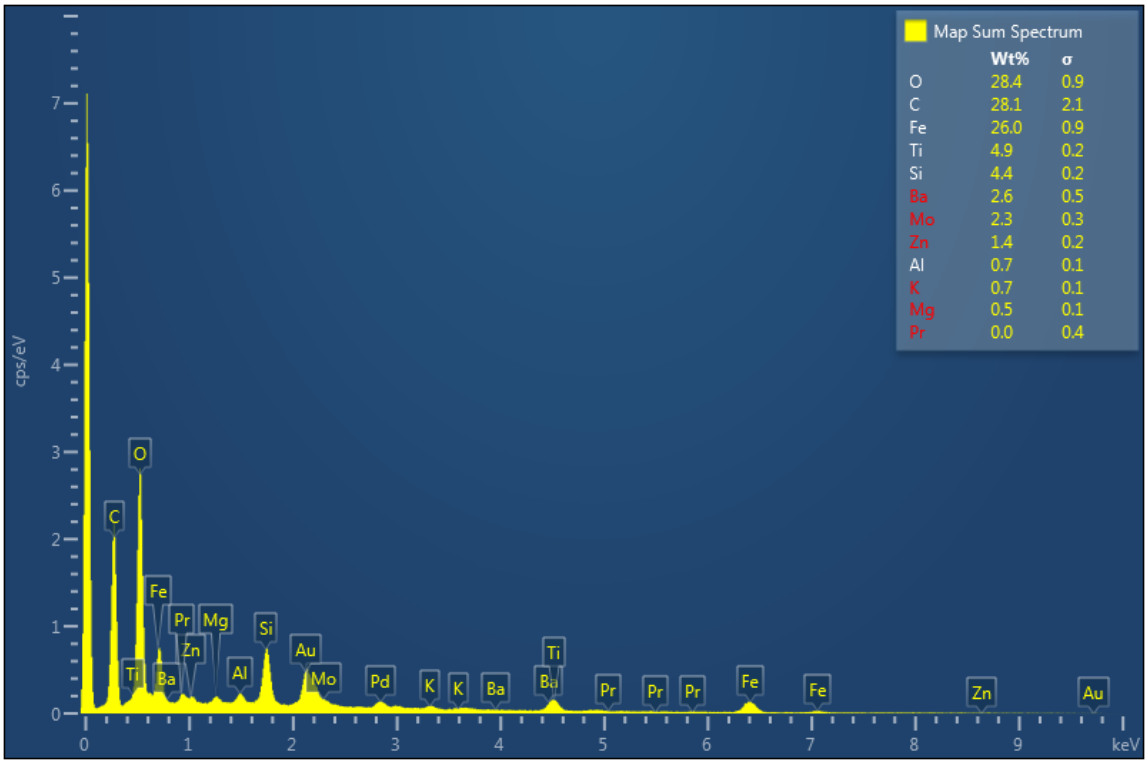

Figure D6. UB influent EDS analysis (Figure D5).

APPENDIX E. AFM DATA

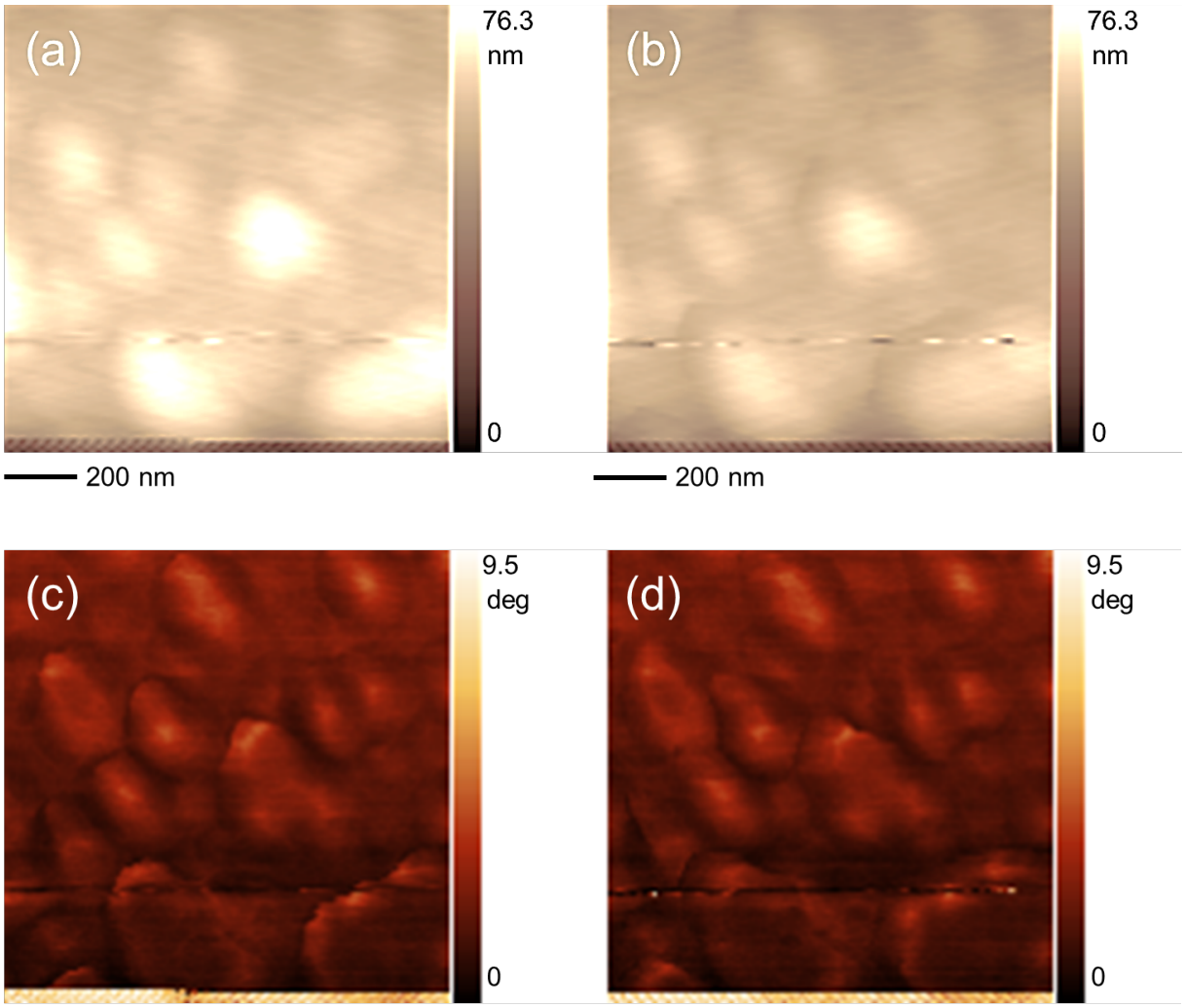

Figure E1. Z-axis (a, b) and phase (c, d), forward (a), and backward (b) images of concentrated wastewater samples with a scan range of 1 µm at a fast scan speed in phase-contrast mode. Height range of approximately 76 nm.

APPENDIX F. DLS DATA

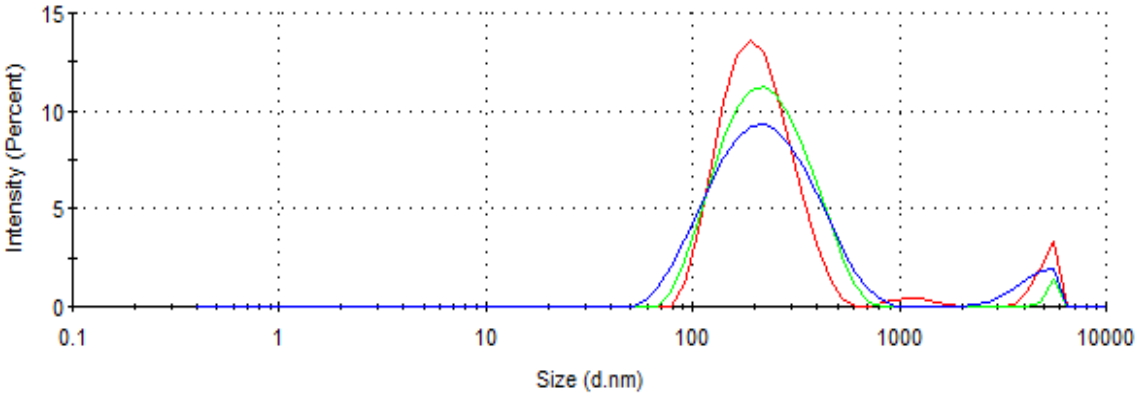

Figure F1. UB influent sample size distribution results.

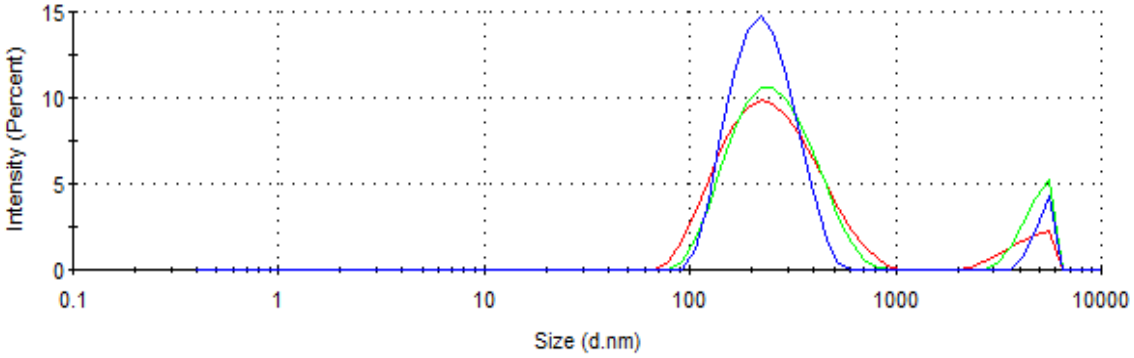

Figure F2. UB effluent sample size distribution results.

REFERENCES

Adamczyk, Zbigniew, and Paweł Weroński. 1999. “Application of the DLVO Theory for Particle Deposition Problems.” *Advances in Colloid and Interface Science* 83(1–3):137–226.

Adegboyega, Nathaniel F., Virender K. Sharma, Karolina M. Siskova, Renata Vecerova, Milan Kolar, Radek Zbořil, and Jorge L. Gardea-Torresdey. 2014. “Enhanced Formation of Silver Nanoparticles in Ag+-NOM-Iron (II, III) Systems and Antibacterial Activity Studies.” *Environmental Science & Technology* 48(6):3228–35.

Alkahtane, Abdullah A. 2015. “Nanosilica Exerts Cytotoxicity and Apoptotic Response via Oxidative Stress in Mouse Embryonic Fibroblasts.” *Toxicological & Environmental Chemistry* 97(5):651–62. doi: 10.1080/02772248.2015.1058050.

Auffan, Melanie, Jerome Rose, Thierry Orsiere, Michel De Meo, Antoine Thill, Ophelie Zeyons, Olivier Proux, Armand Masion, Perrine Chaurand, Olivier Spalla, Alain Botta, Mark R. Wiesner, and Jean Yves Bottero. 2009. “CeO2 Nanoparticles Induce DNA Damage towards Human Dermal Fibroblasts in Vitro.” *Nanotoxicology* 3(2):161–71. doi: 10.1080/17435390902788086.

Azimzada, Agil, Jeffrey M. Farner, Ibrahim Jreije, Madjid Hadioui, Carolyn Liu-Kang, Nathalie Tufenkji, Phil Shaw, and Kevin J. Wilkinson. 2020. “Single-and Multi-

Element Quantification and Characterization of TiO2 Nanoparticles Released from Outdoor Stains and Paints." *Frontiers in Environmental Science* 91.

Bäuerlein, Patrick S., Erik Emke, Peter Tromp, Jan A. M. H. Hofman, Andrea Carboni, Ferry Schooneman, Pim de Voogt, and Annemarie P. van Wezel. 2017. "Is There Evidence for Man-Made Nanoparticles in the Dutch Environment?" *Science of the Total Environment* 576:273–83.

Berry, Catherine Cecilia, Stephen Wells, Stuart Charles, Gregor Aitchison, and Adam S. G. Curtis. 2004. "Cell Response to Dextran-Derivatised Iron Oxide Nanoparticles Post Internalisation." *Biomaterials*. doi: 10.1016/j.biomaterials.2003.12.046.

Brar, Satinder K., and M. Verma. 2011. "Measurement of Nanoparticles by Light-Scattering Techniques." *TrAC Trends in Analytical Chemistry* 30(1):4–17.

Bregoli, Lisa, Francesca Chiarini, Andrea Gambarelli, Gianluca Sighinolfi, Antonietta M. Gatti, Patrizia Santi, Alberto M. Martelli, and Lucio Cocco. 2009. "Toxicity of Antimony Trioxide Nanoparticles on Human Hematopoietic Progenitor Cells and Comparison to Cell Lines." *Toxicology* 262(2):121–29. doi: 10.1016/j.tox.2009.05.017.

Brow, Richard K. 2004. "Introduction." *Journal of the American Ceramic Society* 85(5):1029–1029. doi: 10.1111/j.1151-2916.2002.tb00217.x.

Bvrith, Madhavi Vemula, and Vijaya Bhaskar Reddy. 2013. "An Overview on Research Trends in Remediation of Chromium." *Research Journal of Recent Sciences Res.J.Recent Sci*.

de Castro, Isabela Alves, Robi Shankar Datta, Jian Zhen Ou, Andres Castellanos-Gomez, Sharath Sriram, Torben Daeneke, and Kourosh Kalantar-zadeh. 2017. "Molybdenum Oxides – From Fundamentals to Functionality." *Advanced Materials*.

Cervantes-Avilés, Pabel, and Arturo A. Keller. 2021. "Incidence of Metal-Based Nanoparticles in the Conventional Wastewater Treatment Process." *Water Research* 189:116603.

Chen, Yinduo, and John Bergendahl. 2021. "Identification and Quantification of a Wide Variety of Inorganic Nanoparticles in Municipal Wastewater." *Journal of Hazardous, Toxic, and Radioactive Waste* 25(4):4021030.

Choi, Soohoon, Murray V Johnston, Gen-Suh Wang, and C. P. Huang. 2017. "Looking for Engineered Nanoparticles (ENPs) in Wastewater Treatment Systems: Qualification and Quantification Aspects." *Science of the Total Environment* 590:809–17.

Choi, Soohoon, Murray Johnston, Gen-Suh Wang, and C. P. Huang. 2018. "A Seasonal Observation on the Distribution of Engineered Nanoparticles in Municipal Wastewater Treatment Systems Exemplified by TiO2 and ZnO." *Science of the Total Environment* 625:1321–29.

Chowdhury, Pankaj, Ghodsieh Malekshoar, and Ajay K. Ray. 2017. "Dye-Sensitized Photocatalytic Water Splitting and Sacrificial Hydrogen Generation: Current Status and Future Prospects." *Inorganics*.

Claudia, Altavilla. 2017. "Magnetic Nanoparticles for Drug Delivery." Pp. 313–42 in *Inorganic Nanoparticles: Synthesis, Applications, and Perspectives*. CRC Press.

Doron, Aurbach, and Haik Ortal. 2017. “Inorganic Nanoparticles and Rechargeable Batteries.” Pp. 213–56 in *Inorganic Nanoparticles: Synthesis, Applications, and Perspectives*. CRC Press.

Dwivedi, Amarendra Dhar, Shashi Prabha Dubey, Mika Sillanpää, Young-Nam Kwon, Changha Lee, and Rajender S. Varma. 2015. “Fate of Engineered Nanoparticles: Implications in the Environment.” *Coordination Chemistry Reviews* 287:64–78.

Egerton, Terry A., and Ian R. Tooley. 2012. “UV Absorption and Scattering Properties of Inorganic-Based Sunscreens.” *International Journal of Cosmetic Science*. doi: 10.1111/j.1468-2494.2011.00689.x.

Elsaesser, Andreas, and C. Vyvyan Howard. 2012. “Toxicology of Nanoparticles.” *Advanced Drug Delivery Reviews* 64(2):129–37. doi: 10.1016/j.addr.2011.09.001.

Faure, Bertrand, German Salazar-Alvarez, Anwar Ahniyaz, Irune Villaluenga, Gemma Berriozabal, Yolanda R. De Miguel, and Lennart Bergström. 2013. “Dispersion and Surface Functionalization of Oxide Nanoparticles for Transparent Photocatalytic and UV-Protecting Coatings and Sunscreens.” *Science and Technology of Advanced Materials*.

Fei Yin, Zi, Long Wu, Hua Gui Yang, and Yong Hua Su. 2013. “Recent Progress in Biomedical Applications of Titanium Dioxide.” *Physical Chemistry Chemical Physics*.

Fernández-Nieves, A., and F. J. de las Nieves. 1999. “The Role of ζ Potential in the Colloidal Stability of Different TiO2/Electrolyte Solution Interfaces.” *Colloids and*

Surfaces A: Physicochemical and Engineering Aspects 148(3):231–43. doi: https://doi.org/10.1016/S0927-7757(98)00763-8.

Foss Hansen, Steffen, Laura Roverskov Heggelund, Pau Revilla Besora, Aiga Mackevica, Alessio Boldrin, and Anders Baun. 2016. "Nanoproducts – What Is Actually Available to European Consumers?" *Environmental Science: Nano* 3(1):169–80. doi: 10.1039/C5EN00182J.

Gomoll, Andreas H., Wolfgang Fitz, Richard D. Scott, Thomas S. Thornhill, and Anuj Bellare. 2008. "Nanoparticulate Fillers Improve the Mechanical Strength of Bone Cement." *Acta Orthopaedica*. doi: 10.1080/17453670710015349.

Gondikas, Andreas P., Frank von der Kammer, Robert B. Reed, Stephan Wagner, James F. Ranville, and Thilo Hofmann. 2014. "Release of TiO2 Nanoparticles from Sunscreens into Surface Waters: A One-Year Survey at the Old Danube Recreational Lake." *Environmental Science & Technology* 48(10):5415–22. doi: 10.1021/es405596y.

Hadioui, Madjid, Vladimir Merdzan, and Kevin J. Wilkinson. 2015. "Detection and Characterization of ZnO Nanoparticles in Surface and Waste Waters Using Single Particle ICPMS." *Environmental Science and Technology*. doi: 10.1021/acs.est.5b00681.

Hadioui, Madjid, Caroline Peyrot, and Kevin J. Wilkinson. 2014. "Improvements to Single Particle ICPMS by the Online Coupling of Ion Exchange Resins." *Analytical Chemistry*. doi: 10.1021/ac5004932.

Helsper, Johannes P. F. G., Ruud J. B. Peters, Margaretha E. M. van Bemmel, Zahira E. Herrera Rivera, Stephan Wagner, Frank von der Kammer, Peter C. Tromp, Thilo Hofmann, and Stefan Weigel. 2016. "Physicochemical Characterization of Titanium Dioxide Pigments Using Various Techniques for Size Determination and Asymmetric Flow Field Flow Fractionation Hyphenated with Inductively Coupled Plasma Mass Spectrometry." *Analytical and Bioanalytical Chemistry* 408(24):6679–91. doi: 10.1007/s00216-016-9783-6.

Hidaka, Hisao, Satoshi Horikoshi, Nick Serpone, and John Knowland. 1997. "In Vitro Photochemical Damage to DNA, RNA and Their Bases by an Inorganic Sunscreen Agent on Exposure to UVA and UVB Radiation." *Journal of Photochemistry and Photobiology A: Chemistry* 111(1–3):205–13.

Hoo, Christopher M., Natasha Starostin, Paul West, and Martha L. Mecartney. 2008. "A Comparison of Atomic Force Microscopy (AFM) and Dynamic Light Scattering (DLS) Methods to Characterize Nanoparticle Size Distributions." *Journal of Nanoparticle Research* 10(1):89–96.

Hotze, Ernest M., Tanapon Phenrat, and Gregory V Lowry. 2010. "Nanoparticle Aggregation: Challenges to Understanding Transport and Reactivity in the Environment." *Journal of Environmental Quality* 39(6):1909–24.

Huang, Yuxiong, Arturo A. Keller, Pabel Cervantes-Avilés, and Jenny Nelson. 2021. "Fast Multielement Quantification of Nanoparticles in Wastewater and Sludge Using Single-Particle ICP-MS." *ACS ES&T Water* 1(1):205–13. doi: 10.1021/acsestwater.0c00083.

Ikuma, Kaoru, Andrew S. Madden, Alan W. Decho, and Boris L. T. Lau. 2014. “Deposition of Nanoparticles onto Polysaccharide-Coated Surfaces: Implications for Nanoparticle–Biofilm Interactions.” *Environmental Science: Nano* 1(2):117–22.

Jeng, Hueiwang Anna, and James Swanson. 2006. “Toxicity of Metal Oxide Nanoparticles in Mammalian Cells.” *Journal of Environmental Science and Health - Part A Toxic/Hazardous Substances and Environmental Engineering*. doi: 10.1080/10934520600966177.

Jung, Heejung, David B. Kittelson, and Michael R. Zachariah. 2005. “The Influence of a Cerium Additive on Ultrafine Diesel Particle Emissions and Kinetics of Oxidation.” *Combustion and Flame* 142(3):276–88.

Kaegi, R., A. Ulrich, B. Sinnet, R. Vonbank, A. Wichser, S. Zuleeg, H. Simmler, S. Brunner, H. Vonmont, M. Burkhardt, and M. Boller. 2008. “Synthetic TiO2 Nanoparticle Emission from Exterior Facades into the Aquatic Environment.” *Environmental Pollution* 156(2):233–39. doi: https://doi.org/10.1016/j.envpol.2008.08.004.

Kaegi, Ralf, Brian Sinnet, Steffen Zuleeg, Harald Hagendorfer, Elisabeth Mueller, Roger Vonbank, Markus Boller, and Michael Burkhardt. 2010. “Release of Silver Nanoparticles from Outdoor Facades.” *Environmental Pollution* 158(9):2900–2905. doi: https://doi.org/10.1016/j.envpol.2010.06.009.

Keller, Arturo A., Suzanne McFerran, Anastasiya Lazareva, and Sangwon Suh. 2013. “Global Life Cycle Releases of Engineered Nanomaterials.” *Journal of Nanoparticle*

Research 15(6):1692.

King, Stephen M., and Helen P. Jarvie. 2012. "Exploring How Organic Matter Controls Structural Transformations in Natural Aquatic Nanocolloidal Dispersions." *Environmental Science & Technology* 46(13):6959–67. doi: 10.1021/es2034087.

Kiser, M. A., P. Westerhoff, T. Benn, Y. Wang, J. Pérez-Rivera, and K. Hristovski. 2009. "Titanium Nanomaterial Removal and Release from Wastewater Treatment Plants." *Environmental Science and Technology*. doi: 10.1021/es901102n.

Kiser, Mehlika A., David A. Ladner, Kiril D. Hristovski, and Paul K. Westerhoff. 2012. "Nanomaterial Transformation and Association with Fresh and Freeze-Dried Wastewater Activated Sludge: Implications for Testing Protocol and Environmental Fate." *Environmental Science and Technology*. doi: 10.1021/es300339x.

Lahouij, I., E. W. Bucholz, B. Vacher, S. B. Sinnott, J. M. Martin, and F. Dassenoy. 2012. "Lubrication Mechanisms of Hollow-Core Inorganic Fullerene-like Nanoparticles: Coupling Experimental and Computational Works." *Nanotechnology* 23(37):375701. doi: 10.1088/0957-4484/23/37/375701.

Lam, Chiu-Wing, John T. James, Richard McCluskey, and Robert L. Hunter. 2004. "Pulmonary Toxicity of Single-Wall Carbon Nanotubes in Mice 7 and 90 Days After Intratracheal Instillation." *Toxicological Sciences* 77(1):126–34. doi: 10.1093/toxsci/kfg243.

Li, Fang, Qiming Li, and Hern Kim. 2013. "Spray Deposition of Electrospun TiO 2 Nanoparticles with Self-Cleaning and Transparent Properties onto Glass." *Applied*

Surface Science. doi: 10.1016/j.apsusc.2013.03.103.

Li, Lingxiangyu, Georg Hartmann, Markus Döblinger, and Michael Schuster. 2013. "Quantification of Nanoscale Silver Particles Removal and Release from Municipal Wastewater Treatment Plants in Germany." *Environmental Science & Technology* 47(13):7317–23.

Lübbe, Andreas Stephan, Christian Bergemann, Winfried Huhnt, Thomas Fricke, Hanno Riess, Jeffery Walter Brock, and Dieter Huhn. 1996. "Preclinical Experiences with Magnetic Drug Targeting: Tolerance and Efficacy." *Cancer Research* 56(20):4694–4701.

Matsumura, Yasuhiro, and Honnavara N. Ananthaswamy. 2004. "Toxic Effects of Ultraviolet Radiation on the Skin." *Toxicology and Applied Pharmacology* 195(3):298–308.

Maurer-Jones, Melissa A., Ian L. Gunsolus, Catherine J. Murphy, and Christy L. Haynes. 2013. "Toxicity of Engineered Nanoparticles in the Environment." *Analytical Chemistry* 85(6):3036–49.

Merrifield, Ruth C., Chady Stephan, and Jamie Lead. 2017. "Determining the Concentration Dependent Transformations of Ag Nanoparticles in Complex Media: Using SP-ICP-MS and Au@ Ag Core–Shell Nanoparticles as Tracers." *Environmental Science & Technology* 51(6):3206–13.

Miriam, Raifailovich. 2017. "Inorganic Particles against Reactive Oxygen Species for Sun Protective Products." Pp. 355–66 in *Inorganic Nanoparticles: Synthesis,*

Applications, and Perspectives. CRC Press.

Mohn, D., M. Zehnder, T. Imfeld, and W. J. Stark. 2010. "Radio-Opaque Nanosized Bioactive Glass for Potential Root Canal Application: Evaluation of Radiopacity, Bioactivity and Alkaline Capacity." *International Endodontic Journal*. doi: 10.1111/j.1365-2591.2009.01660.x.

Mylon, Steven E., Kai Loon Chen, and Menachem Elimelech. 2004. "Influence of Natural Organic Matter and Ionic Composition on the Kinetics and Structure of Hematite Colloid Aggregation: Implications to Iron Depletion in Estuaries." *Langmuir* 20(21):9000–9006.

Naasz, Steffi, Stefan Weigel, Olga Borovinskaya, Andrius Serva, Claudia Cascio, Anna K. Undas, Felice C. Simeone, Hans J. P. Marvin, and Ruud J. B. Peters. 2018. "Multi-Element Analysis of Single Nanoparticles by ICP-MS Using Quadrupole and Time-of-Flight Technologies." *Journal of Analytical Atomic Spectrometry* 33(5):835–45.

Navratilova, Jana, Antonia Praetorius, Andreas Gondikas, Willi Fabienke, Frank von der Kammer, and Thilo Hofmann. 2015. "Detection of Engineered Copper Nanoparticles in Soil Using Single Particle ICP-MS." *International Journal of Environmental Research and Public Health* 12(12):15756–68.

Nina, Perkas, Gedanken Aharon, Wehrschuetz-Sigl Eva, Perelshtein Ilana, and Applerot Guy. 2017. "Innovative Inorganic Nanoparticles with Antibacterial Properties Attached to Textiles by Sonochemistry." Pp. 367–92 in *Inorganic Nanoparticles: Synthesis, Applications, and Perspectives*. CRC Press.

Nuzzo, Regina. 2014. “Scientific Method: Statistical Errors.” *Nature News* 506(7487):150.

Oberdörster, Günter, Andrew Maynard, Ken Donaldson, Vincent Castranova, Julie Fitzpatrick, Kevin Ausman, Janet Carter, Barbara Karn, Wolfgang Kreyling, David Lai, Stephen Olin, Nancy Monteiro-Riviere, David Warheit, Hong Yang, and A. report from the ILSI Research Foundation/Risk Science Institute Nanomaterial Toxicity Screening Working Group. 2005. “Principles for Characterizing the Potential Human Health Effects from Exposure to Nanomaterials: Elements of a Screening Strategy.” *Particle and Fibre Toxicology* 2(1):8. doi: 10.1186/1743-8977-2-8.

Perugini, P., S. Simeoni, S. Scalia, I. Genta, T. Modena, B. Conti, and F. Pavanetto. 2002. “Effect of Nanoparticle Encapsulation on the Photostability of the Sunscreen Agent, 2-Ethylhexyl-p-Methoxycinnamate.” *International Journal of Pharmaceutics* 246(1–2):37–45.

Peters, Ruud J. B., Greet van Bemmel, Zahira Herrera-Rivera, Hans P. F. G. Helsper, Hans J. P. Marvin, Stefan Weigel, Peter C. Tromp, Agnes G. Oomen, Anton G. Rietveld, and Hans Bouwmeester. 2014. “Characterization of Titanium Dioxide Nanoparticles in Food Products: Analytical Methods To Define Nanoparticles.” *Journal of Agricultural and Food Chemistry* 62(27):6285–93. doi: 10.1021/jf5011885.

Polesel, Fabio, Julia Farkas, Marianne Kjos, Patricia Almeida Carvalho, Xavier Flores-Alsina, Krist V. Gernaey, Steffen Foss Hansen, Benedek Gy Plósz, and Andy M. Booth. 2018. “Occurrence, Characterisation and Fate of (Nano)Particulate Ti and Ag in Two Norwegian Wastewater Treatment Plants.” *Water Research* 141(0043–1354):19–31. doi: 10.1016/j.watres.2018.04.065.

Qian, Wen Yu, Dong Mei Sun, Rong Rong Zhu, Xi Ling Du, Hui Liu, and Shi Long Wang. 2012. “PH-Sensitive Strontium Carbonate Nanoparticles as New Anticancer Vehicles for Controlled Etoposide Release.” *International Journal of Nanomedicine*. doi: 10.2147/IJN.S34773.

Rompelberg, Cathy, Minne B. Heringa, Gerda van Donkersgoed, José Drijvers, Agnes Roos, Susanne Westenbrink, Ruud Peters, Greet van Bemmel, Walter Brand, and Agnes G. Oomen. 2016. “Oral Intake of Added Titanium Dioxide and Its Nanofraction from Food Products, Food Supplements and Toothpaste by the Dutch Population.” *Nanotoxicology*. doi: 10.1080/17435390.2016.1222457.

Scott, Thomas B. 2011. “Inorganic Nanoparticles for Environmental Remediation.” *Inorg. Nanopart* 393–439.

Semaan, Mars E., C. A. Quarles, and Leszek Nikiel. 2002. “Carbon Black and Silica as Reinforcers of Rubber Polymers: Doppler Broadening Spectroscopy Results.” *Polymer Degradation and Stability* 75(2):259–66. doi: https://doi.org/10.1016/S0141-3910(01)00227-0.

Shandilya, Neeraj, Olivier Le Bihan, Christophe Bressot, and Martin Morgeneyer. 2015. “Emission of Titanium Dioxide Nanoparticles from Building Materials to the Environment by Wear and Weather.” *Environmental Science and Technology*. doi: 10.1021/es504710p.

Sharma, Virender K., Jan Filip, Radek Zboril, and Rajender S. Varma. 2015. “Natural Inorganic Nanoparticles–Formation, Fate, and Toxicity in the Environment.”

Chemical Society Reviews 44(23):8410–23.

Shi, Liange, and Fanglin Du. 2007. "Solvothermal Synthesis of SrCO3 Hexahedral Ellipsoids." *Materials Letters*. doi: 10.1016/j.matlet.2006.11.050.

Smeraldi, Josh, Rajagopalan Ganesh, Turaj Hosseini, Leila Khatib, Betty H. Olson, and Diego Rosso. 2017. "Fate and Toxicity of Zinc Oxide Nanomaterial in Municipal Wastewaters." *Water Environment Research* 89(9):880–89. doi: 10.2175/106143017x14902968254773.

Somiya, S. 1988. "'Science and Technology of Zirconia III.'"

Song, Y., X. Li, and X. Du. 2009. "Exposure to Nanoparticles Is Related to Pleural Effusion, Pulmonary Fibrosis and Granuloma." *European Respiratory Journal* 34(3):559–67. doi: 10.1183/09031936.00178308.

Stumm, Werner. 1987. *Aquatic Surface Chemistry: Chemical Processes at the Particle-Water Interface*. Vol. 87. John Wiley & Sons.

Toro, Patricio, Raúl Quijada, Mehrdad Yazdani-Pedram, and José Luis Arias. 2007. "Eggshell, a New Bio-Filler for Polypropylene Composites." *Materials Letters* 61(22):4347–50. doi: https://doi.org/10.1016/j.matlet.2007.01.102.

Toshima, Naoki. 2011. "Inorganic Nanoparticles for Catalysis." *ChemInform* 42(11):no.

Tuoriniemi, Jani, Geert Cornelis, and Martin Hassellöv. 2012. "Size Discrimination and Detection Capabilities of Single-Particle ICPMS for Environmental Analysis of Silver Nanoparticles." *Analytical Chemistry* 84(9):3965–72.

Villalobos-Hernández, J. R., and C. C. Müller-Goymann. 2005. “Novel Nanoparticulate Carrier System Based on Carnauba Wax and Decyl Oleate for the Dispersion of Inorganic Sunscreens in Aqueous Media.” *European Journal of Pharmaceutics and Biopharmaceutics*. doi: 10.1016/j.ejpb.2004.11.002.

Wang, Yonggang, Matthew D. Becker, Vicki L. Colvin, Linda M. Abriola, and Kurt D. Pennell. 2014. “Influence of Residual Polymer on Nanoparticle Deposition in Porous Media.” *Environmental Science & Technology* 48(18):10664–71. doi: 10.1021/es500523p.

Yamaguchi, Tsutomu. 1994. “Application of ZrO2 as a Catalyst and a Catalyst Support.” *Catalysis Today*. doi: 10.1016/0920-5861(94)80003-0.